APPLYING NEW STRUCTURE, LAYOUT AND PROCESS FOR CONSTRUCTING THE METAMATERIAL AND STUDYING ITS ADVANCEMENT IN MICROWAVE CIRCUITS

(MEMBINA STRUKTUR BARU, BENTUK DAN PROSES UNTUK METAMATERIAL DAN MENYELIDIK SECARA LANJUT DALAM APLIKASI LITAR MIKROJALUR)

MOHAMAD KAMAL A. RAHIM

RESEARCH VOTE NO:
78034

Jabatan Kejuruteraan Radio
Fakulti Kejuruteraan Elektrik
Universiti Teknologi Malaysia

2008

UNIVERSITI TEKNOLOGI MALAYSIA

**BORANG PENGESAHAN
LAPORAN AKHIR PENYELIDIKAN**

JUDUL: **Applying New Structure, Layout and Process for
Constructing the Metamaterial and Studying its
Advancement in Microwave Circuits**

Saya   **MOHAMAD KAMAL A. RAHIM**
                                    (HURUF BESAR)

mengaku membenarkan **Laporan Akhir Penyelidikan** ini disimpan di Perpustakaan
Universiti Teknologi Malaysia dengan syarat-syarat kegunaan seperti berikut:

1. Tesis adalah hak milik Universiti Teknologi Malaysia.

2. Perpustakaan Universiti Teknologi Malaysia dibenarkan membuat salinan untuk tujuan
    pengajian sahaja.

3. Perpustakaan dibenarkan membuat salinan tesis ini sebagai bahan pertukaran antara
    institusi pengajian tinggi.

4. *Sila tandakan (✓)

☐ SULIT   (Mengandungi maklumat yang berdarjah keselamatan atau
                         kepentingan Malaysia seperti yang termaktub di dalam
                         AKTA RAHSIA RASMI 1972)

☐ TERHAD   (Mengandungi maklumat TERHAD yang telah ditentukan
                         oleh organisasi/badan di mana penyelidikan dijalankan)

☑ TIDAK TERHAD

                                              Disahkan oleh,

                                        _____
                                        (TANDATANGAN KETUA PENYELIDIK)

                                        _____
                                        Nama & Cop Ketua Penyelidik

                                        Tarikh : _____

CATATAN: * Jika tesis ini SULIT atau TERHAD, sila lampirkan surat daripada pihak
berkuasa/organisasi berkenaan dengan menyatakan sekali sebab dan tempoh tesis ini perlu dikelaskan sebagai
SULIT atau TERHAD

VOT 78034

APPLYING NEW STRUCTURE, LAYOUT AND PROCESS FOR CONSTRUCTING THE METAMATERIAL AND STUDYING ITS ADVANCEMENT IN MICROWAVE CIRCUITS

(MEMBINA STRUKTUR BARU, BENTUK DAN PROSES UNTUK METAMATERIAL DAN MENYELIDIK SECARA LANJUT DALAM APLIKASI LITAR MIKROJALUR)

MOHAMAD KAMAL A. RAHIM

Jabatan Kejuruteraan Radio
Fakulti Kejuruteraan Elektrik
Universiti Teknologi Malaysia

JUN 2008

DECLARATION

I declare that this thesis entitled "Applying New Structure, Layout and Process for Constructing the Metamaterial for Studying its Advancecment in Microwave Circuits" is the result of my own research except as cited in the references

Signature   : ....

Name of Supervisor : PROF. MADYA DR. MOHAMAD KAMAL B.

          ABD. RAHIM

Date   : JUNE 2008

ACKNOWLEDGEMENT

APPLYING NEW STRUCTURE, LAYOUT AND PROCESS FOR CONSTRUCTING THE METAMATERIAL AND STUDYING ITS ADVANCEMENT IN MICROWAVE CIRCUITS

(Keywords: Left-handed metamaterial, Negative refraction, Microstrip antenna)

The speculation and invention of Left-Handed Meta Material (LH MTM) has sparked the interest of many researchers globally. This material is said to have simultaneous negative parameters or double negative parameters (DNG Parameters) of the permittivity and permeability that led to the reversal of multiple theories and laws. Besides, it has the ability to improve the gain of antenna due to its focusing effect from its negative refractive index (NRI) characteristics.

Nowadays, conventional microstrip antennas have low gain and directivity compared to other antennas available in the market nowadays. However, this type of antenna is still being used due to its ease of fabrication, light weight characteristics, just to name a few. Therefore, as a mean to make this type of antenna more worthwhile, the integration of LH MTM to this type of antennas was studied through simulations and experiments to prove the hypothesis of the focusing effect. As of the structure design, the combination of the Square Rectangular Split Ring and the Thin Wire Structure was used for fabrication purposes on an FR-4 Board using the Wet Etching Technique.

From the simulation done, the gain of the antenna had increased 1.2 dB. This has proven that the focusing effect of the LH MTM really enhance the gain of the antenna. On the other hand, the Return Loss (S_{11}) was improved by 9.62 dB and 12.29 dB in the simulation. Therefore, we could also conclude that LH MTM also contributes to the betterment of the matching of the antenna. Lastly, more alternative designs of LH MTM should be explored in the future and a parameter study should be done to further understand this peculiar LH MTM.

Key Researcher :

Assoc. Prof. Dr. Mohammad Kamal A. Rahim (Head)
Mr. Thelaha Masri
Mr Nazri A. Karim
Mr Huda A. Majid
Mr Osman Ayop

e-mail :   mkamal@fke.utm.my
Tel No. :   07-5536038
Vote No. :   78034

MEMBINA STRUKTUR BARU, BENTUK DAN PROSES UNTUK METAMATERIAL DAN MENYELIDIK SECARA LANJUT DALAM APLIKASI LITAR MIKROJALUR

(Katakunci: Metamaterial tangan kiri, Negatif pembiasan, Antena mikrojalur)

Spekulasi dan rekacipta *Left-Handed Meta Material* (LH MTM) telah menarik perhatian ramai pakar di seluruh dunia ini. Bahan ini dipercayai mempunyai kedua-dua parameter yang negatif (ε dan μ) dalam julat frekuensi tertentu dan ini telah membuka pintu kepada pelbagai teori and hukum yang bertentangan dengan apa yang diketahui ramai. Selain itu, bahan ini berpotensi untuk meningkatkan gandaan sesuatu antenna dengan kebolehannya memfokus gelombang yang melaluinya dengan index biasannya yang negatif.

Pada era yang serba moden ini, antena mikrojalur masih mempunyai gandaan dan kearahan yang rendah berbanding dengan jenis-jenis antena yang lain. Walaubagaimanapun, antena mikrojalur masih digunakan dengan meluas kerana ia mudah dihasilkan, ringan dan sebagainya. Oleh itu, adalah logik untuk meningkatkan gandaan dan kearahan antena ini dengan integrasi LH MTM untuk menjadikannya lebih bernilai dan pada masa yang sama membuktikan hipotesis bahawa gelombang boleh difokus apabila melalui LH MTM.

Untuk melaksanakan simulasi LH MTM, konfigurasi *Square Rectangular Split Ring* dan *Thin Wire Structure* digunakan. Daripada simulasi yang dijalankan, gandaan antena telah meningkat sebanyak 1.2 dB. Dengan ini, projek ini telah membuktikan kebolehan memfokus LH MTM dapat meningkatkan gandaan antena. Pada masa yang sama, *Return Loss* (S_{11}) telah berkurang sebanyak 9.62 dB dan 12.29 dB bagi simulasi. Oleh sebab itu, integrasi LH MTM telah membaiki padanan antena tersebut. Akhirnya, untuk memahami bahan ini dengan lebih mendalam, lebih banyak rekaan LH MTM perlu diterokai dan kajian parameter perlu dilaksanakan.

Penyelidik :

Prof. Madya Dr. Mohamad Kamal A. Rahim (Ketua)
Mr. Thelaha Masri
Mr Nazri A. Karim
Mr Huda A. Majid
Mr Osman Ayop

e-mail :   mkamal@fke.utm.my
Tel No. :   07-5536038
Vote No. :   78034

TABLE OF CONTENT

LIST OF TABLES

LIST OF FIGURES

LIST OF SYMBOLS

a	-	Inner Radius of Smaller Rings in Split Ring Resonator
c	-	Speed of Light
d	-	Thickness of the slab (LH MTM)
E	-	Electric Field
H	-	Magnetic Field
k	-	Complex wavenumber
l	-	Length of Transmission Line
n	-	Refractive Index
p	-	Periodicity / Average Cell Size
R'	-	Resistance of metal in Split Ring Resonators
S	-	Poynting Vector
w	-	Width of the rings in Split Ring Resonators
Z	-	Impedence
ε	-	Permittivity
μ	-	Permeability
ω	-	Radian Frequency
λ	-	Wavelength
β	-	Propagation Constant
δ	-	Radial Spacing between Split Ring Resonator
ζ	-	Damping factor due to metal losses
σ	-	Conductivity of Metal
η	-	Normalized wave impedence
Ź	-	Transmission term
Γ	-	Reflection Coefficient
υ_p	-	Phase Velocity

υ_g	-	Group Velocity
ω_{0m}	-	Magnetic Plasma Frequency
ω_{pe}	-	Electric Plasma Frequency

LIST OF ABBREVIATIONS

DNG   -   Double Negative

LH MTM   -   Left Handed Meta Material

NRI   -   Negative Refractive Index

NRW   -   Nicolson-Ross-Weir

TW   -   Thin Wire

SRR   -   Split Ring Resonator

CHAPTER 1

INTRODUCTION

1.0   Introduction

In the 21st Century, there have been numerous study and research by physicists and students around the globe regarding a double negative material (negative value of permeability, μ and permittivity, ε) that contradicted a lot of the Physic laws. However, before venturing further into this interesting topic, let us look at the permittivity-permeability diagram Figure 1.1 which depicts the classification of materials available in the world today.
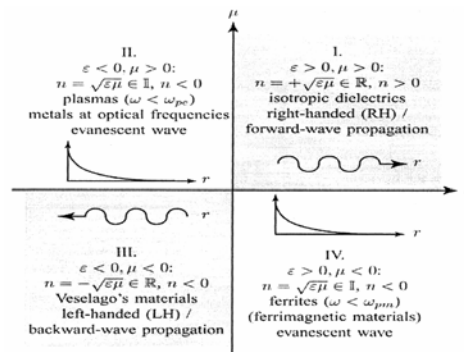
Figure 1.1 Permittivity-permeability diagram. The angular frequencies ω_{pe} and ω_{pm} represent the electric and magnetic plasma frequencies [1].

From the diagram above, almost all materials are categorized in group I where the μ and ε are both positive with a forward-wave propagation. These materials are referred to as right-handed materials (derived from the fact that the Poynting vector is determined by using the right hand). Besides, for materials which belong to group II, they are normally made of metals at optical frequencies. For example, the metal Thin-wire (TW) structure proposed by Prof. JB Pendry [2] exhibits such characteristics. On the other hand, group III materials are actually ferromagnetic materials where its μ is less than zero. Lastly, group IV are materials of interest in this whole thesis where it is hand made, effectively homogeneous (when periodicity of unit cell $< \lambda_g/4$) and exhibits a series of highly unusual properties [1]. In terms of implementation of the Left-handed Metamaterial (LH MTM) and to further clarify the word hand made materials, they are typically realized artificially as composite structures that are constructed from arrays of metallic inclusions in dielectric substrates [1].

1.1   The History of Left-Handed Meta Material (LH MTM)

In year 1967, Victor Vesalago, a Russian Physicist made a theoretical speculation on the existence of substances with simultaneously negative ε and μ, which serves as the origin of all research on LH MTMs. However, there was not much progress until year 1999 when Prof J.B Pendry proposed his design of Thin-Wire (TW) structure that exhibits the negative value of permittivity, ε [2] and the Split Ring Resonator (SRR) with a negative permeability, μ value. Following this interesting discovery, Dr. Smith from Duke University combined the 2 structures and became the first to fabricate the LH MTM in his lab.

Subsequently, with the paths paved by the pioneers, more and more researchers emerged to study this peculiar material in many fields. Among them was a study on specific reduction rate in a muscle cube with SRR [3]. The significance of this study was

to reduce the electromagnetic waves that reached the human brain when communicating via mobile phones. In the experiment, the muscle cube was a substitute of a human brain and the SRR were designed to function at 900 MHz and 1800MHz (the well known cellular phone's frequency band). By the end of the experiment, it was evident that the S21 was reduced in the specific frequencies. On the other hand, many researches were done to improve the response of microstrip antennas in particular since this type of antenna is desired for its low cost properties but with the compromise in the gain and directivity. According to some studies done [4]-[5], the LH MTM could actually increase the directivity of the microstrip antennas by locating a LH MTM cover in front of the propagating face of the antenna. Furthermore, there was also a study for filter applications by utilizing the microstrip technology as well [6]. Through this particular experiment, it proved that SRR is also a frequency selective device and could be treated as a filter.

1.2   Fundamental Theories of LH MTM

What has made these Metamaterials such a big focus of interest especially in the microwave engineering? It certainly deserves more than an increased gain in the microstrip technology and its application in filtering any unwanted signals. Therefore, a fair amount of explanation has to be made known in order to showcase the nobility of this newly discovered material.

First and foremost, referring to figure 1.1, a LH MTM is distinct from its peers in terms of its value of ε and μ where both of them are negative at the a given frequency region. It is important to note that only in this particular range of frequency, this material exhibits the LH properties. Therefore, it is very crucial to design the LH MTM at a desired frequency range and this actually proved that LH MTM are hand made and not readily found in anywhere in the world.

1.3   Problem Statement

Due to soaring interest in this particular material and its vast potential in various applications, it is a subject worth studying. Therefore, the study on the new theories developed was carried out and at the same time the claims of the journals and papers published were verified via simulation processes. This is because some experiments showed that this particular substance could increase the gain and directivity of the antenna and should this claim be verified, it would open more doors to future researches in University Technology of Malaysia.

1.4   The Scope of Research

The scope of this project is to design and simulate the a material with simultaneous negative permeability and permittivity or the so-called LH MTM and serves as the pioneer project in University of Technology Malaysia (UTM) regarding this new theory. It is also desired to integrate this material into the current existing antennas developed by previous scholars to enhance the characteristics of the antenna – especially the Return Loss and also the Gain and Directivity. As predicted by previous studies, all the 3 parameters were believed to have an improvement with integration of LH MTM into the antenna, particularly the microstrip antenna.

1.5   Objective of Research

According to some papers published in the media, this LH MTM would increase the gain of an antenna and a whole lot of room for discovery and development when the laws of physics we have come to accept since our childhood are bound to be reversed. Therefore, the paramount objectives of this research are:

- To investigate the antenna properties (Return Loss, Gain, Directivity, Half Power Beam Width, Cross Polar Isolation, etc.) of the antenna during the presence of LH MTM.

- To verify some all the claims such as the Double Negative Parameters (DNG Parameters), Negative Refractive Index (NRI) and Backward Wave Propagation stated in the books and papers through simulation processes.

- To understand the fundamentals of LH MTM that has been the hot issue in the arena of physics and microwave engineering.

1.5   Methodology

Firstly, a research on LH MTM was carried out to understand the fundamentals of the newly discovered substance relying on the books and papers from the IEEEXplore as the prime reference. Subsequently, the CST Microwave Studio was chosen as the ultimate software to simulate the structure as this software is desirable for a 3D platform in simulating a full wave simulation. After obtaining the S-parameters from the software, they were exported to MathCAD to calculate the effective values of

permittivity and permeability as well as the refractive index by utilizing the Nicolson-Ross-Weir (NRW) Approach. Eventually, the backward wave and the negative refractive index properties were also being investigated by simulating the E-field in the Left Handed frequency range in CST Microwave Studio.

1.6   Organisation of Thesis

This thesis starts with the brief history of LH MTM, the problem statement, the scope and objective of the research as well as the methodology in implementing this research in Chapter 1. Subsequently, it was written in such a way to provide an insight into the novelty of LH MTM and some of its basic concepts that reversed the laws and theories we were accustomed with in Chapter 2. Furthermore, a few applications of LH MTM in the microstrip technology were presented and discussed in the same chapter to portray the practicality of this new substance. At the same time, some different structures of LH MTM were also shown. After understanding some of the concept of LH MTM, the design of LH MTM using CST Microwave Studio and MathCAD was discussed in Chapter 3. For the sake of completeness, the equation design specifications of the square patch antenna were also presented in that particular chapter.

Subsequently, an experiment was done to design and simulate the LH MTM and this was shown in Chapter 4 where the simulation results were presented. The results included the Return Loss, Gain, Directivity, Half Power Beam Width and a comparison table were tabulated. Lastly, it was concluded in Chapter 5 that LH MTM could be used to enhance the current conventional microstrip antennas in terms of the gain and directivity. In addition, the list of references and appendices were listed at the end of this thesis.

CHAPTER 2

LITERATURE REVIEW

2.0   Introduction

Literature Review is one of the most crucial parts of a thesis. It gives the author or researcher the source of knowledge, idea and inspiration. In this thesis, the literature review is divided into a few main components where the basic theories would be discussed first followed by some applications of LH MTM to provide the insights to the usefulness of this peculiar material. Lastly, the whole chapter would be summarized in the summary of this chapter.

2.1   Double Negative (DNG) Properties

This state-of-the-art material has peculiar properties that one could not help mentioning especially the simultaneous negative value of μ and ε. As mentioned in the section 1.1, Prof JB Pendry was the first to realized the speculation of the Russian

Physicist and demonstrated the double negative properties of LH MTM through the simulation and theoretical assumptions made. As for the TW Structure, the negative-ε is obtained theoretically from the following formula:

$$\varepsilon_r(\omega) = 1 - \frac{\omega_{pe}^2}{\left(\omega^2 + \zeta^2\right)} + j\frac{\xi\omega_{pe}^2}{\omega(\omega^2 + \zeta^2)}$$

(2.1)

where

$$\omega_{pe} = \sqrt{\frac{2\pi c^2}{p^2 \ln(p/a)}}$$

ω_{pe} = electric plasma frequency, tunable to GHz range

c = speed of light, a = radius of the wire, p = average cell size « λ_g

$$\zeta = \frac{\varepsilon_0 (p\omega_{pe}/a)^2}{\pi\sigma} = \text{damping due to metal losses}$$

σ: conductivity of the metal

Therefore, it was obvious that

$$\text{Re}(\varepsilon_r) < 0 \text{ for } \omega^2 < (\omega_{pe}^2 - \zeta^2)$$

(2.2)

which reduces if ζ = 0 to

$$\varepsilon_r < 0 \text{ for } \omega < \omega_{pe}$$

(2.2a)

As for the positive negative-μ /positive-ε SRR Structure, the equation is given as below:

$$\mu_r = 1 - F\omega^2 \frac{(\omega^2 - \omega_{0m}^2)}{(\omega^2 - \omega_{0m}^2)^2 + (\omega\zeta)^2} + j\frac{F\omega^2\zeta}{(\omega^2 - \omega_{0m}^2)^2 + (\omega\zeta)^2}$$

(2.3)

where

$F = \pi(a/p)^2$, a = inner radius of the smaller ring

$$\omega_{0m} = c\sqrt{\frac{3pc^2}{\pi \ln(2w/\delta)a^3}}$$ = magnetic resonance frequency, tunable to GHz range

w = width of the rings

δ = radial spacing between the rings

$$\varsigma = \frac{2pR'}{a\mu_0}$$ = damping factor due to metal losses

R': metal resistance per unit length

From the experiments done, it appeared that

$$\mu_r < 0, \text{ for } \omega_{0m} < \omega < \frac{\omega_{0m}}{\sqrt{(1-F)}} = \omega_{pm \text{ (magnetic plasma frequency)}} \qquad (2.4)$$

From these assumptions made, it was obvious that a material with negative values of μ and ε could actually be fabricated for a certain band of frequency. However, it is important to note that when a LH MTM is produced, it would be a combination of these 2 structures and the coupling interactions would yield properties totally different from the superposition of the properties of each structure taken separately. Therefore, these formulas could only be served as a guide where the combined structure would act as a LH MTM.

In order to illustrate this point, some exemplary calculations were done with MathCAD on Figure 2.1(a) and (b) to acquire the graph of the effective parameters that are shown in Figure 2.2 and Figure 2.3. In the numerical simulation, the following values were assigned to the following parameters:

Thin Wire Structure   **Split Ring Resonator Structure**

p = 50 mm (period of the unit cells)   p = 50 mm (period of unit cells)

a = 20 mm (radius of the TW)   w = 1 mm (width of the ring)

δ = 0.1 mm (radial spacing between the ring)

a = 20 mm (inner radius of the SRR)
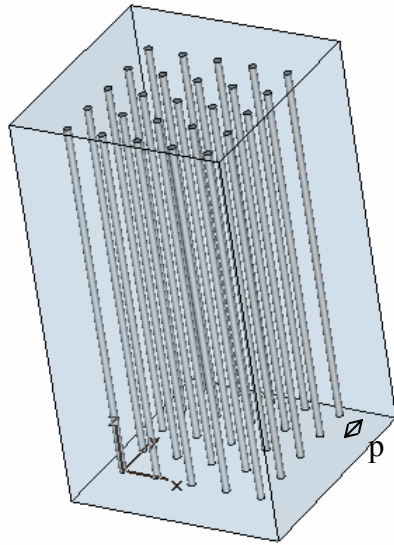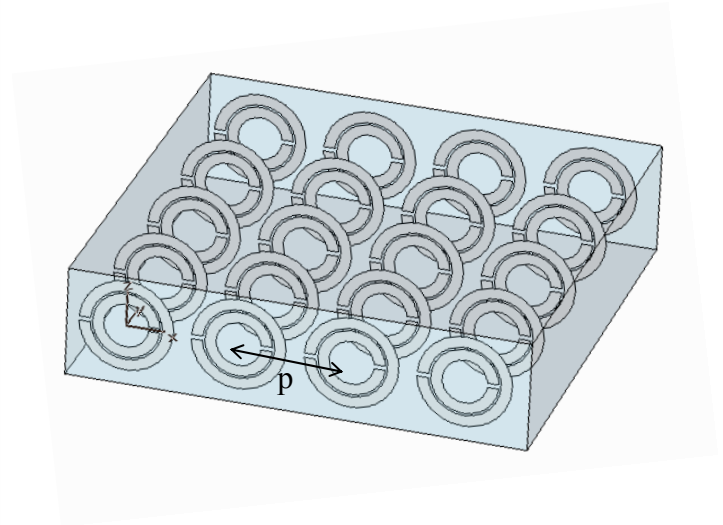
(a)   (b)

Figure 2.1: Diagrams acquired from CST Microwave Studio, (a) The TW Structure Design which gives the -ε_r (b) SRR Structure Design which produces the -μ_r
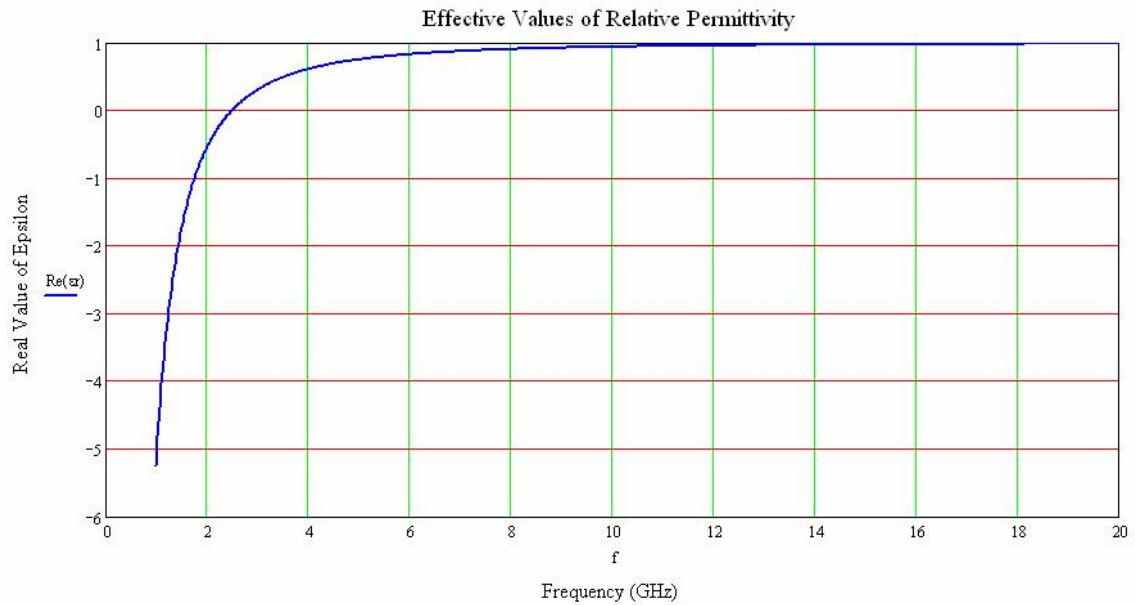
Figure 2.2: Effective values of Relative Permittivity calculated from MathCAD
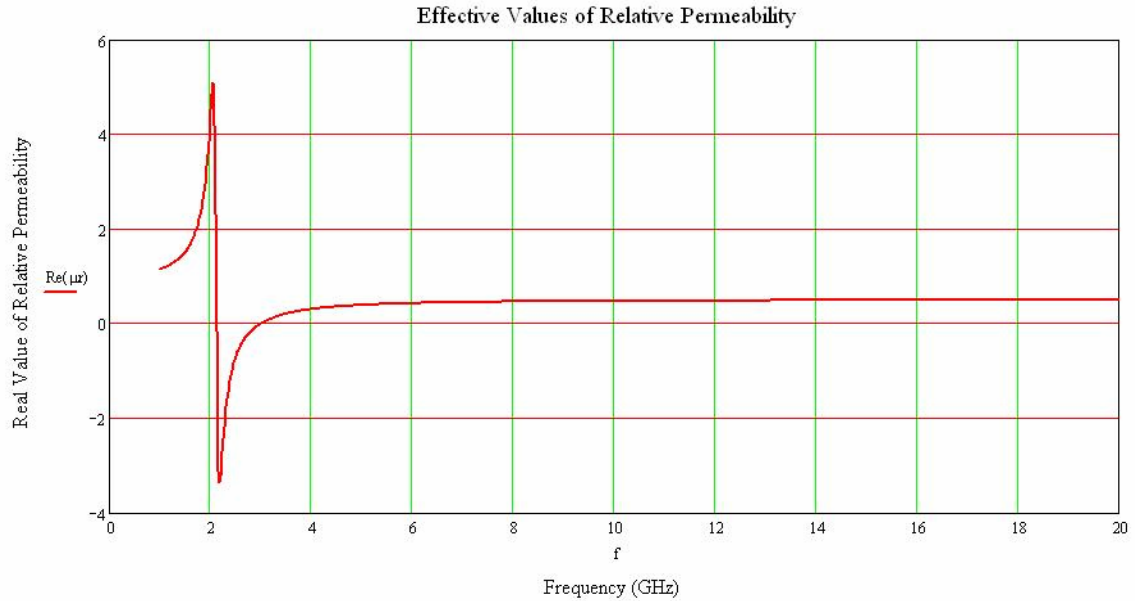
Figure 2.3: Effective values of Relative Permeability calculated from MathCAD

From the 2 graphs obtained, one could observe that the frequency range where LH MTM existed – where both effective parameters were simultaneously negative – was from 2.14 GHz to 2.482GHz. Therefore, from this example, there is a possibility that a LH MTM could be obtained if the 2 structures were superimposed. Figure 2.4 and 2.5 shows the practical implementation of the LH MTM which was done by Dr. Smith from Duke University.
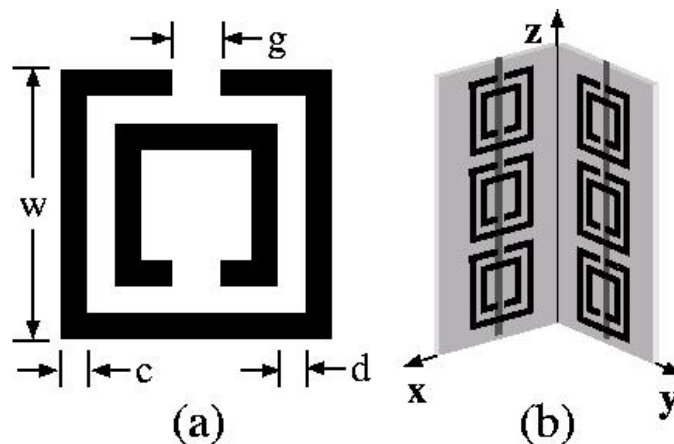
Figure 2.4: a) The model of LH MTM constructed by Dr. Smith from UCSD with his team which mimics the SRR structure. b) The prototype of the LH MTM after the combination of the SRR structure and the TW structure – bidimensional LH MTM [1]
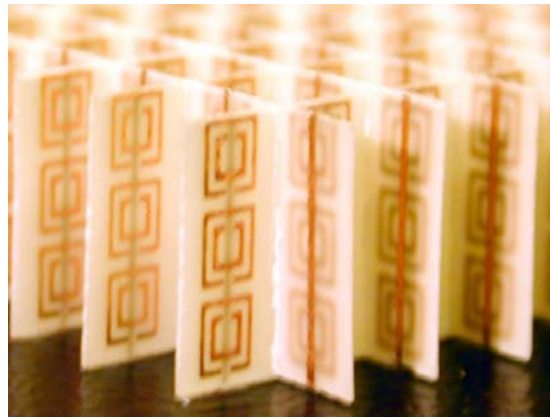
Figure 2.5: The prototype of LH MTM designed by Dr. Smith and this team. [1]

However, there are some papers [13, 14] suggested different approaches altogether when the 2 structures were superimposed. From [14], the author used the lossless transmission line model to predict the LH MTM region. By using the ABCD matrix of a two-port network representation of a lossless transmission line [15] as shown in equation 2.5,

$$\begin{pmatrix} A & B \\ C & D \end{pmatrix} = \begin{pmatrix} \cos(\beta l) & jZ_0\sin(\beta l) \\ jY_0\sin(\beta l) & \cos(\beta l) \end{pmatrix} \tag{2.5}$$

the effective parameters are extracted as follows:

$$\beta = \omega\sqrt{\varepsilon\mu} \tag{2.6}$$

$$Z_0 = \sqrt{\frac{\varepsilon}{\mu}} \tag{2.7}$$

Assuming that l/λ is small, the relative permeability can then be extracted from (2.5) and the matrix elements can then be extracted by calculating the expression

$$\frac{B}{A} = j\frac{Z_0\sin(\beta l)}{\cos(\beta l)} = jZ_0\tan(\beta l) \cong jZ_0\beta l \tag{2.8}$$

By combining (2.6), (2.7) and (2.8), one then obtains

$$\mu_r = \frac{B}{j\omega\mu_0 lA} \tag{2.9}$$

Similarly, the relative permittivity can be extracted by first calculating the expression

$$\frac{C}{A} = j\frac{Y_0 \sin(\beta l)}{\cos(\beta l)} = jY_0 \tan(\beta l) \cong jY_0 \beta l \tag{2.10}$$

By combining (2.6), (2.7) and (2.10), one then obtains

$$\varepsilon_r = \frac{C}{j\omega\varepsilon_0 lA} \tag{2.11}$$

Therefore, from equation (2.9) and (2.11), it is apparent that the negative parameters could be gained from the lossless transmission line formula. Eventually, this could be used as a guide of the resonant frequency as in lossy cases, the bandwidth of the resonant frequency would increase and decrease the amplitude of the parameters but would not shift the frequency to any point.

Since the above mentioned method used the ABCD Matrix and the calculations were performed based on a lossless transmission line, it would not really be an ideal model for the extraction of the said parameters. In order to get more accurate approximation, the modified NRW Approach were studied and applied in this project [13]. The NRW approach begins by introducing the composite terms

$$V_1 = S_{21} + S_{11} \tag{2.12}$$
$$V_2 = S_{21} - S_{11} \tag{2.13}$$

and deriving the following quantities:

$$X = \frac{1+V_1V_2}{V_1+V_2} = \frac{1+Z'^2}{2Z'} \tag{2.14a}$$

$$Y = \frac{1-V_1V_2}{V_1-V_2} = \frac{1+\Gamma^2}{2\Gamma} \tag{2.14b}$$

where $\acute{Z}$ = transmission term, Γ = reflection coefficient

Consequently, equation (2.15) and (2.16) are obtained.

$$Z' = X \pm \sqrt{(X^2-1)} \tag{2.15}$$

$$\Gamma = Y \pm \sqrt{(Y^2-1)} \tag{2.16}$$

From (2.15) and (2.16), the signs have to be chosen properly to maintain the value of $|\acute{Z}| \leq 1$ and $|\Gamma| \leq 1$. However, this had been proven to be unreliable as the values of S_{11} and S_{21} are highly frequency dependent and achieve values near zero and unity. Besides, the results were unsatisfactory from numerous tests done in [13] particularly in the frequency regions where the permittivity and permeability resonances were expected. Therefore, a few more derivations were done from (2.15) and (2.16) and obtained

$$Z' = \frac{V_1-\Gamma}{1-\Gamma V_1} \tag{2.17}$$

$$\Gamma = \frac{Z'-V_2}{1-Z'V_2} \tag{2.18}$$

From (2.17) and (2.18), one could acquire

$$1 - Z' = \frac{(1-V_1)(1+\Gamma)}{(1-\Gamma V_1)} \tag{2.19}$$

$$\eta = \frac{1+\Gamma}{1-\Gamma} = \frac{(1+Z')(1-V_2)}{(1-Z')(1+V_2)} \tag{2.20}$$

where η = normalized wave impedence, d = thickness of the slab (LH MTM)

Assuming that the electrical thickness of the MTM slab is not too large, i.e., $k_{real}d < 1$
and knowing that the complex wavenumber k = $\omega\sqrt{\frac{\varepsilon_r \mu_r}{c}}$ = $k_0 \sqrt{\varepsilon_r \mu_r}$, Z' ≈ 1 – jkd to
obtain the approximate results for the wave impedence and permeability

$$k \approx \frac{(1-V_1)(1+\Gamma)}{jd(1+V_2)} \tag{2.21}$$

$$\mu_r \approx \frac{2(1-V_2)}{jk_0 d(1+V_2)} \tag{2.22}$$

Furthermore, it was found that when $k_{real}d < 1$,

$$S_{11} \approx \frac{2jkd(\eta^2 - 1)}{(\eta+1)^2 - (\eta-1)^2} = \frac{2jkd(\eta^2 - 1)}{4\eta} \tag{2.23}$$

$$\varepsilon_r = \mu_r + j\frac{2S_{11}d}{k_0} \tag{2.24}$$

As a result, equation (2.22) and (2.24) were used to determine the negative parameters.

2.2 Negative Refractive Index (NRI)

Due to its peculiarity in its DNG values, where the ε and μ are both negative, many other properties of this material are altered altogether. The most obvious alteration is the refractive index where it takes on a negative value as given by the formula

$$n = \pm\sqrt{\varepsilon\mu} \qquad (2.25)$$

Theoretically, this is due to the fact that n is a real negative number whenever the materials are classified in Group III in Figure 1.1 and through experiments, it was also shown that the wave that propagates through the LH MTM bends the 'wrong' way as shown in Figure 2.6.
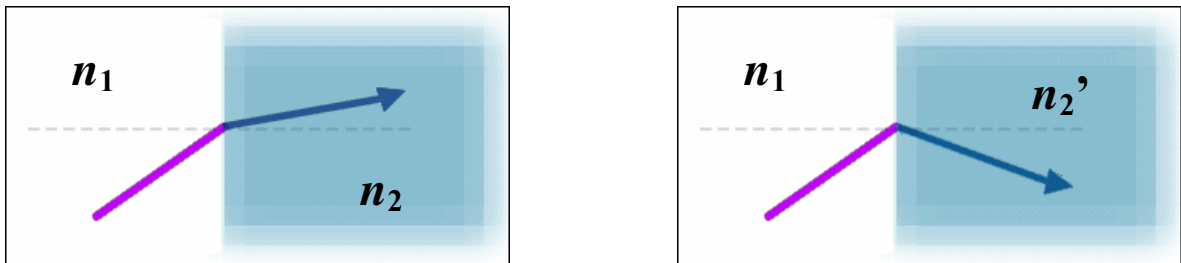
Figure 2.6: (a) The refracted ray in a RH Medium, (b) The refracted ray in a LH Medium

In Figure 2.6(b), the refractive index of $n_2' = - n_2$ and it is evident that the ray is refracted to the opposite side compared to the ray propagating in RH Medium. In addition, even though the ray bends the opposite direction, the Snell's Law is still satisfied when a negative value of n is substituted into the equation,

$$n_1 \sin \theta_1 = n_2 \sin \theta_2 \qquad (2.26)$$

and $\theta_2 < 0$ is obtained. Therefore, it is also proven in equation 2.26 that $-\theta_2$ would produce a refracted ray in the opposite direction. In terms of simulations done in the past [7], it could be shown in Figure 2.7.
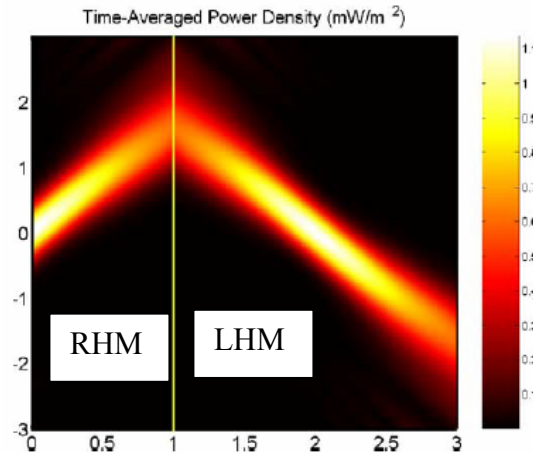
Figure 2.7: The negative refractive index obtained from experiment [7]

Due to its negative refractive index, it is apparent that rays propagating through a LH MTM slab would be focused internally and a refocus point would be created as the ray leaves the slab. This could be shown in Figure 2.8 and if we were to translate this idea into the microwave engineering, we would be able to enhance the directivity and gain of a particular antenna [8]. From the simulation results, it is evident that the wave radiated from the circular patch antenna could be focused inside the LH MTM and further increase the directivity of the antenna. In other words, the beam width of the wave was decreased and an increase in gain was observed.

RH　　　**LH**　　　**RH**
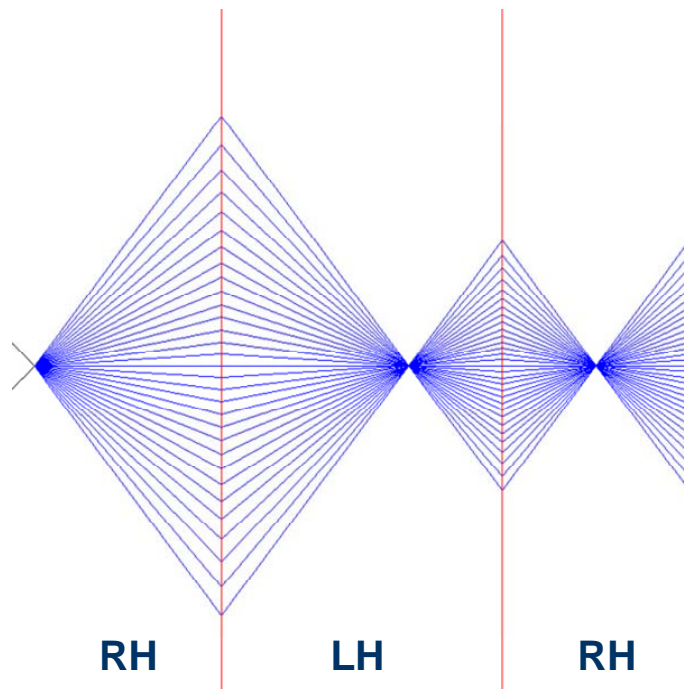
Figure 2.8: The refocused ray when entering and exiting the LH MTM Slab

2.3 Backward Wave Propagation

On the other hand, the subsequent peculiar characteristic of this material is the Backward Wave (BW) propagation.
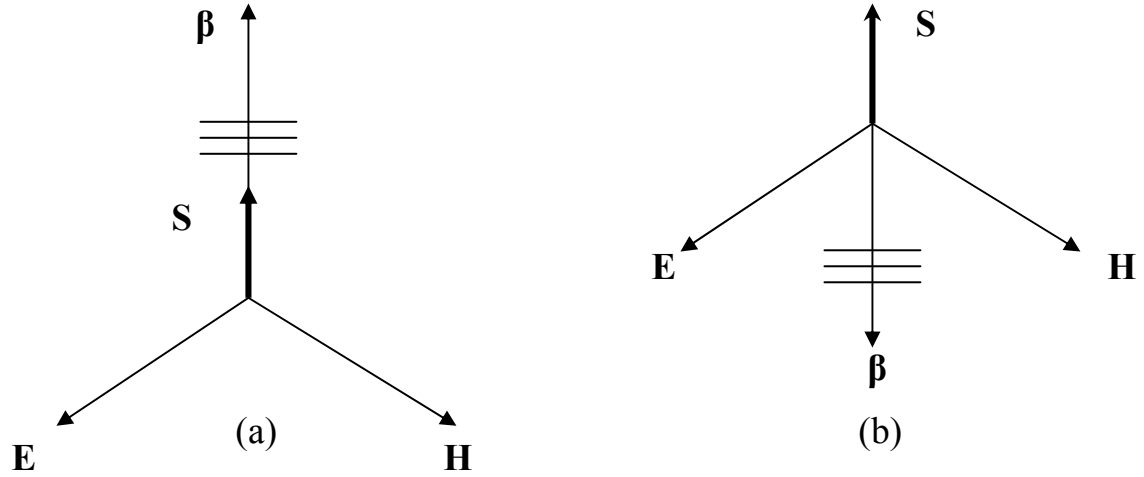
Figure 2.9: Electric field-magnetic field-wave vector triad (**E**, **H**, **β**) and the Poynting vector **S** for an electromagnetic wave. (a) conventional Right-handed (RH) medium, (b) Left-handed (LH) medium

From the Maxwell Equations and considering a lossless medium in region without sources (**M**s = **J**s = 0), we could obtain the following equation:

$$\boldsymbol{\beta} \times \mathbf{E} = +\omega|\mu|\mathbf{H,}$$
(2.27a)
$$\boldsymbol{\beta} \times \mathbf{H} = -\omega|\varepsilon|\mathbf{E}$$
(2.27b)

which built the familiar RH triad (**E**, **H**, **β**) shown in Figure 3 (a). Besides, when the values of μ and ε < 0, since |μ| > 0 and |ε| > 0,

$$\boldsymbol{\beta} \times \mathbf{E} = -\omega|\mu|\mathbf{H,}$$
(2.28a)
$$\boldsymbol{\beta} \times \mathbf{H} = +\omega|\varepsilon|\mathbf{E}$$
(2.28b)

which built the LH triad (**E**, **H**, **β**) shown in Figure 3 (b). Furthermore, we could observe the opposite direction of the **β** and therefore, we could conclude that the value of β is

negative. At the same time, the phase velocity which is described by the following equation,

$$v_p = \frac{\omega}{\beta}$$ (2.29)

would eventually acquire the negative value from β as the frequency always employs the positive value.

Besides, the Poynting vector **S** which is defined as,

$$\mathbf{S} = \mathbf{E} \times \mathbf{H}^*$$ (2.30)

is associated to the power flow P_0 and therefore, oriented towards the direction of the propagation of energy over time. Subsequently, **S** is parallel to the group velocity (velocity of a modulated signal in a distortionless medium),

$$v_g = \nabla_\beta \omega$$ (2.31)

In a nutshell, from figure 3 and all the equations derived, we could summarize that (considering positive direction of the power flow),

RH Medium: $v_p > 0$ ($\beta > 0$) and $v_g > 0$

(2.32a)

LH Medium: $v_p < 0$ ($\beta < 0$) and $v_g > 0$

(2.32b)

and this exhibits the antiparallel characteristic of LH MTM.

In terms of simulations and experiments done in the past, there were numbers of them which studied the backward wave propagation in periodic waveguide structures [9, 10, 11]. Taking [11] as an example, they had successfully fabricated the SRR and TW Structures and tested the propagation of the wave in the waveguides with one inclusion of the structures at one time. From the 2 experiments done separately, it was discovered

that the propagation of backward waves below the cutoff frequency was a pattern of H Field (when only the SRR structure was included) or E Field (when only the TW Structure was included). Upon verifying the backward wave propagation of the single inclusion, they numerically tested the inclusion of both structures (LH MTM) with a commercial FEM Simulator (HFSS) and proved that the wave in the LH MTM region propagated in an opposite way with the energy flow.

Until this point of discussion, one may ask how we determine the propagation of a backward wave. Besides observing the propagation of E Field and H Field from any 3D Simulator (CST Microwave Studio), one may also investigate the unwrapped phase of S_{21} [9]. It was mentioned that just below the LH MTM operating frequency region, the unwrapped phase of S_{21} increases with frequency which is caused by a negative value of the group delay of the LH MTM. In other words, when the increase in the unwrapped phase is observed, there is a clue that backward wave propagation may be in progress.

2.4   LH MTM Applications in Microstrip Technology

Up to press time, this special material is still under a lot of research works and numerous applications are discovered as time goes by both in the optical and microwave domain. Since the scope of this project does not extend beyond the microwave domain, it is only wise to study the applications in Microstrip Technology. Subsequently, the application of LH MTM in enhanced gain microstrip antenna, filtering unwanted signals and the broad bandwidth, miniaturized cells would be discussed.

2.4.1 Enhancement of Gain and Directivity of the Circular Patch Antenna [8]
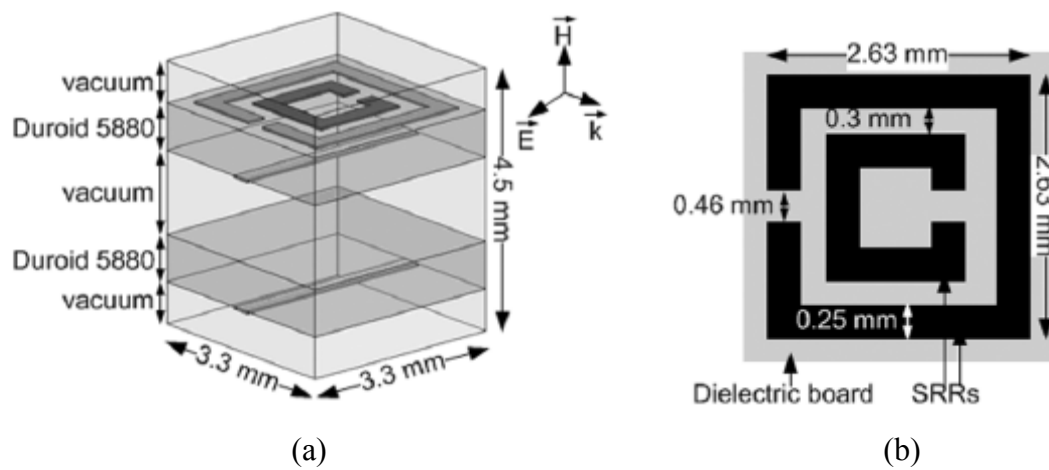

Figure 2.10: (a) Unit cell of the LHM consisting of SRRs and electrical wires. (b) Dimensions of the SRR.
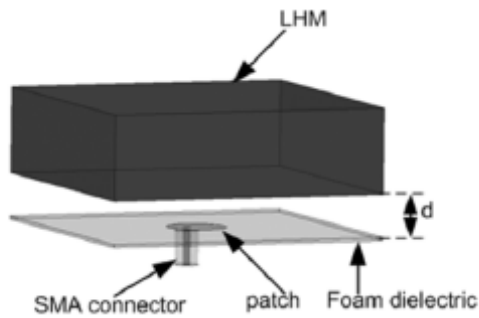

Figure 2.11: Experimental setup of the integration of LH MTM with the circular patch antenna

Although this investigation [8] was only done theoretical, the results obtained from the simulation were very convincing and encouraging. The construction of the LH

MTM is shown in Figure 2.10 which represented the unit cell of LH MTM and the simulation was done on the setup depicted in Figure 2.11. The distance between the LH MTM slab and the circular patch antenna, d must be half of the thickness of the LH MTM slab and in this case, it was set to 5.5 mm with the thickness of slab equals to 11 mm. This optimum value used in this paper was to ensure a focusing effect was achieved.

In this paper, first of all, the LH frequency were tested under the waveguide setup as would be explained in more detail in section 2.4.3 and using the following equations obtained from [18] and [19],

$$Z = \pm \sqrt{\frac{(1+r)^2 - t^2 e^{2jkd}}{(1-r)^2 - t^2 e^{2jkd}}} \qquad (2.33)$$

$$\cos(nkd) = X = \frac{e^{-jkd}}{2t}(1 - r^2 + t^2 e^{2jkd}) \qquad (2.34)$$
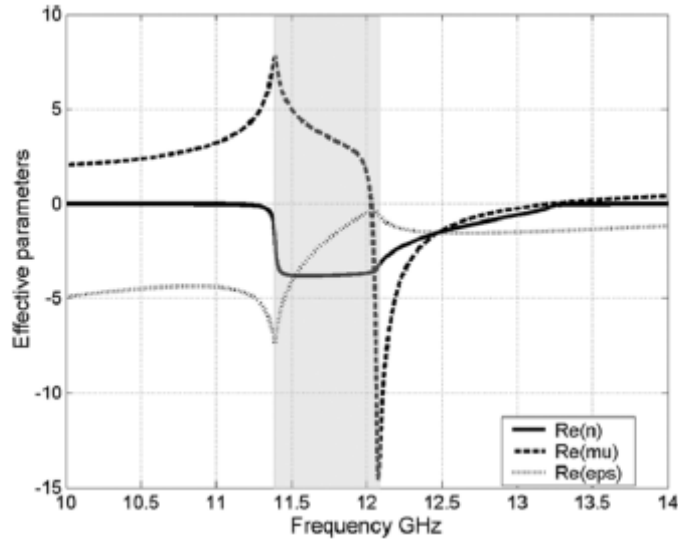
Figure 2.12: Extraction of the real effective values of Permittivity, Permeability and Refractive Index

From Figure 2.12, it could be observed that LH MTM region lies in the 12.25 – 13.3 GHz range. Since the effective ε and μ are equal to -1.55 around 12.4GHz, this

frequency was chosen as the choice of resonant frequency for the circular patch antenna. The S_{11} parameter of the antenna designed is shown in Figure 2.13(a). Subsequently, with the integration of LH MTM, the S_{11} parameter obtained was slightly different due to the frequency-varying effective parameters of the LH MTM. However, what was paramount was the greater dip of the S_{11} parameter to almost -30 dB compared to -23.5 dB previously.
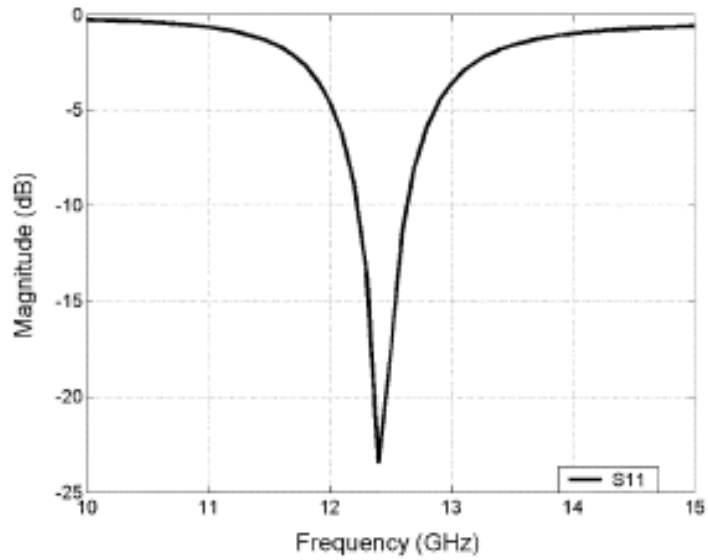
(a)
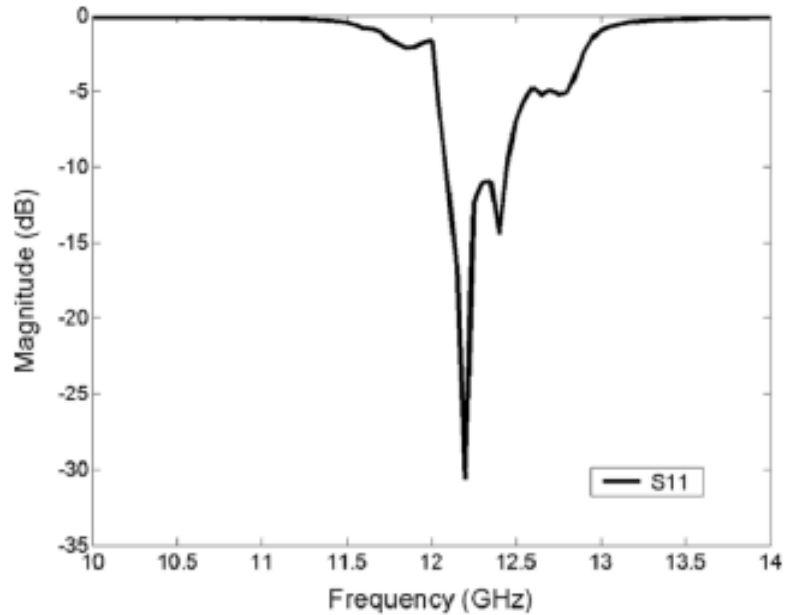
(b)

Figure 2.13: S_{11} Parameter of the (a) circular patch antenna constructed at a resonant frequency of 12.4GHz and (b) antenna with LH MTM

Besides looking at the S_{11} parameter, the radiation pattern of the antenna with and without the LH MTM was also taken to measure the gain and directivity. From Figure 2.14 and Figure 2.15, it was seen that the maximum power received for the H-Field and E-Field increased approximately 3 dB and 2 dB respectively.

(a)
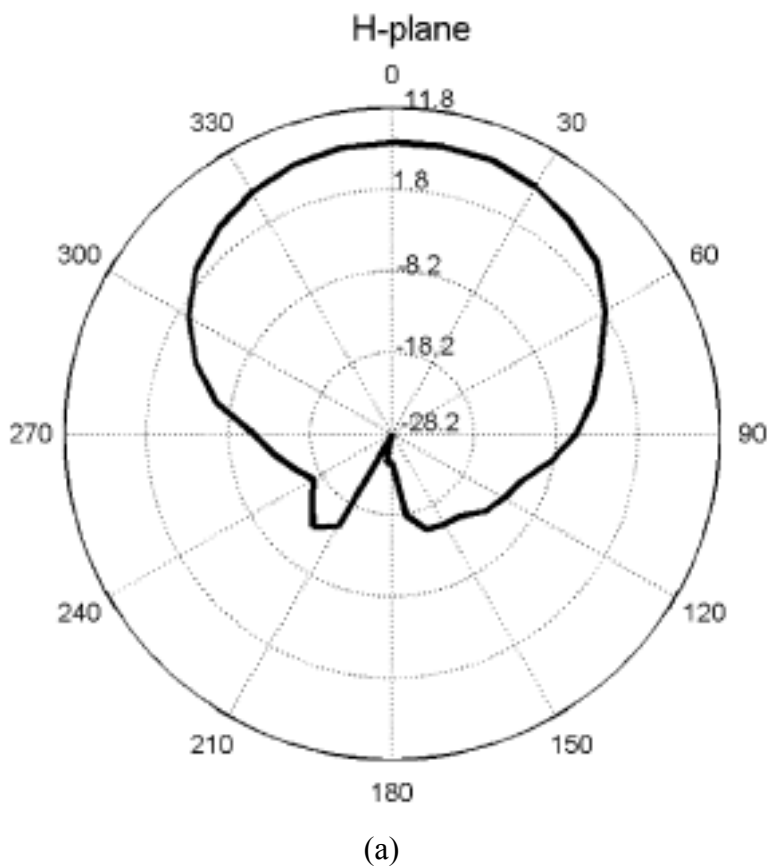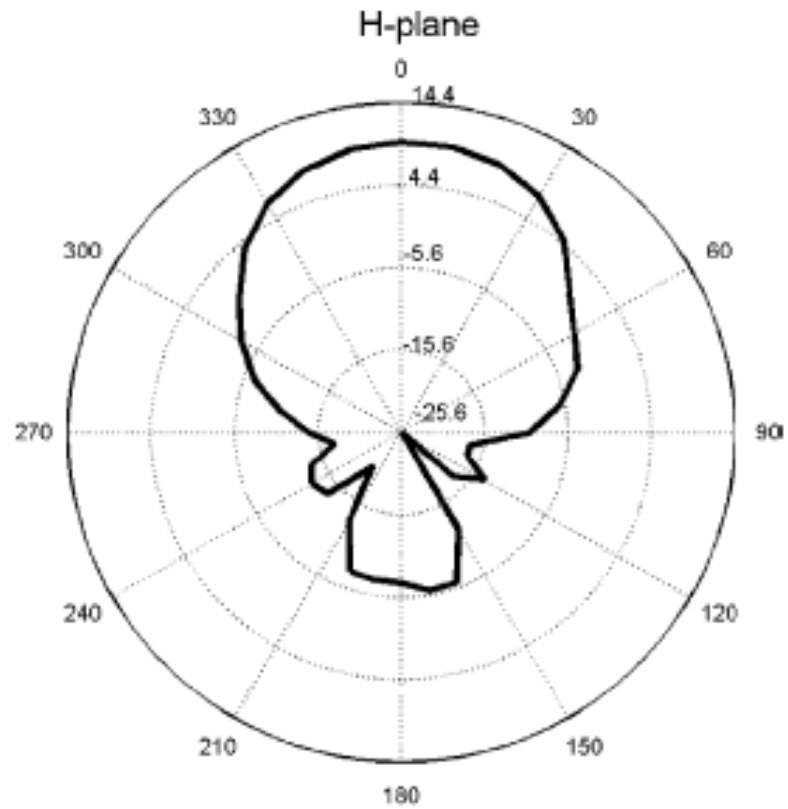
(b)

Figure 2.14: H-Plane of circular patch antenna (a) Without LH MTM and (b) With LH MTM Slab

E-plane

(a)

E-plane

(b)
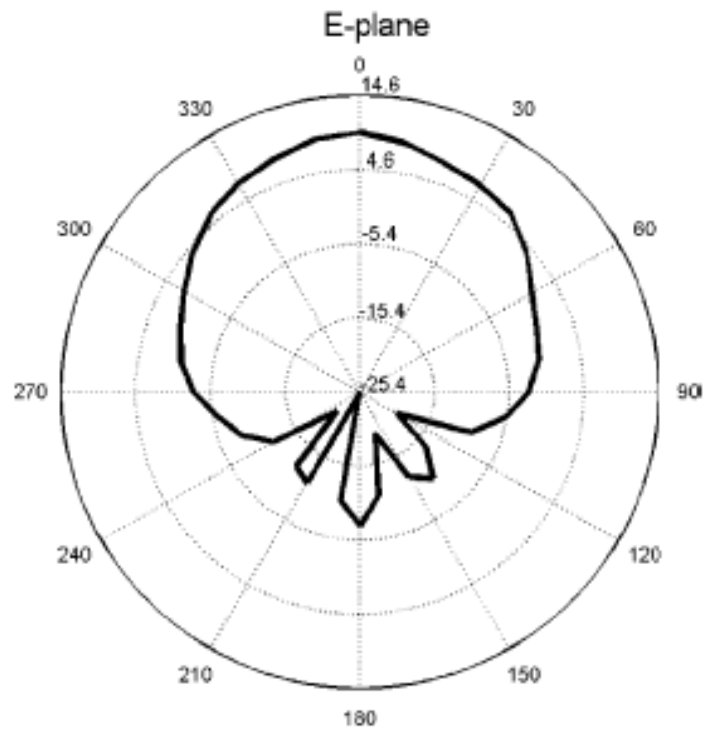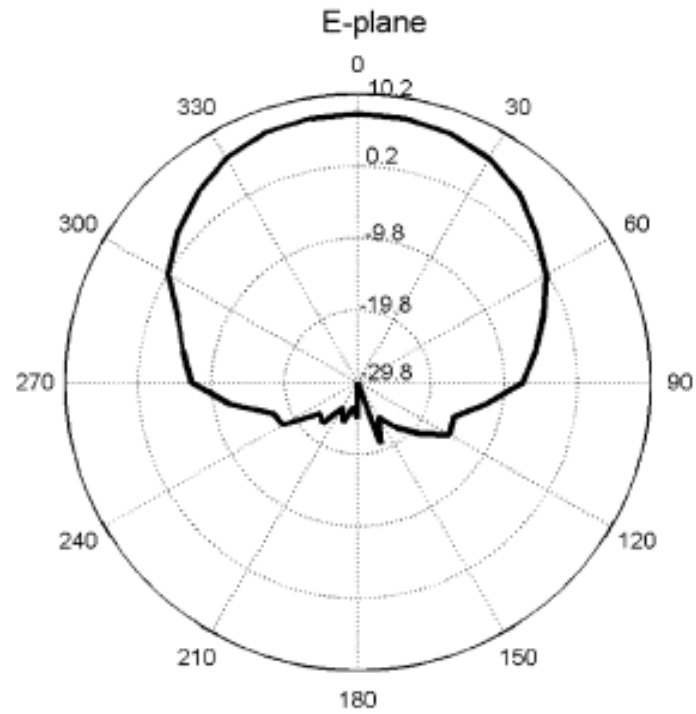
Figure 2.15: E-Plane of the circular patch antenna (a) Without LH MTM Slab and (b) With LH MTM Slab

Subsequently, the E Field of the patch antenna was simulated (Figure 2.16(a)) and that was set as the reference point of the radiation pattern. Lastly, by placing the LH MTM on top of the patch antenna, the E Field was once again simulated and the results observed (Figure 2.16(b)) clearly suggested that the LH MTM could focus the propagation of waves and in turn increase the directivity and the gain of the patch antenna.
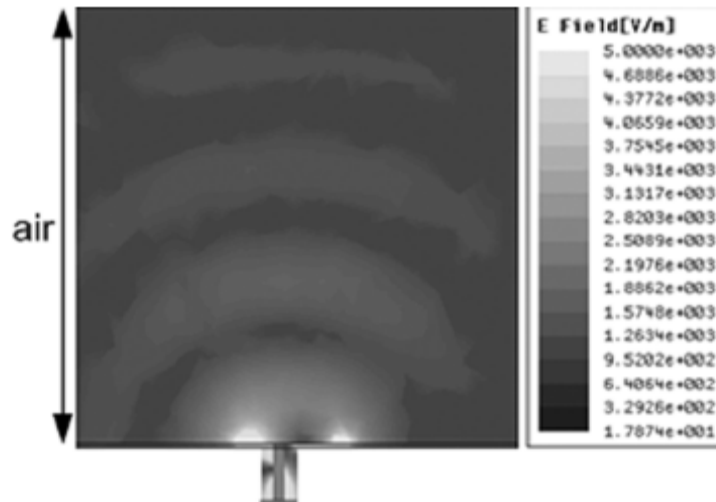
(a)
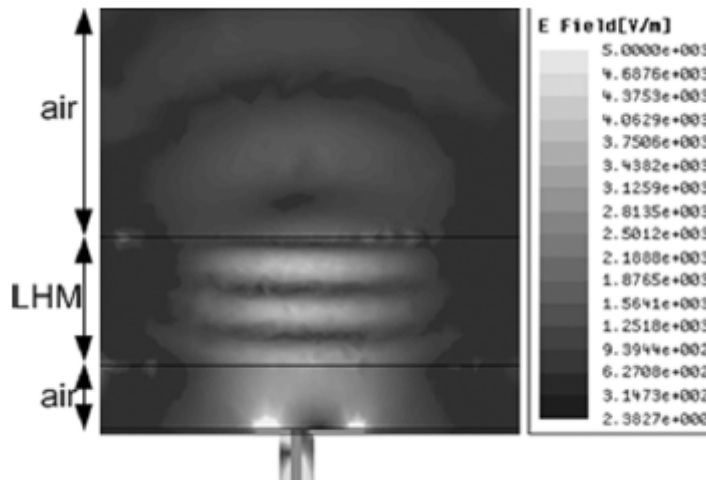
(b)

Figure 2.16: Simulated E-Field Magnitude (a) Without LH MTM Slab and (b) With LH MTM Slab

As a conclusion, an improvement of gain by 2.8 dB was achieved and a more directional antenna was obtained when the LHM was placed on top of the antenna. In the case of lower losses and better wave impedence matching, a gain of 12 dB could be achieved. On the other hand, a more directional antenna was obtained even without the use of an array of several elements.

2.4.2   LH MTM for Filter Applications [6]

(a)   (b)
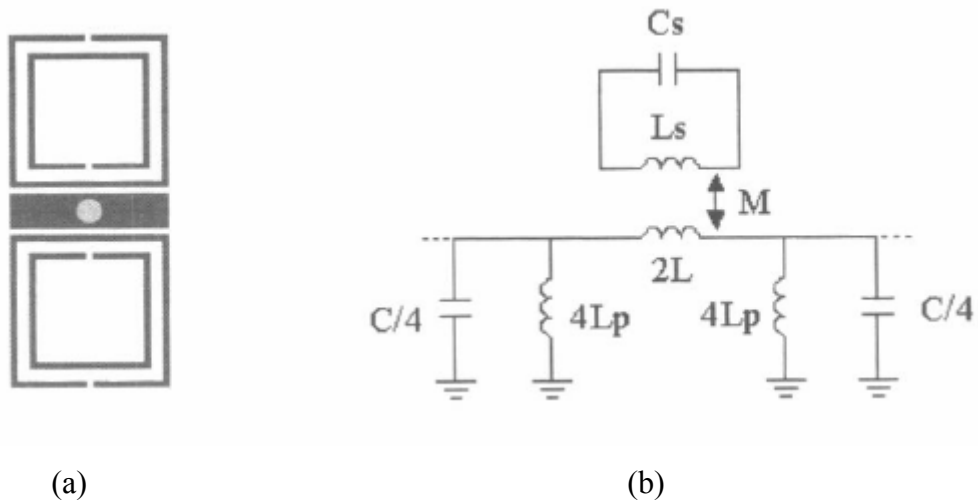
Figure 2.17: (a) Basic cell of the LHM microstrip line (upper side) and (b) equivalent circuit model (due to symmetry, the magnetic wall concept has been used).
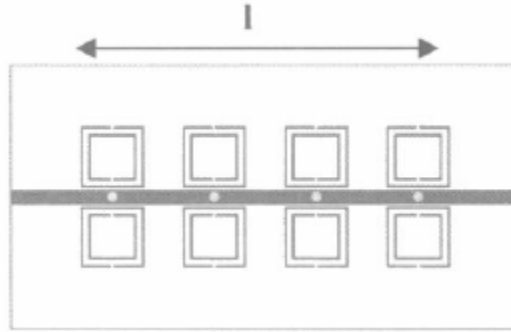
Figure 2.18: Layout of fabricated LH MTM Microstrip Line

Due to high selectivity of SRR Structures, LH MTM was desired to be constructed as filters. As proven in [6], the SRR Structures were loaded periodically and etched in close proximity to the conductor strip and via holes (Figure 2.18). As discussed earlier, these SRR provided negative permeability characteristic to the medium in a narrow band above their resonant frequency while the vias act as shunt connected inductors or more popular known as the TW Structure, which exhibit the negative permittivity property.

From the dispersion relation, it was previously demonstrated [20] that a periodic structure described by the elemental cell of Figure 2.17(b) supports backward waves in a narrow band above the resonant frequency of the coupled tank. Actually, the structure is transparent (i.e. backward waves are allowed) in the interval delimited by the frequencies given by:

$$f_L = \frac{1}{2\pi} \sqrt{\frac{1}{C'_x (2L + 8L_p)} + \frac{1}{L'_s C'_s}}$$ (2.35)

$$f_H = \frac{1}{2\pi} \sqrt{\frac{1}{2C'_s L} + \frac{1}{L'_s C'_s}}$$ (2.36)

with $C'_s = L_s/(M^2\omega_0^2)$, $L'_s = C'_s M^2\omega_0^2$ and $\omega_0^2 = 1/(L_s/C_s) = 1/(L'_s C'_s)$. As long as f_L is close to $f_0 = \omega_0/2\pi$ where a transmission zero is present, the structure exhibits a backward band pass behavior with a sharp cutoff in the lower band edge. At the limits of the propagation region, the phase, Φ, and Bloch impedance, Z_B, take its extreme values. Thus, at f_L, $\Phi = \pi$ and $Z_B =$, whilst at f_H, $\Phi = 0$ and $Z_B = 0\Omega$.

Through the simulation done, the result of S_{21} was obtained and shown in Figure 2.19. There were actually 2 types of simulations done where Figure 2.19(a) shows the simulation done by full wave electromagnetic simulation while Figure 2.19(b) shows the circuit simulation on the equivalent circuit model. It was apparent that the simulated results acquired proved the selectiveness of the microstrip line where the transmission of signal was only efficient around 3GHz with approximately 4% fractional bandwidth. Subsequently, after the fabrication and measurement were obtained, the graph of S_{21} and S_{11} were plotted as in Figure 2.20 which correlated very well with the simulated results.
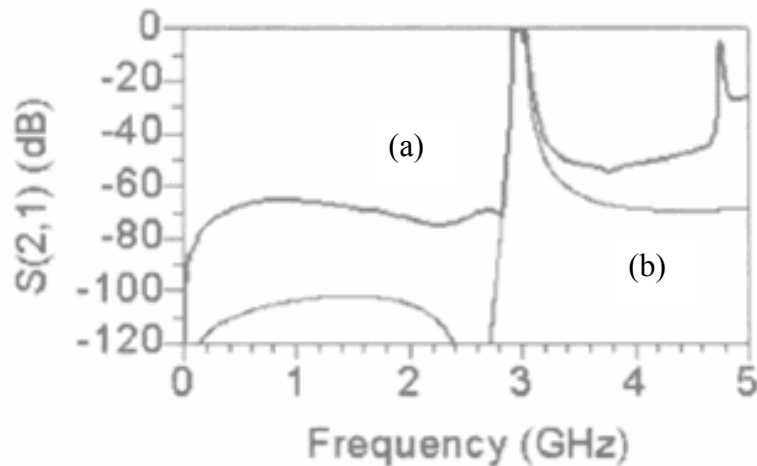
Figure 2.19: (a) frequency response obtained by full wave electromagnetic simulationand compared to (b) that obtained from circuit simulation on the equivalent circuit model. The estimated parameters for the equivalent circuit model are $L_x = 2.68$ nH, $C_s = 1.05$ pF, $M = 1.15$ nH, $L=1.01$ nH, $C=0.4l$ pF, $L_P = 0.22$ nH. For SRRs, $c = 0.2$ mm, $d=0.4$ mm, $I_L = I_0 = 5$ mm.
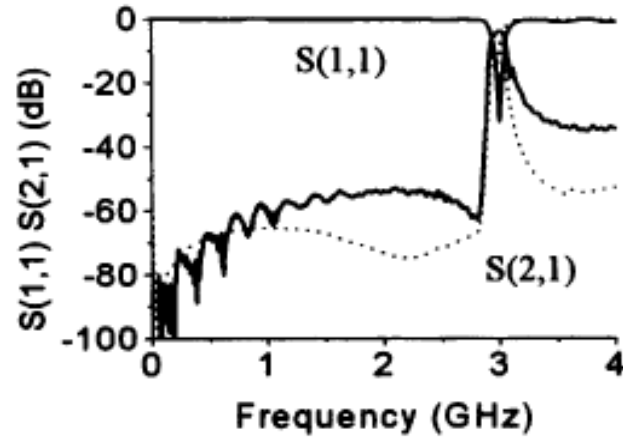
Figure 2.20: Measured (solid lines) and simulated (with losses included) (dashed lines) Insertion and Return Losses for the fabricated prototype device.

In a nutshell, this experiment has proven that LH MTM could also be used to construct filters due to its high selectivity characteristic.

2.4.3   Broadband and Miniaturized LH MTM Cell [12]

(a)   (b)
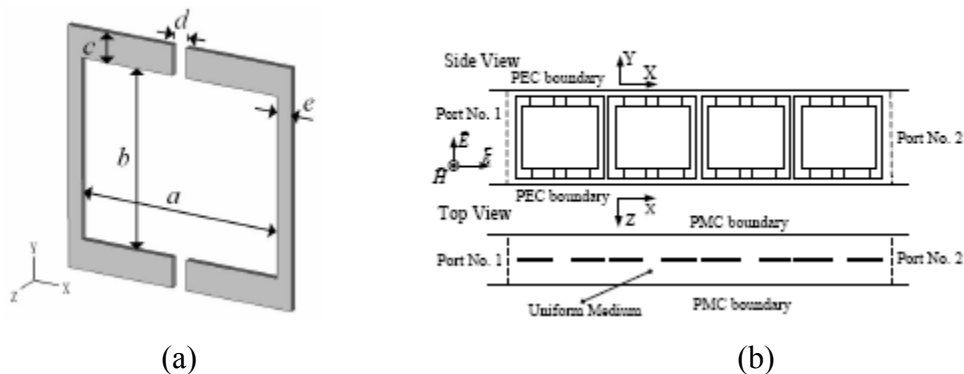
Figure 2.21: (a) The Unit Cell and (b) Simulation Model of LHM Slab

Although the high selectivity property of the LH MTM could be utilized to fabricate filters, it would not be able to prove its worth in other application due to its narrow band of its LH region. Therefore, this experiment [12] had been done to increase the LH region as well as miniaturizing the unit cell of the LH MTM.

The setup of the C Band planar LH MTM and the orientation of the materials in the waveguide are illustrated in Figure 2.21(a) and (b) respectively. From the simulations done in CST Microwave Studio, a broadband LH region was obtained (Figure 2.22) from approximately 4.2GHz – 7.5GHz. In addition, the negative parameters of permeability and permittivity were obtained based on the Nicolson-Ross-Weir (NRW) Approach (Equation 2.12 – 2.20) and the results were plotted in Figure 2.23. The calculations were done using Matlab to obtain the graphs.

With this experiment, it was proven that a broadband LH MTM could be fabricated but some consideration needs to be taken when realizing the structure in Figure 2.10 as it was assumed that the materials were as if embedded in a waveguide. Besides, the NRW Approach was found to have difficulties with LH MTM cases when in the region where the resonant and resulting LH region was thought to occur [13].
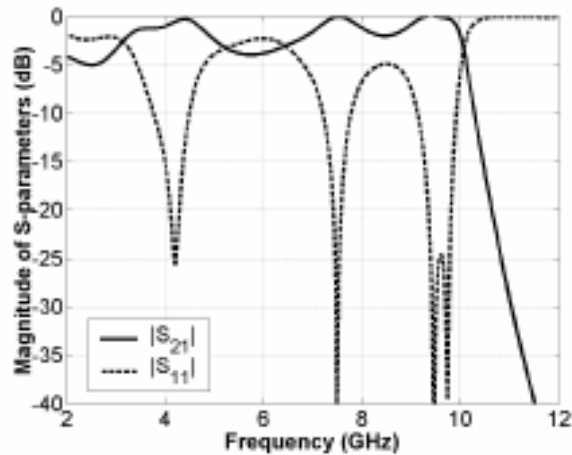
Figure 2.22: S-Parameter Magnitude

(a)   (b)
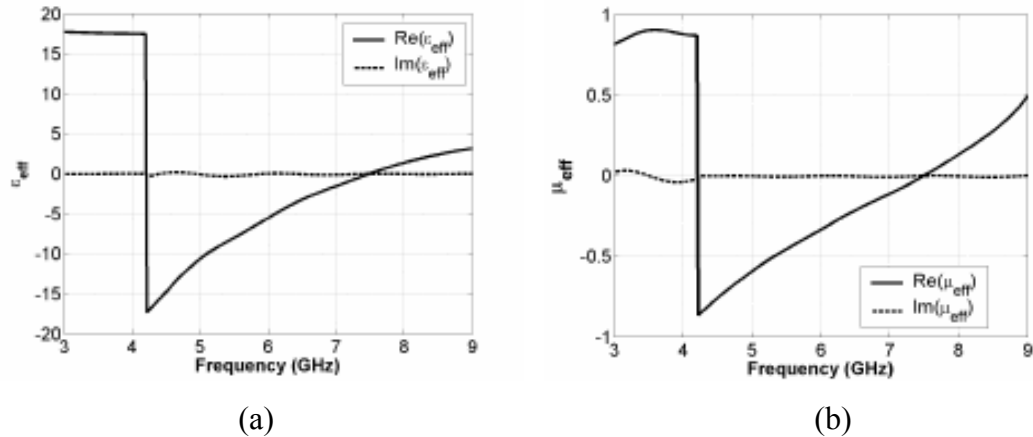
Figure 2.23: The Effective Parameters (a) The effective permittivity values and (b) The effective permeability values

From this experiment done, besides obtaining a wide bandwidth of approximately 3.3GHz or 56.4%, the miniaturization of the cell was also successful by having a unit electrical cell size of 0.067. From this paper and the discussions with the author, the design of LH MTM using the CST Microwave Studio and the method to calculate the effective DNG Parameters were determined.

2.4.4 Compact Size Highly Directive Antennas based on the SSR Metamaterial Medium [21]

As the name implied, this experiment was realized by the utilization of Split Ring Resonator (SRR) structure to create highly directive antenna compared to the photonic crystal. This experiment was done by using 2 monopole antennas obtained by removing the dielectric cladding and the metal shield of a microwave coaxial cable, one transmitting and the other receiving, to transfer signal via an SRR structure. These antennas had a length of 7cm, which were optimized for operation around 4GHz. Subsequently, the transmission coefficients of the single SRR structure were measured

by an HP-8510C network analyzer and the E-Field distribution simulated are shown in Figure 2.24 and 2.25 respectively. From the results obtained (Figure 2.24), it was clear that the SRR structure was a resonant magnetic dipole because at the resonance frequency, solenoidal currents flowed along the SRR structure as illustrated in Figure 2.25. Moreover, the SRR structure had localized the incident E-Field within its close vicinity. In other words, E-Field was concentrated in the gaps of the SRR structure. Therefore, it was clear that by arranging them in regular pattern, the resulting SRR structure could be regarded as an array antenna.

On the other hand, for comparison purposes, the experiment was also done to the closed SRR structure, which had two complete rings. The transmission data for a single-SRR structure showed a strong dip around 3.65 GHz and this dip was not observed in the transmission spectrum of the closed SRR structure. As a result, we could conclude that the SRR structure is indeed the suitable one to achieve the resonant magnetic dipole characteristics.
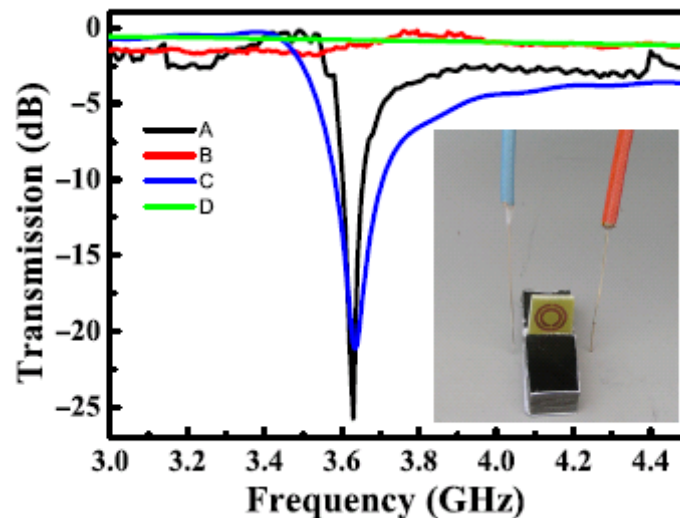
Figure 2.24: The experiment set up and the frequency response. Measured transmission spectrum of (A) SRR structure and (B) closed SRR structure[1]. Simulated transmission spectrum of (C) SRR structure and (D) closed SRR structure.

---

[1] This is so when the rings are constructed without the gap. In other words, the rings are completely round without any cuts.
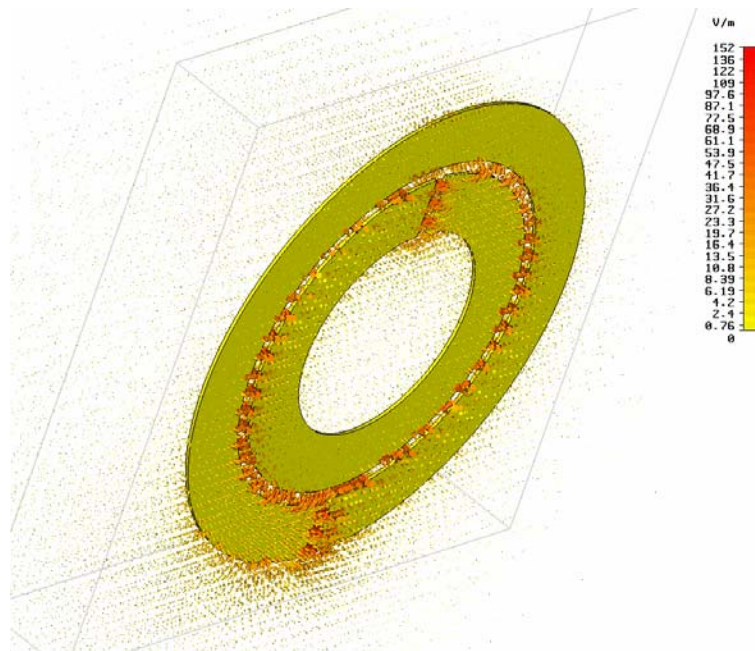
Figure 2.25: Simulated electric-field distribution within the unit cell of SRR metamaterial medium

Subsequently, the research was extended to a collection of the SRR structures by duplicating the same structure as shown in the Figure 2.26.
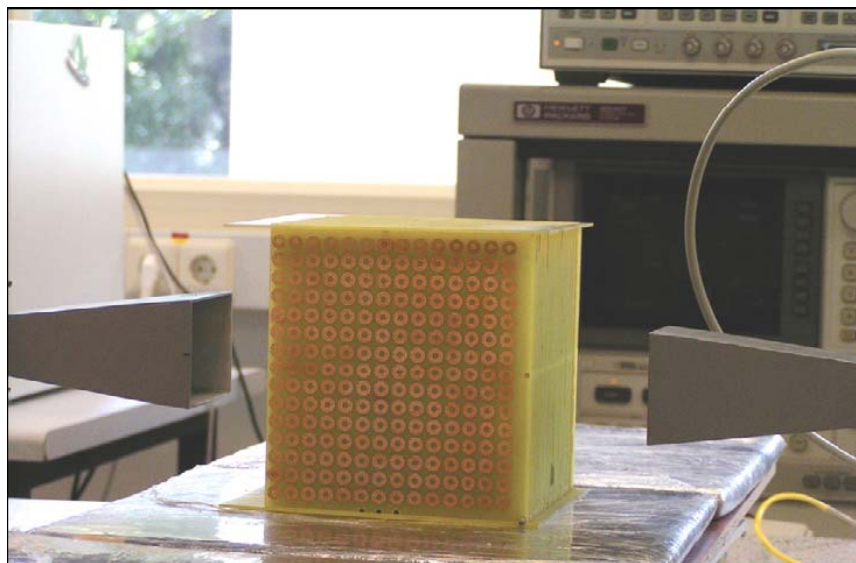
Figure 2.26: Experiment set up of the SRR structure.
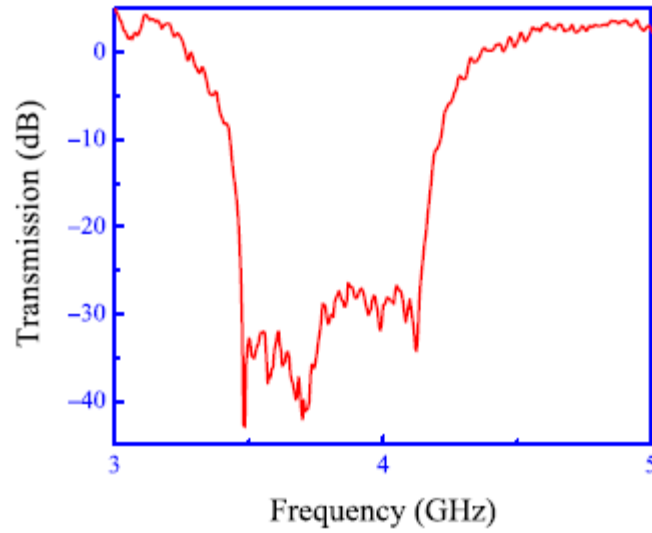
Figure 2.27: Transmission spectrum of electromagnetic waves through the SRR metamaterial medium

As expected from an array of SRR structure, the dip in the transmission spectrum was observed as in Figure 2.27. Apparently, the bandwidth of the transmission spectrum had increased dramatically. This actually showed that the SRR structure promotes the band gap at the frequency range of 3.4 GHz to 4.3 GHz and it could also be summarized that the array of SRR structure were acting as a resonant magnetic dipole at that particular frequency range.

Lastly, the Far-field radiation was done via measurements where a monopole antenna were placed inside the array of SRR structure and a horn antenna were used to transmit the signal. The results of the measurement are shown in Figure 2.28 for the SRR structure and Figure 2.29 for the closed SRR structure. Ignoring the Far-field radiation pattern in the E-plane, because no TW structure were present and nothing were expected from the E-plane, the Far-field radiation pattern in the H-plane were seen to be more directional as in Figure 2.28(a) compared to the measurement taken at an-off resonance frequency in Figure 2.28(b). As a mean of comparing the closed and normal SRR structure, results in Figure 2.29 were obtained and no sign of a directed signal was observed in the Far-field radiation pattern in both the E-plane and H-plane.

Figure 2.28: Far-field radiation pattern in the H-Plane (lines) and E-Plane (dotted) (a) near the resonance frequency of SRR structure and (b) at an off-resonance frequency for SRR structure

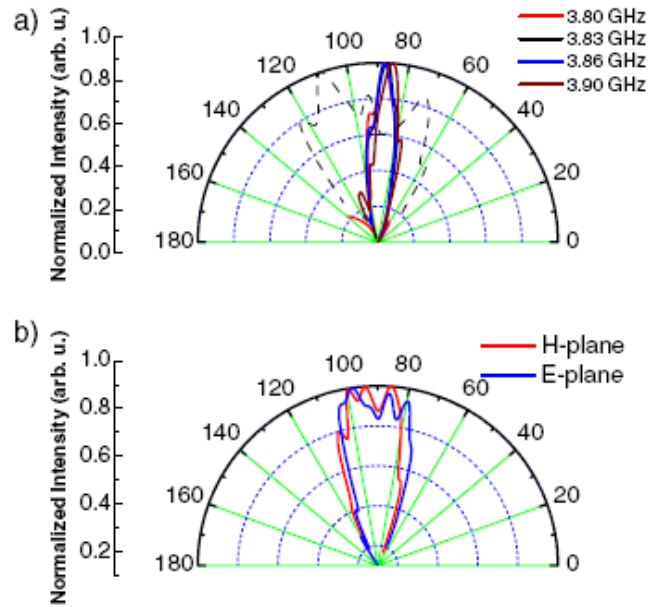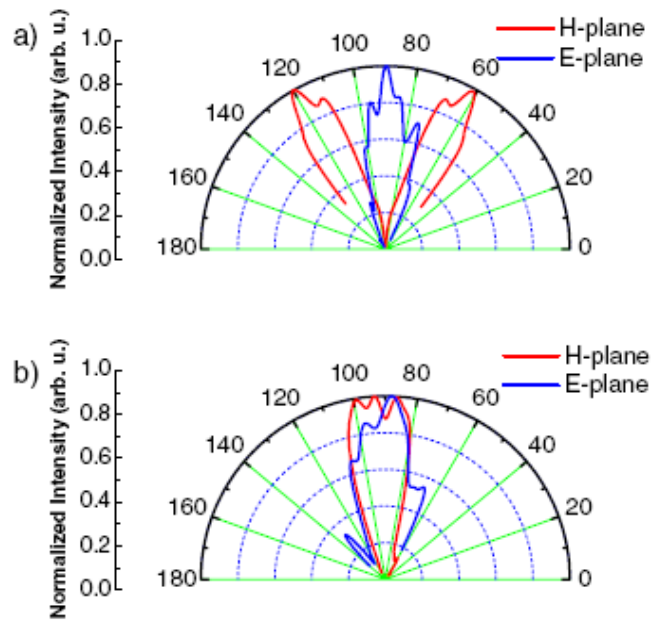**Figure 2.29:** Far-field radiation pattern in the H-Plane (lines) and E-Plane (dotted) (a) near the resonance frequency of SRR structure and (b) at an off-resonance frequency for closed SRR structure
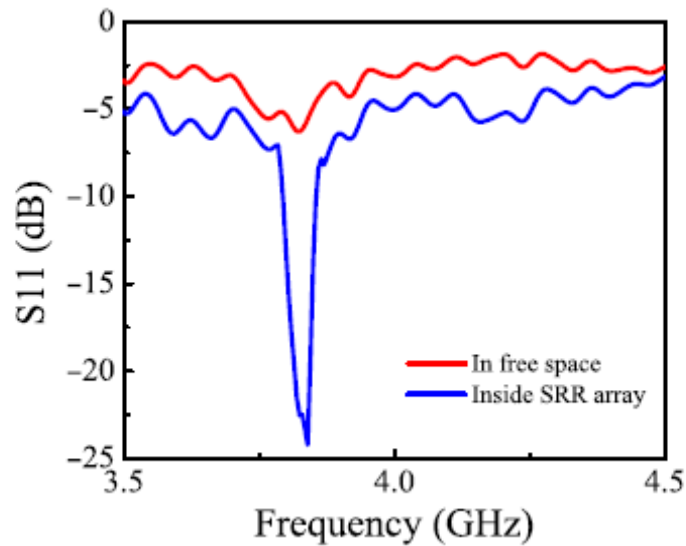
Figure 2.30: S_{11} parameter of monopole antenna

Lastly, the S_{11} parameter of the monopole antenna was measured when the antenna was placed in the array of SRR structure compared to its location in the free space. From Figure 2.30, it was apparent that the S_{11} reduced to -24 dB in the SRR array and this proved an enhanced coupling efficiency. This could be attributed to the high local electric fields near the SRRs.

After obtaining a number of results on some of the parameters of an antenna, it was only logical to conclude that the SRR structure truly contributed to the enhancement of directivity of the antenna. However, due to the resonant nature of the SRR structure, the high directivity of the antenna could only be obtained at a certain frequency. In other words, the design would be only applicable to a frequency band and if one were to apply this theory to another operating frequency, one would have to redesign the whole structure again. Nonetheless, ignoring the hassle aside, the SRR structure also improved the coupling efficiency of the antenna.

2.5 Summary

After discussing all the literature review that was related to the study at press time, there seemed to be different formula of the effective DNG Parameters for different LH MTM structure. However, in this thesis, the modified NRW approach was still preferred as it provided the equations when the TW and SRR structures were combined and the utilization of S parameters contributed to the ease of calculations. Besides discussing the equations in detail about the DNG Parameters, the NRI and Backward Wave Propagation characteristics were also presented.

Subsequently, a few applications related to the gain and directivity of the LH MTM was discussed in detail as in section 2.4.1 and 2.4.4. On the other hand, the application of LH MTM in the filter application was depicted in section 2.4.2 and lastly, the structure of a broadband and a miniaturized cell of LH MTM were shown in section 2.4.3.

In a nutshell, these papers had provided the basic idea and some fundamental knowledge about LH MTM. This is certainly useful for the implement of this research.
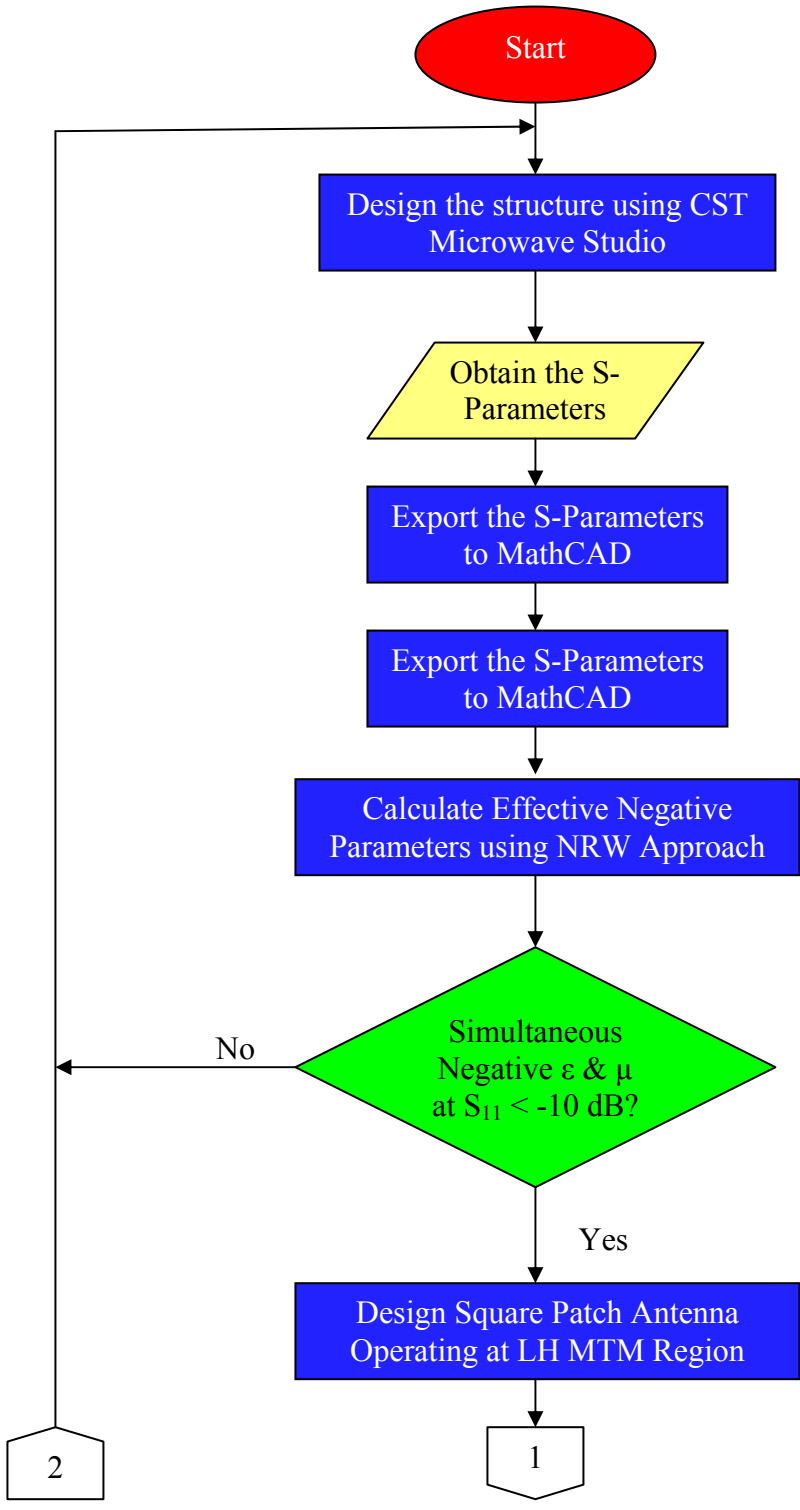
CHAPTER 3

METAMATERIAL DESIGN & SIMULATION

3.0   Introduction

This chapter discusses the process on designing the left-handed metamaterial. This chapter also shows a few results in simulation and the flow chart of the project.
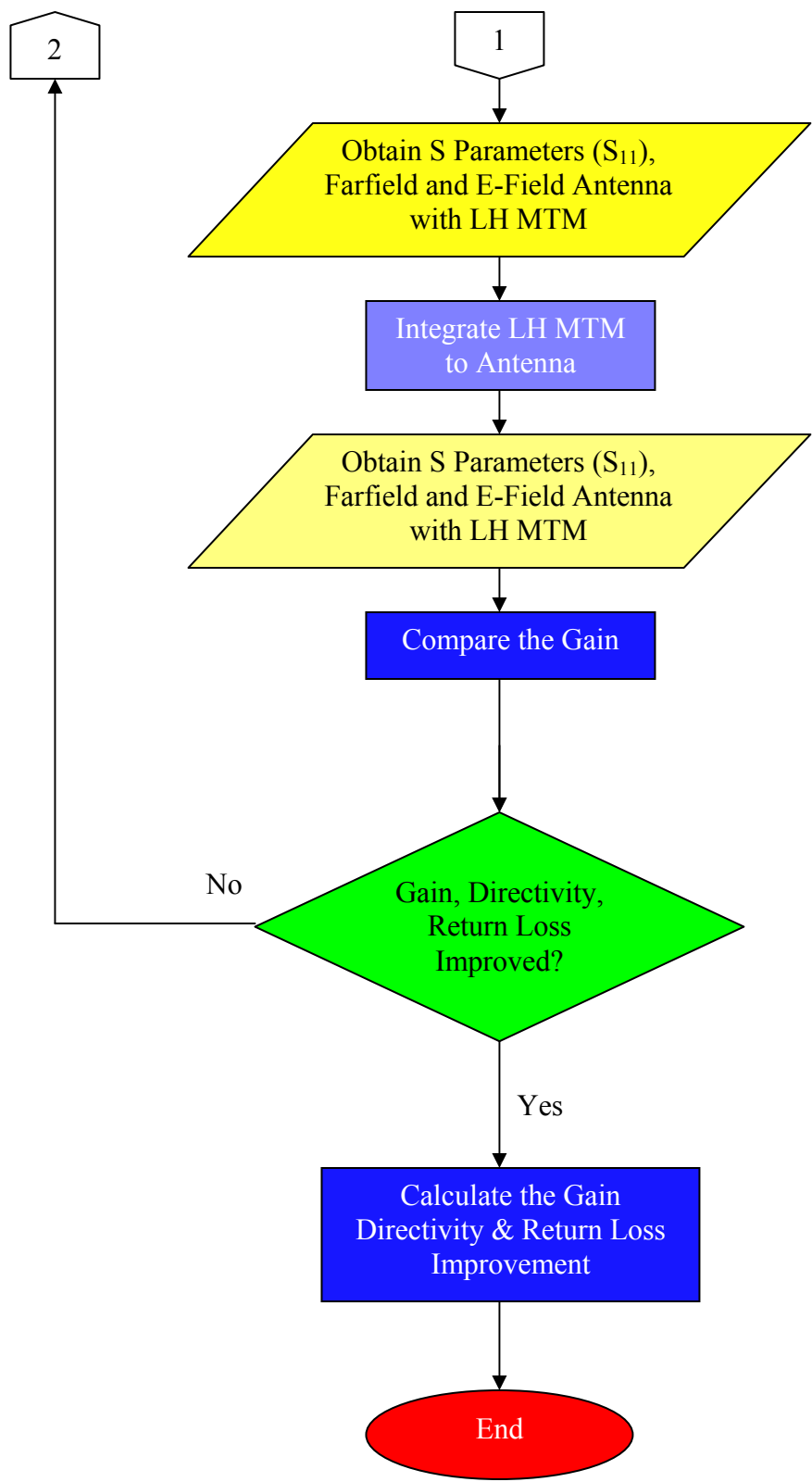
3.1 The Flow of Design Process

```
                    ┌─────────────┐
                    │    Start    │
                    └──────┬──────┘
                           │
        ┌──────────────────┤
        │                  ▼
        │        ┌───────────────────────┐
        │        │ Design the structure  │
        │        │ using CST Microwave   │
        │        │ Studio                │
        │        └───────────┬───────────┘
        │                    ▼
        │          ╱─────────────────╲
        │         │ Obtain the S-     │
        │          ╲ Parameters      ╱
        │                    ▼
        │        ┌───────────────────────┐
        │        │ Export the S-         │
        │        │ Parameters to MathCAD │
        │        └───────────┬───────────┘
        │                    ▼
        │        ┌───────────────────────┐
        │        │ Export the S-         │
        │        │ Parameters to MathCAD │
        │        └───────────┬───────────┘
        │                    ▼
        │        ┌───────────────────────┐
        │        │ Calculate Effective   │
        │        │ Negative Parameters   │
        │        │ using NRW Approach     │
        │        └───────────┬───────────┘
        │                    ▼
        │               ◇─────────◇
   No   │          Simultaneous
 ◄──────┤          Negative ε & μ
        │          at S₁₁ < -10 dB?
        │               ◇─────────◇
        │                    │ Yes
        │                    ▼
        │        ┌───────────────────────┐
        │        │ Design Square Patch   │
        │        │ Antenna Operating at  │
        │        │ LH MTM Region          │
        │        └───────────┬───────────┘
        ▼                    ▼
      ⬡ 2                  ⬡ 1
```

Flowchart elements:

- **Start**
- Design the structure using CST Microwave Studio
- Obtain the S-Parameters
- Export the S-Parameters to MathCAD
- Export the S-Parameters to MathCAD
- Calculate Effective Negative Parameters using NRW Approach
- Simultaneous Negative ε & μ at $S_{11} < -10$ dB? — No → 2 ; Yes → Design Square Patch Antenna Operating at LH MTM Region → 1

Figure 3.1: Flow Chart of Designing LH MTM

3.2   LH MTM Design with CST Microwave Studio

In order to determine the dimension of the structure, equation (2.1) and (2.3) are first calculated to obtain the desired LH MTM frequency region. For easy reference and to avoid confusions, the equations as well as the value of the parameters are written again as follows:

$$\varepsilon_r(\omega) = 1 - \frac{\omega_{pe}^2}{\left(\omega^2 + \zeta^2\right)} + j\frac{\xi\omega_{pe}^2}{\omega(\omega^2 + \zeta^2)}$$

where

p = 50 mm = periodicity of the structure

a = 20 mm = radius of the thin wire

$$\mu_r = 1 - F\omega^2 \frac{(\omega^2 - \omega_{0m}^2)}{(\omega^2 - \omega_{0m}^2)^2 + (\omega\zeta)^2} + j\frac{F\omega^2\zeta}{(\omega^2 - \omega_{0m}^2)^2 + (\omega\zeta)^2}$$

where

p = 50 mm = periodicity of the structure

a = 20 mm = inner radius of the smaller ring

w = 5 mm = width of the ring

δ = 0.1 mm = radial spacing of the ring
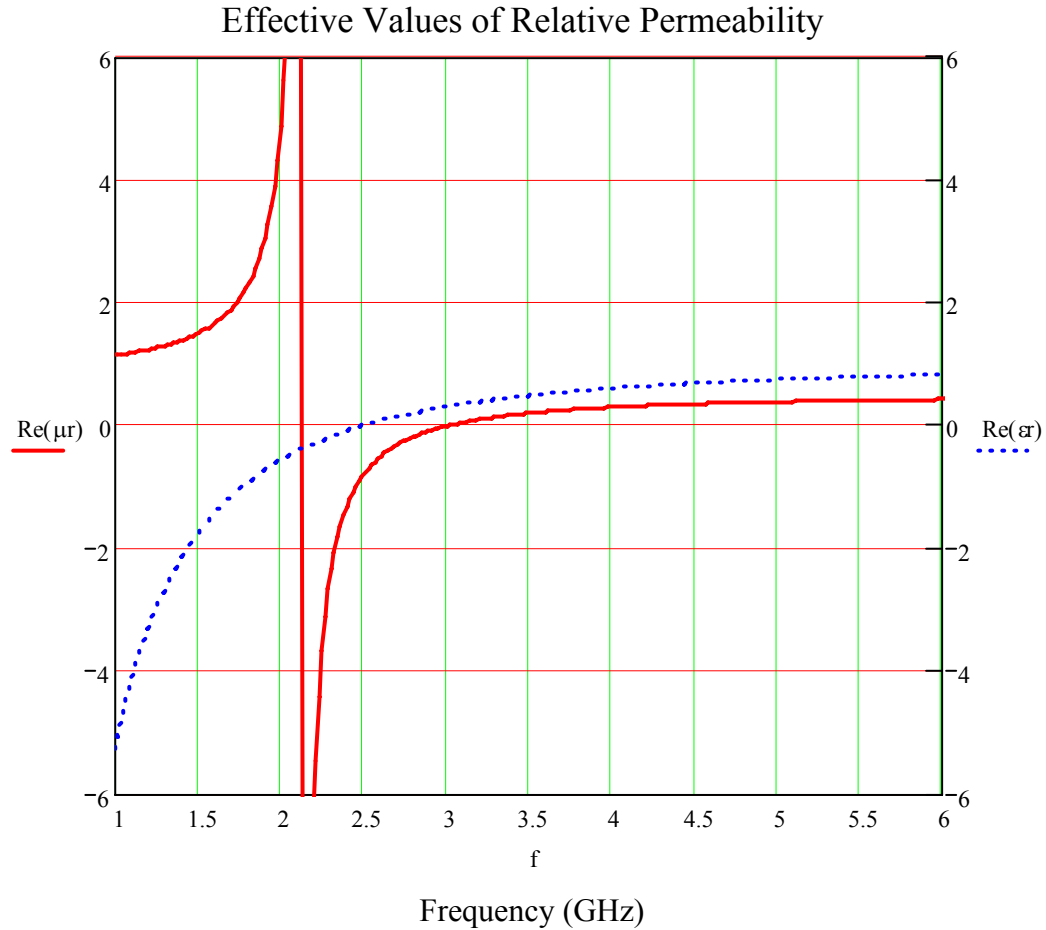
Effective Values of Relative Permeability

Figure 3.2: The effective parameters obtained from the equation 2.1 and 2.3.

From the graph acquired from Figure 3.2, it was apparent that the LH MTM region was between 2.14 GHz to 2.482 GHz. It may be tempting to think that the LH MTM could be constructed at one of the ISM Band (2.4GHz) from the results obtained in the above graph. However, one must keep in mind that the equations were only applicable to the structures – the TW and SRR structures – when excited separately. Nonetheless, the values obtained gave a rough indication that the LH MTM would be around that frequency range.

Subsequently, by using the values obtained from the calculations above, the LH MTM was designed using CST Microwave Studio and again, the effective parameters were calculated using the modified NRW approach as stated in the following equations:

$$S_{11} \approx \frac{2\,jkd\,(\eta^2 - 1)}{(\eta + 1)^2 - (\eta - 1)^2} = \frac{2\,jkd\,(\eta^2 - 1)}{4\eta}$$

$$\varepsilon_r = \mu_r + j\frac{2S_{11}d}{k_0}$$

There had been a change in some of the parameters to make the structure realizable in the fabrication process later. For example, the radial spacing of 0.1 mm could hardly be realized and it had been change to 1 mm. Besides, similar alterations were done to the radius of the TW structure as the value seemed illogical. On the other hand, in equation 2.1, the length of the TW structure was assumed to be infinity and that could not be possibly realized.

As a result, the graph in Figure 3.3 and 3.4 were obtained. From there, it was proven that the LH MTM region fell in the range of 3.7 GHz to 4.9GHz. Since there are no specific equations for a certain LH MTM structure at the moment, one could only guess where the LH MTM would exist by transferring the S_{11} and S_{21} parameters to the MathCAD to calculate the effective parameters.
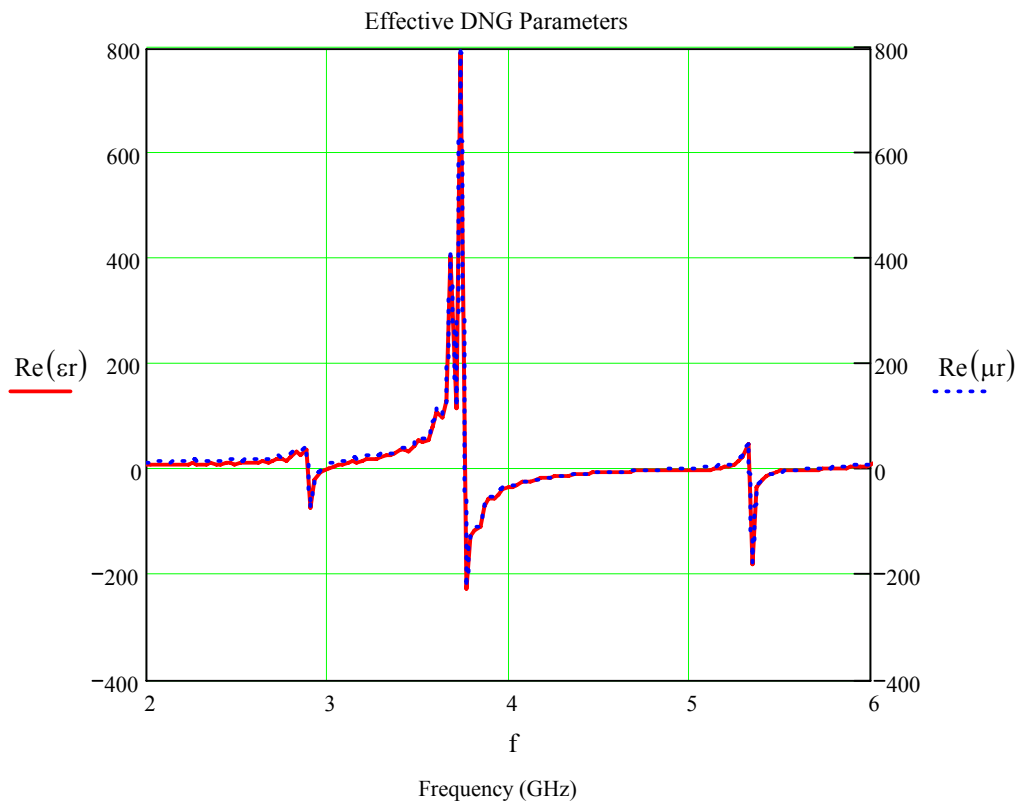
Figure 3.3: Real Effective Values of Permittivity and permeability gained from MathCAD
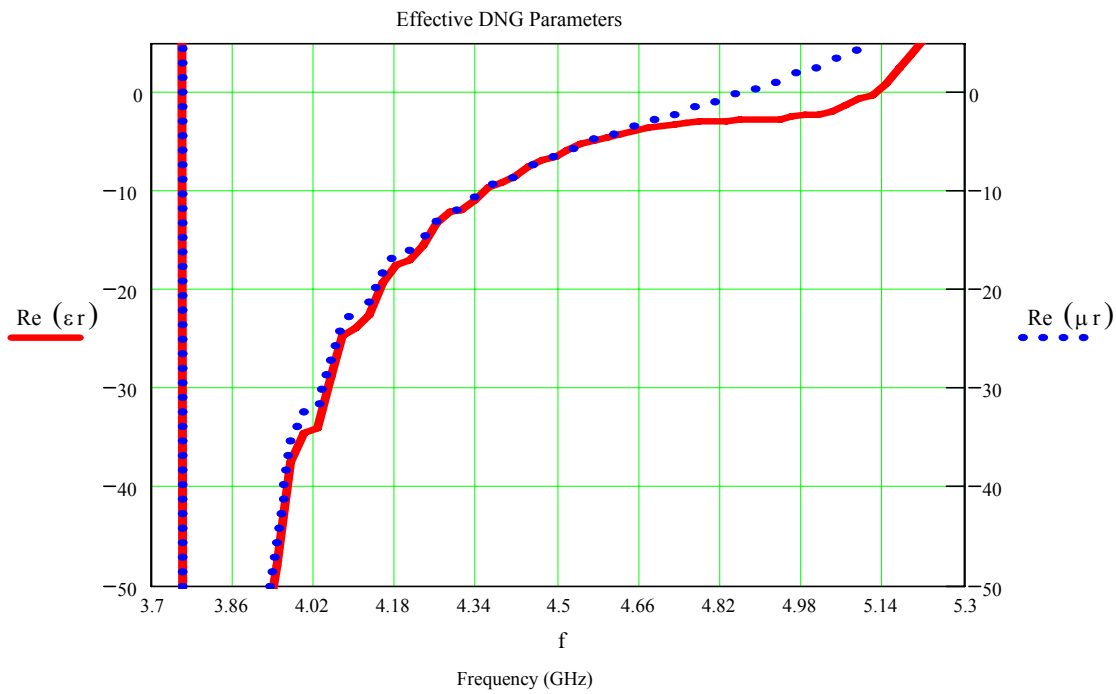

Figure 3.4: Zoomed Real Effective Values of Permittivity and permeability gained from MathCAD

From the results gained from Figure 3.3 and 3.4, the dimensions of the metamaterial where it will be predicted to act as a metamaterial were recorded and the design process of the metamaterial was done. The structure from [8] was chosen as the guide to implement the LH MTM structure and the dimensions of the structures are shown in Table 3.1.

	Magnitude	Unit
Operating Frequency	3.7 – 4.9	GHz
TW Structure		
Radius (a)	1	mm
Length	30	mm
SRR Structure		
Inner Ring Smallest Parameter	10 x 10	mm
Width of Ring (w)	2	mm
Spacing between Rings (δ)	1	mm
Gap of the Opening at Each Ring	2	mm
Periodicity (p)	10	mm

Table 3.1: LH MTM Design Specification

Since the combination of Figure 2.1(a) and (b) could be realized practically on a dual layer FR-4 Board, the structure is simulated as shown in Figure 3.5.
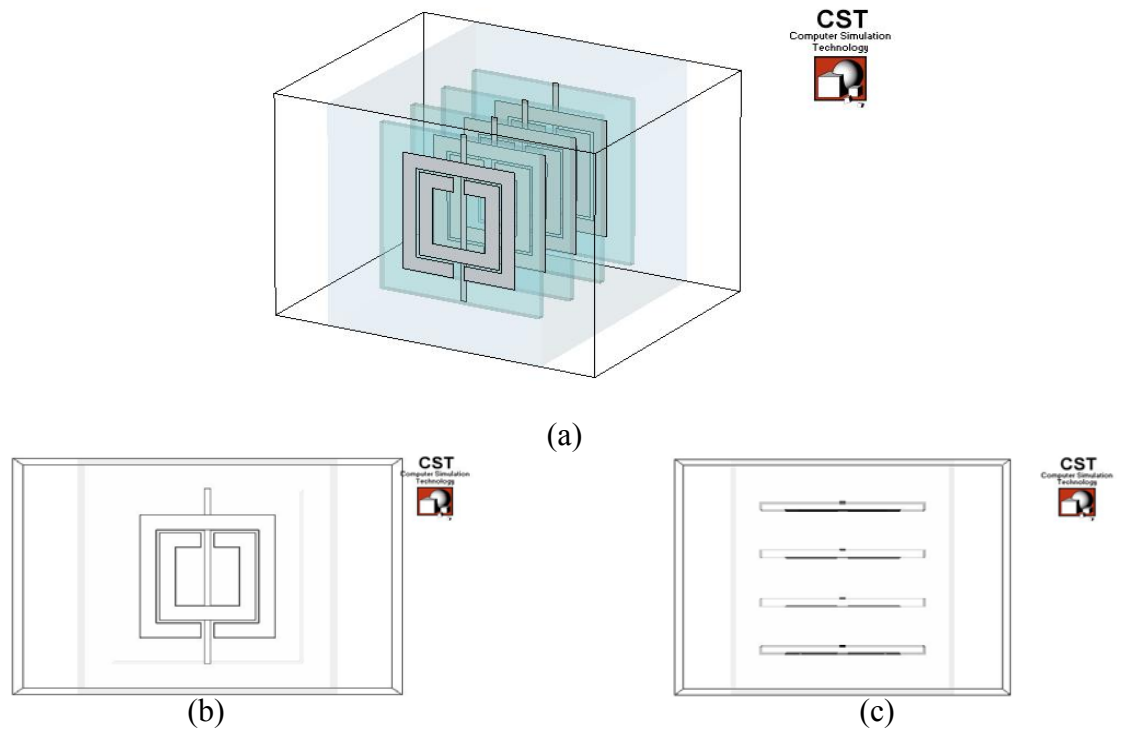
(a)

(b)

(c)

Figure 3.5: (a) 3D Perspective View (b) Front View and (c) Top View of the proposed structure realizable on FR-4 Board

Referring to Figure 3.5(b), the excitation of the signal was done from the left side to the right side of the structure assuming the surrounding was air with the permeability and permittivity equals to 1. This could be illustrated more clearly in Figure 3.6.
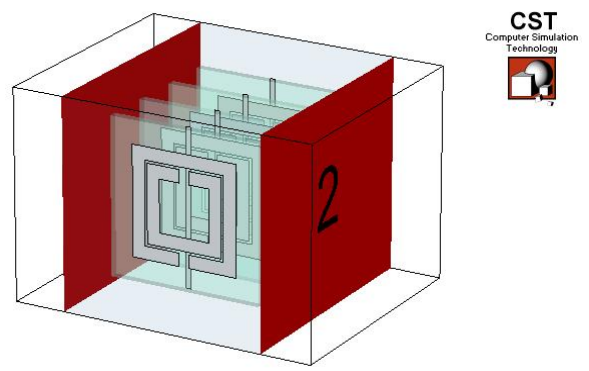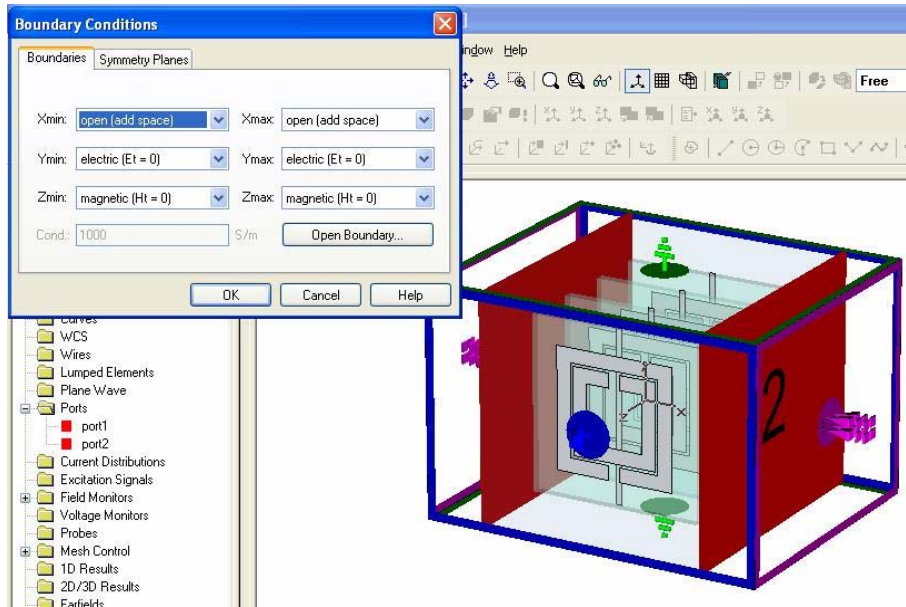

Figure 3.6: Waveguide Ports (in red)

Figure 3.7: Boundary Condition of Structure

In Figure 3.7, Y-Plane was defined as Perfect Electric Boundary (PEB) and Z-Plane was defined as the Perfect Magnetic Boundary (PMB). Subsequently, the wave was excited from the negative X-axis (Port 1) towards the positive X-axis (Port 2). This setup mimicked the waveguide and it was suitable to calculate the S-Parameters for the extraction of the effective parameters later on.

Through this configuration, the S-Parameters (S_{11} and S_{21}) were obtained and exported to MathCAD for the calculation of the LH MTM region using the NRW Approach. Subsequently, after plotting the effective parameters (ε & μ), a square patch antenna which operated in the LH MTM region (3.7GHz – 4.9GHz) was designed. In this case, a patch antenna operating at 3.9GHz was designed and discussed further in Section 3.4.

3.3   Calculation Process in MathCAD

This powerful tool was used twice in the design of the whole LH MTM. First of all MathCAD was used to determine the approximate dimensions of the LH MTM via equation (2.1) and (2.3). This gave a very rough idea of where the LH MTM region was and the dimensions used were transferred to CST Microwave Studio to design the structure (Figure 3.5).

Knowing that the combination of the 2 structures would yield a different response altogether, the modified NRW Approach [Equation (2.22) and (2.24)] were used to calculate the effective parameters of the LH MTM. This was done by exporting the S-Parameters from CST Microwave Studio to MathCAD so that the calculation processes could commence. Further optimization procedures of the design were needed to acquire the desired LH MTM frequency region.

Once the LH MTM region was obtained, the exact dimensions of the structure were transferred to CST Microwave Studio for further simulation and subsequent fabrication processes. The sample calculations that produced the graph in Figure 3.2 and Figure 3.3 are shown as follows.

Calculations for to Produce Figure 3.2

Parameters to calculate the Effective Permeability

f :=

	0
0	1
1	1.019
2	1.038
3	1.057
4	1.076

$\omega := 2\pi f \cdot 10^9$ $p := 0.050$ $a := 0.02$ width $:= 0.001$

sp $:= 0.0001$

R1 $:= 50$ $\mu o := 1.2566 10^{-6}$ $n := 0, 1 .. 1000$

Note:
f = frequency from 1GHz to 6 GHz

p = periodicity of the cell

width = width of the rings

sp = radial spacing between the rings

R1 = metal resistance per unit length

a = inner radius of the smaller ring

n = the index used for the steps of frequency. In this case, there are 1000 steps available

Formulas to calculate the Effective Permeability

$$F1 := \pi \cdot \left(\frac{a}{p}\right)^2 \qquad \zeta := \frac{2 \cdot p \cdot R1}{a \cdot \mu o} \qquad \omega 1 := \left(3 \cdot 10^8\right) \cdot \sqrt{\frac{3 \cdot p}{\pi \cdot \left(\ln\left(\frac{2 \cdot \text{width}}{sp}\right)\right) \cdot a^3}}$$

$$\mu r_n := 1 - \left[\frac{F1 \cdot \left[\left(\omega_n\right)^2\right] \cdot \left[\left(\omega_n\right)^2 - \omega 1^2\right]}{\left[\left(\omega_n\right)^2 - \omega 1^2\right]^2 + \left(\omega_n \cdot \zeta\right)^2}\right] + \left[\frac{i \cdot F1 \cdot \left[\left(\omega_n\right)^2\right] \cdot \zeta}{\left[\left(\omega_n\right)^2 - \omega 1^2\right]^2 + \left(\omega_n \cdot \zeta\right)^2}\right]$$

$\text{Re}(\mu r) =$

	0
0	1.142
1	1.149
2	1.156
3	1.164
4	1.172
5	1.18
6	1.189
7	1.198
8	1.207
9	1.217
10	1.228
11	1.238
12	1.25
13	1.262
14	1.274
15	1.287

Note:

$\omega 1$ = *magnetic plasma frequency*

F1 = F

Parameters to calculate the Effective Permittivity

f :=

	0
0	1
1	1.019
2	1.038
3	1.057
4	1.076

$\omega := 2\pi f \cdot 10^9$ $p := 0.050$ $a := 0.02$ $\sigma := 1000$

$\varepsilon o := 8.854 \cdot 10^{-12}$ $n := 0, 1 .. 1000$

Note:

f = frequency from 1GHz to 6 GHz

p = periodicity of the cell

a = radius of Thin Wire

n = the index used for the steps of frequency. In this case, there are 1000 steps available

σ = conductivity of the metal

Formulas to calculate the Effective Permittivity

$$\omega 1 := \sqrt{\frac{2\pi \cdot \left(3 \cdot 10^8\right)^2}{p^2 \cdot \ln\left(\frac{p}{a}\right)}}$$

$$\zeta := \left[\frac{\left(\frac{p \cdot \omega 1}{a}\right)^2 \cdot \varepsilon o}{\pi \sigma}\right]$$

$$\varepsilon r := 1 - \left(\frac{\omega 1^2}{\omega^2 + \zeta^2}\right) + \left[\frac{i \cdot \zeta \cdot \left(\omega 1^2\right)}{\omega \cdot \left(\omega^2 + \zeta^2\right)}\right]$$

Note:

ω1 = electric plasma frequency

ζ = damping factor due to metal losses

$Re(\varepsilon r) =$

	0
0	-5.253
1	-5.022
2	-4.804
3	-4.597
4	-4.401
5	-4.215
6	-4.039
7	-3.871
8	-3.712
9	-3.56
10	-3.416
11	-3.278
12	-3.147
13	-3.021
14	-2.901
15	-2.787

Calculations to produce Figure 3.3

Parameters to be used in the Modified NRW Approach

s11 :=

	0
0	-0.515+0.28i
1	-0.554+0.332i
2	-0.502+0.387i
3	-0.462+0.353i
4	-0.511+0.345i
5	-0.517+0.426i
6	-0.438+0.45i
7	-0.431+0.397i
8	-0.498+0.442i
9	-0.438+0.575i
10	-0.254+0.571i
11	-0.18+0.402i
12	-0.284+0.285i
13	-0.4+0.317i
14	-0.425+0.399i
15	-0.396+0.447i

s21 :=

	0
0	-0.411-0.635i
1	-0.388-0.672i
2	-0.462-0.685i
3	-0.492-0.61i
4	-0.45-0.597i
5	-0.487-0.634i
6	-0.55-0.579i
7	-0.517-0.525i
8	-0.53-0.564i
9	-0.642-0.487i
10	-0.558-0.274i
11	-0.265-0.31i
12	-0.221-0.637i
13	-0.516-0.766i
14	-0.676-0.568i
15	-0.57-0.465i

$$\varepsilon o := 8.854187817 \ e^{-12} \qquad \mu o := 1.256637061 \ e^{-6} \qquad w := 2 \cdot \pi \cdot h \qquad n := 0, 1 .. 500$$

$$d := 3mm \qquad h := f \cdot GHz \qquad c = 2.998 \times 10^8 \ \frac{m}{s}$$

Formulas to be used in the Modified NRW Approach

Note :

d = thickness of slab

c = speed of light

w = radian frequency

n = *the index used for the steps of frequency. In this case, there are 1000 steps available*

$$v1 := s21 + s11 \qquad v2 := s21 - s11$$

$$\mu r_n := \frac{\left[2 \cdot (1 - v2_n)\right] \cdot c}{w_n \cdot d \cdot i \cdot (1 + v2_n)} \qquad \varepsilon r_n := \mu r_n + \frac{(2 \cdot s11_n \cdot i) \cdot c}{w_n \cdot d}$$

	0
0	9.701
1	8.111
2	8.895
3	10.383
4	8.934
5	8.134
6	9.806
7	10.158
8	8.505
9	8.984
10	11.835
11	9.155
12	8.904
13	10.763
14	12.036
15	10.072

$Re(\varepsilon r) =$ (left table above)

	0
0	14.152
1	13.324
2	14.898
3	15.78
4	14.154
5	14.494
6	16.447
7	15.949
8	14.88
9	17.17
10	19.866
11	14.752
12	12.819
13	15.072
14	17.404
15	16.024

$Re(\mu r) =$ (right table above)

3.4 Square Patch Antenna Design

As usual, the path of designing a conventional microstrip antenna was taken. Microstrip antenna was chosen instead of other type of antennas because the hardware (FR-4 Board and all the fabrication tools) was easily obtained and the ease of design. By using the well-known formulas in equation (3.1) to (3.8), the design specification was obtained as in Table 3.2. This simulation process was done with AWR Microwave Office due to its easy declaration of port and ideal software for simple 2D simulation tasks.

$$W = \frac{\lambda_0}{2} \tag{3.1}$$

$$\varepsilon_{eff} = \frac{\varepsilon_r + 1}{2} + \frac{\varepsilon_r - 1}{2}(1 + \frac{10h}{w})^{-1/2} \tag{3.2}$$

$$\Delta l = \frac{0.412h(\varepsilon_{eff} + 0.3)\left(\dfrac{w}{h} + 0.264\right)}{\left(\varepsilon_{eff} - 0.258\right)\left(\dfrac{w}{h} + 0.8\right)} \tag{3.3}$$

$$L = \frac{c}{2f\sqrt{\varepsilon_{eff}}} - 2\Delta l \tag{3.4}$$

$$G = \frac{\pi W}{\eta \lambda_0}\left[1 + \frac{(kh)^2}{24}\right] \tag{3.5}$$

$$R_e = \frac{1}{2G} \tag{3.6}$$

$$R_i = R_e \sin^2 \frac{\pi x}{L} \tag{3.7}$$

$$x = \frac{L}{\pi} \sin^{-1} \sqrt{\frac{R_i}{R_e}} \tag{3.8}$$

where

c = speed of light

R_e = the input resistance at the edge of the patch

R_i = the input resistance = 50 Ω

W = width of the patch

L = length of the patch

$k = \beta = \dfrac{2\pi}{\lambda_0}$

λ_0 = operating wavelength

h = thickness of substrate = 1.6 mm

x = distance from the patch center
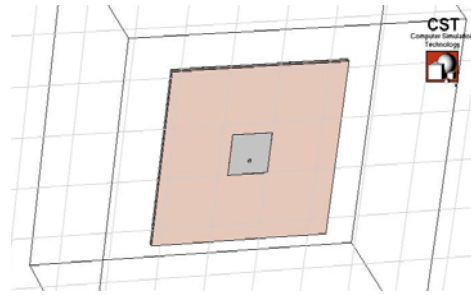
(a)

Figure 3.8: Square Patch Antenna Constructed in CST Microwave Studio

	Magnitude	Unit
Operating Frequency	3.9	GHz
Length (L)	15.7116	mm
Width (W)	15.7116	mm
Feed	Coaxial	-
Feed Location	X=7.8, Y=5.2	mm

Table 3.2: Design Specification for Square Patch Antenna

3.5   Integration of LH MTM to Antenna

After designing and simulating the antenna, ensuring that it operates at the desired frequency and recording its gain, the integration of LH MTM and the antenna was carried out as in Figure 3.6. In this simulation, the boundary conditions were set to open space since the antenna would be operating in such conditions. Subsequently, the simulation was done on varying distance with a step of 5 mm between the LH MTM and

the antenna to observe the gain of the antenna with LH MTM compared to the original gain obtained earlier without the LH MTM. Besides, the Return Loss (S_{11}) was also obtained at the same time and analyzed.

(a)
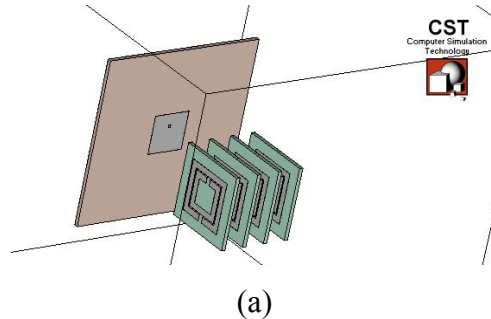
Figure 3.9: (a) 3D View, (b) and (c) of the Integration of LH MTM and Patch Antenna Setup

3.6   Summary

This chapter had presented some of the basic theories and equations to be used in designing LH MTM. However, one has to keep in mind that during the production of this thesis, there has not been a concrete equation to guide the design process of LH MTM. Therefore, the modified NRW approach was used as the last determining factor of the LH MTM frequency range.

Eventually, the design using CST Microwave Studio was explained briefly with some important dimensions for the LH MTM as well as the square patch antenna. In addition, the integration of the antenna with LH MTM was also presented in section 3.5 and the distance between the 2 structures were altered by a step of 5 mm to observe the influence of the LH MTM towards the antenna at different distances.

CHAPTER 4

RESULTS & DISCUSSIONS

4.0   Introduction

Looking at the reversed theories discussed in Chapter 2, there would a lot of new and interesting results to be obtained in experiments involving the LH MTM. Although the full potential of the LH MTM has not been fully discovered at the moment, there had been pretty established hypothesis and results about the gain and directivity of a particular antenna in the presence of LH MTM. In this thesis, the gain, directivity, the coupling efficiency or the Return Loss as well as other supporting characteristics of antenna such as the Cross Polar Isolation and Back Lobe Magnitude were measured and discussed.

4.1   Return Loss Improvement

The Return Loss (S_{11}) holds the paramount importance in any antenna design as it depicts how well the signal could be transmitted from the antenna. By the rule of thumb, as long as the Return Loss is below -10 dB at the desired frequency range, the antenna would be classified as a good antenna.

As for comparison purposes, the simulated results were shown in Figure 4.1.
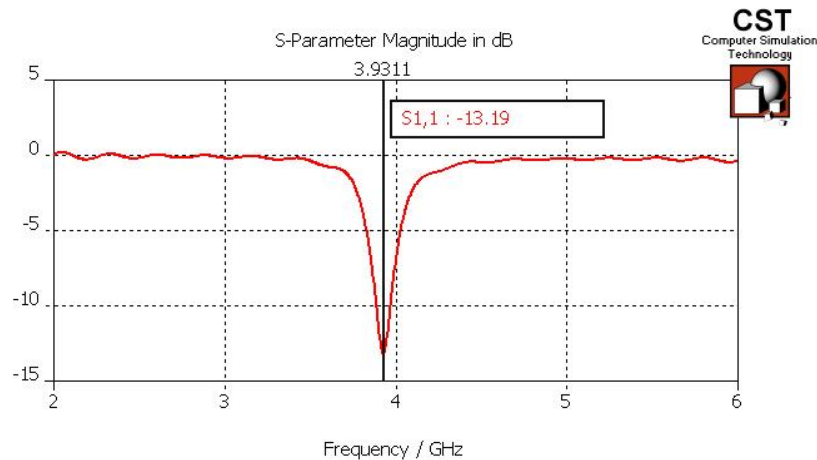
Figure 4.1: Simulated S_{11}

Subsequently, with the integration of LH MTM to the designed patch antenna, the distance between them was varied and the following results (Figure 4.2) were obtained from simulation. In other words, the S_{11} improved with the increment of the distance until the distance was 30 mm.

On the other hand, difference observed between the Return Loss obtained at different distance of the LH MTM to the antenna was because of the frequency-varying effective parameters of LH MTM as well as the focusing effects of the LH MTM which would only be effective at that particular distance. Theoretically, the distance should be half of the thickness of the LH MTM and the magnitude of the permittivity should be same as the FR-4 Board to obtain the optimum focusing effect and hence, the maximum gain. In addition, the presence of LH MTM had introduced a better matching of the antenna which showed in the decrement of the Return Loss.

From the S_{11} results, we could sum up that the LH MTM certainly improves the Return Loss of the antenna which operates in the LH MTM region although with some minor shift of resonant frequency.
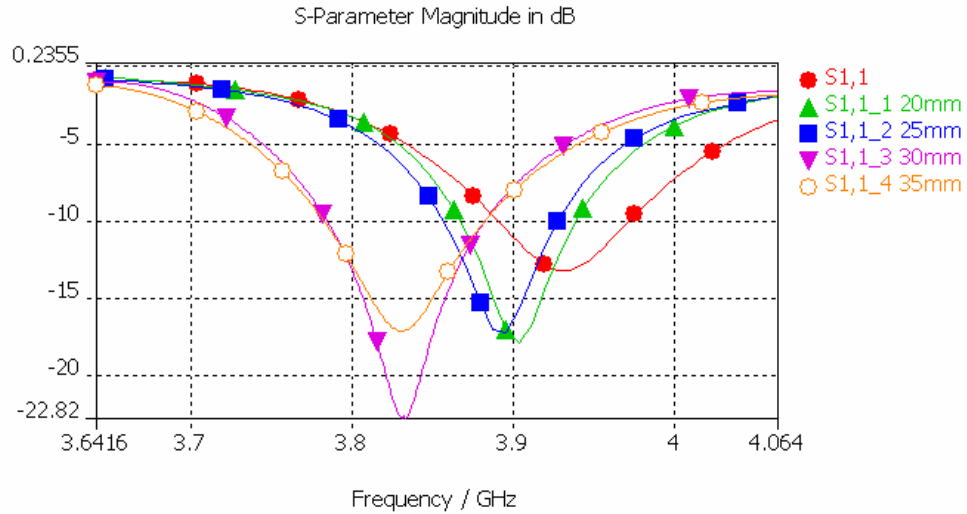
(a)

Figure 4.2: Simulated S_{11} with variation in the distance between LH MTM and antenna

4.2 Gain & Directivity Enhancement

This is the main characteristic of interest in this research and it is very important especially in Microstrip Antennas as researchers have been trying to increase the gain by introducing a lot of other methods such as making use of a supersubstrate of either high permittivity or permeability above the patch antenna [16] and to sandwich the antenna by dielectric layers of the same permittivity [17]. As predicted by the author of [8], the gain of the antenna could be increased with the integration of LH MTM to the antenna and from the simulations and experiments; it was to prove that those speculations were actually true.

Figure 4.3 shows the comparison of 3D radiation pattern of the antenna with the one integrated with LH MTM. At the same time, the polar plot radiation patterns were

also simulated and measured and shown in Figure 4.4. For the sake of a clearer view of the gain and directivity, Figure 4.4 is referred. Looking at the radiation pattern, this radiated signal seemed more directed after the insertion of LH MTM with the 3 dB Beam Width of 52.4^o from the previous 87.9^o. This showed a decrement of 35.5^o in the beam Width and from the simulation results as well, the directivity increased from 6.928 dBi to 8.621 dBi which represented an increase of approximately 1.7 dB.

On the other hand, Figure 4.5 shows the gain of the antenna with and without the LH MTM. Apparently, the gain had increased from 4.5 dB to 5.7 dB. This shows an increase of 1.2 dB in the gain.

(a)

(b)
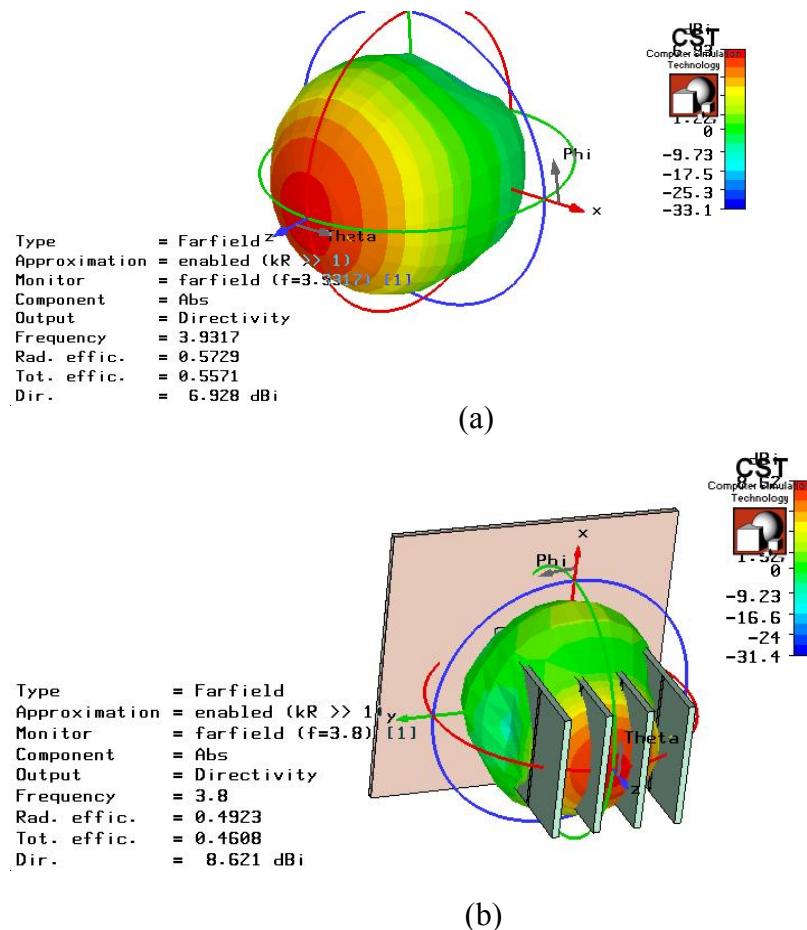
Figure 4.3: 3D Directivity Radiation Pattern of (a) Patch Antenna and (b) Patch Antenna with LH MTM

Farfield 'farfield (f=3.9317) [1]' Directivity_Abs(Theta)

Frequency = 3.9317
Main lobe magnitude = 6.9 dBi
Main lobe direction = 0.0 deg.
Angular width (3 dB) = 87.9 deg.
Side lobe level = -16.4 dB

(a)

Farfield 'farfield (f=3.8) [1]' Directivity_Abs(Theta)

Frequency = 3.8
Main lobe magnitude = 8.6 dBi
Main lobe direction = 0.0 deg.
Angular width (3 dB) = 52.4 deg.
Side lobe level = -9.2 dB

(b)
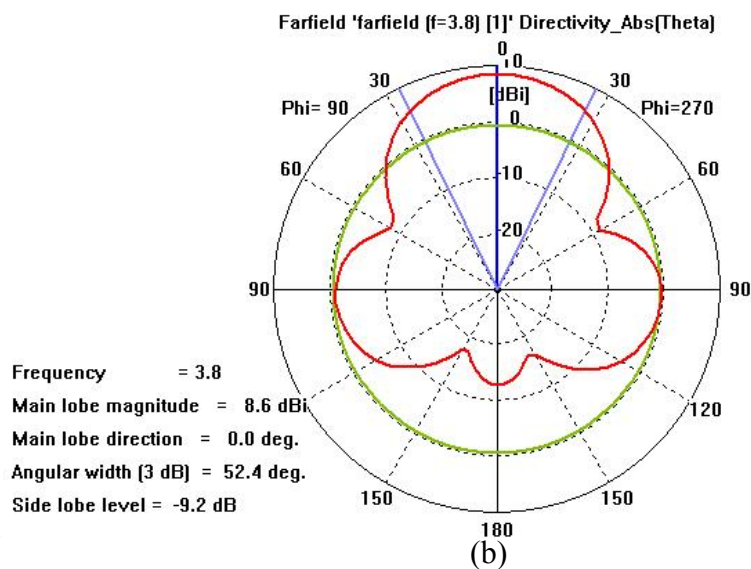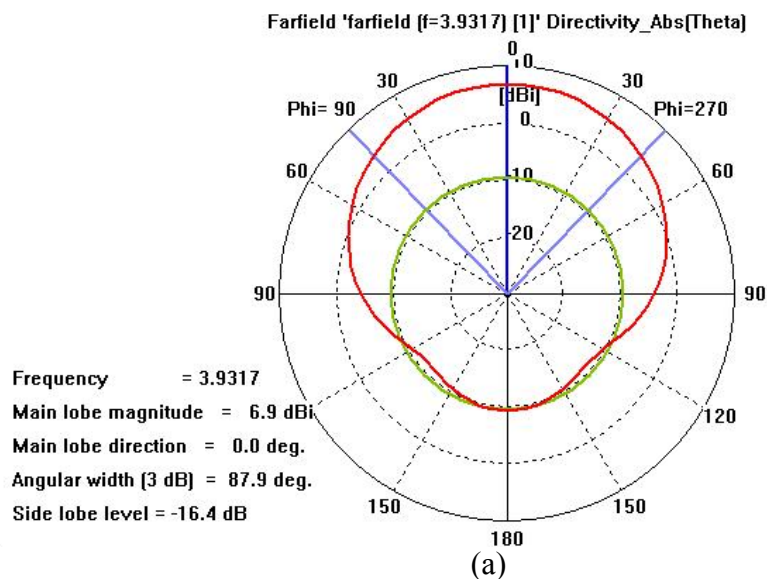
Figure 4.4: Polar Plot Directivity Radiation Pattern of (a) Patch Antenna and (b) Patch Antenna with LH MTM
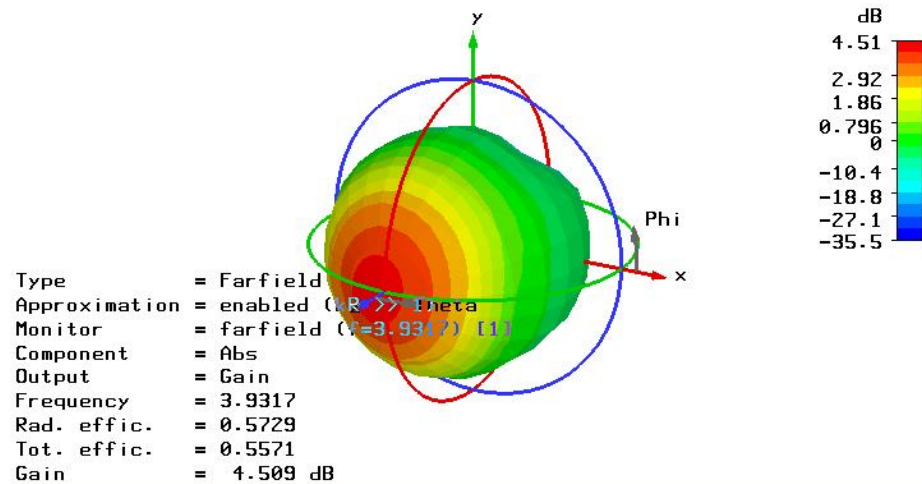
(a)
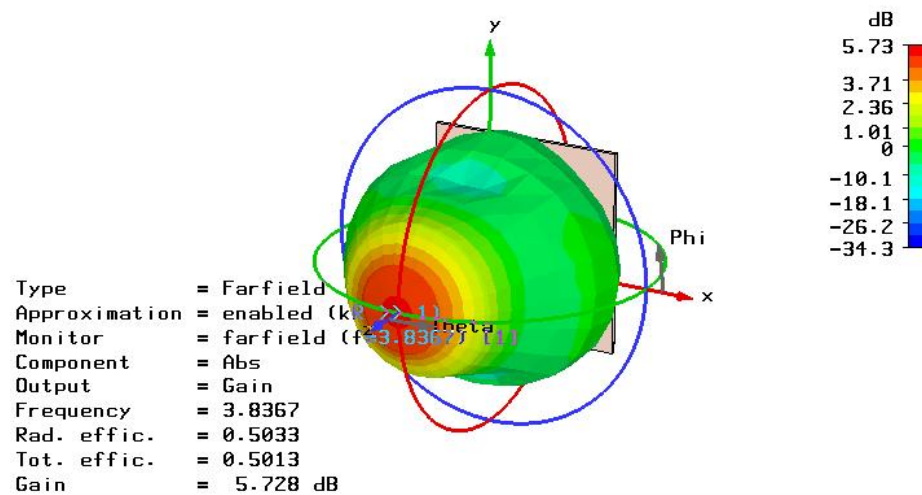
(b)

Figure 4.5: 3D Gain Radiation Pattern of (a) Patch Antenna and (b) Patch Antenna with LH MTM

Therefore, as a whole, the gain and directivity of the antenna increased in the presence of LH MTM due to the focusing effect that was previously explain in Section 4.1. In order to illustrate the comparison between all the parameters stated above, the values were tabulated as in Table 4.1.

Table 4.1: Simulation Results Comparison

No	Parameters	Without LH MTM (3.9GHz)	With LH MTM (3.83GHz)
1	Return Loss (S_{11})	-13 dB	-22.8 dB
2	Gain	4.509 dB	5.728 dB
3	Directivity	6.9 dBi	8.6 dBi
4	Half Power Beam Width	87.9°	52.4°


```
Type        = E-Field (peak)
Monitor     = e-field (f=3.9317) [1]
Component   = Abs
Plane at x  = 8
Frequency   = 3.9317
Phase       = 0 degrees
Maximum-2d  = 1200.39 V/m at 8.20464 / 8.35582 / -1.6
```
(a)


```
Type        = E-Field (peak)
Monitor     = e-field (f=3.8367) [1]
Component   = Abs
Plane at x  = -2
Frequency   = 3.8367
Phase       = 0 degrees
Maximum-2d  = 1340.56 V/m at -1.79536 / 8.35582 / -36.6
```
(b)
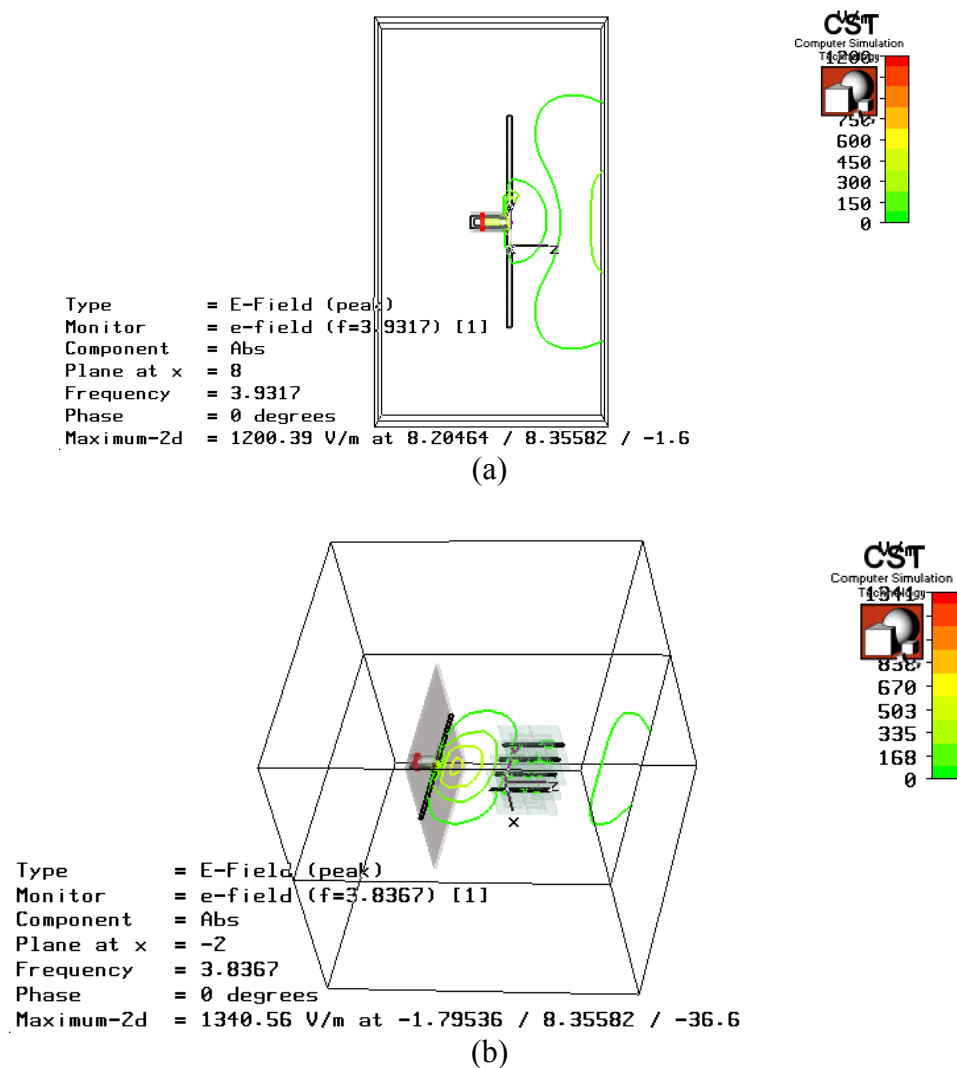
Figure 4.6: Simulated E-Field of (a) Antenna (b) Antenna with LH MTM

4.3   extension results

Figure 1 illustrates the LHM structure where it is a combination of a modified (SRR) and two (CLS). The modified SRR will produce magnetic material-like responses and exhibit the negative permittivity and the CLS will produce strong dielectric-like responses and exhibit the negative permeability [5 and 6].
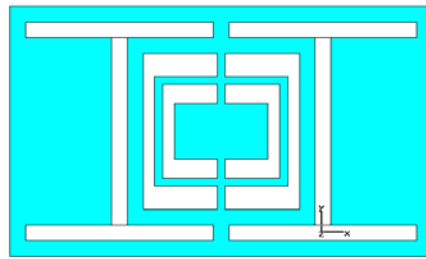
Figure 4.7:   Front view of LHM
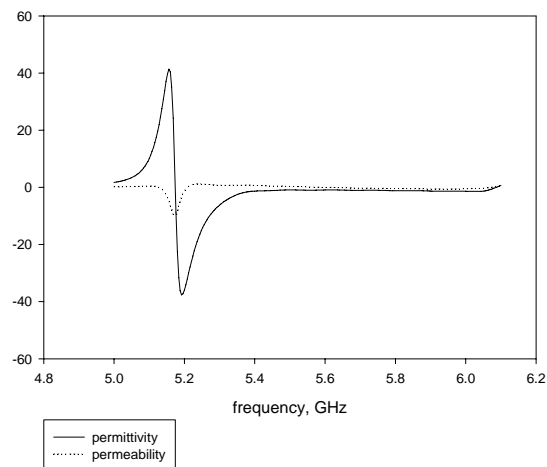
Figure 4.8:   Negative permittivity and negative permeability value

From Figure 3, the range of the negative permittivity and negative permeability (-ε and -μ) starts from 5.17 GHz to 6.0 GHz. A single patch microstrip antenna was then designed to operate at the frequencies where the value of negative permittivity and negative permeability are almost the same. The centre frequency of 5.64 GHz was

chosen as the operating frequency of the microstrip antenna. The same material of LHM was used for the microstrip antenna and a coaxial feed was used to feed the patch of microstrip antenna. The LHM structure was placed in front of the microstrip antenna with a distance of 11.6 mm as shown in Figure 4. The simulated return loss (s_{11}) of the antenna with and without the LHM structure is shown in Figure 5. The simulated radiation pattern of the antenna is shown in Figure 6 and the radiation pattern of the antenna integrated with LHM structures is shown in Figure 7.
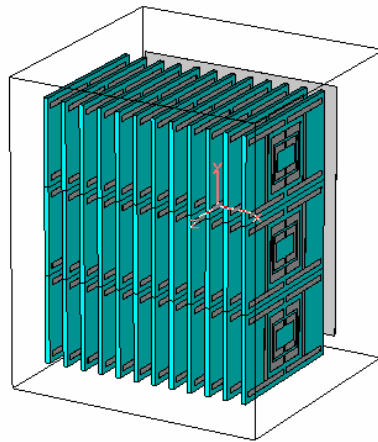
Figure 4.9: Single patch antenna integrated with LHM structure
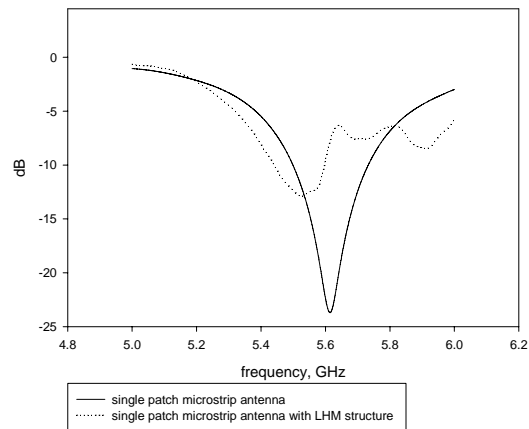
Figure 4.10: Return losses

```
Type          = Farfield
Approximation = enabled (kR >> 1)
Monitor       = farfield (f=5.64) [1]
Component     = Abs
Output        = Gain
Frequency     = 5.64
Rad. effic.   = 0.7260
Tot. effic.   = 0.7192
Gain          =  5.384 dB
```
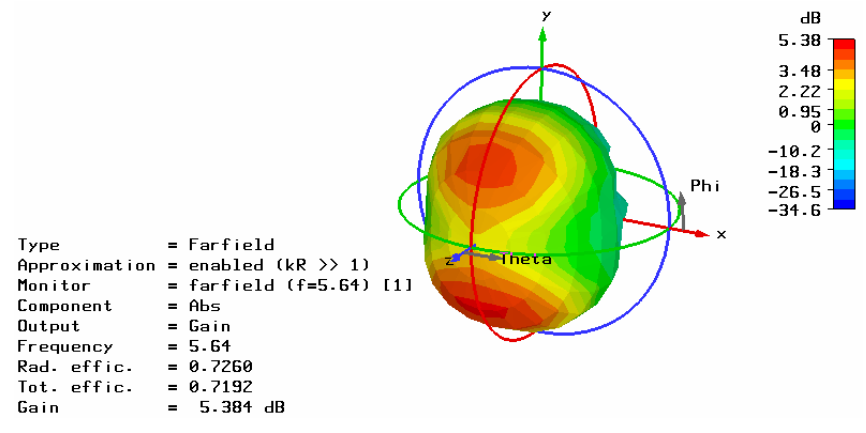
Figure 4.11:   Radiation pattern of single patch microstrip antenna


```
Type          = Farfield
Approximation = enabled (kR >> 1)
Monitor       = farfield (f=5.64) [1]
Component     = Abs
Output        = Gain
Frequency     = 5.64
Rad. effic.   = 0.7973
Tot. effic.   = 0.6111
Gain          =  8.615 dB
```
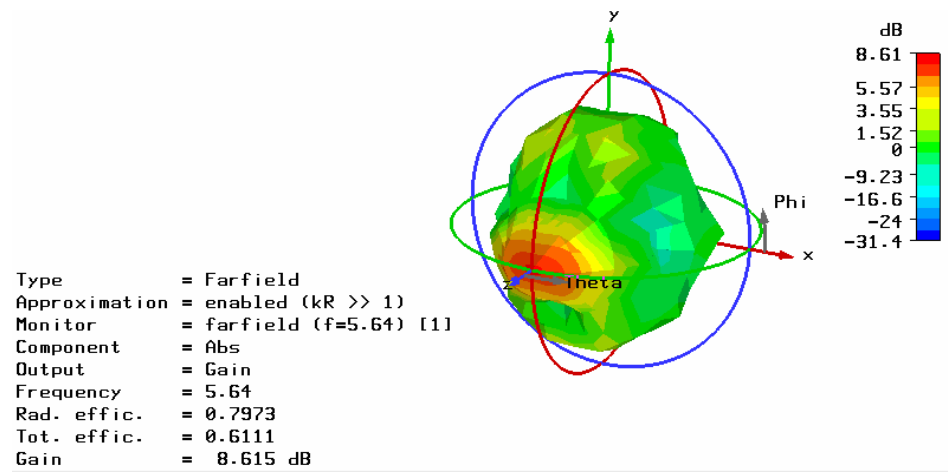
Figure 4.12:   Radiation pattern of single patch microstrip antenna with LHM structure

4.4   Summary

Looking at the encouraging results gained from simulations and experiments, one could conclude that LH MTM is truly a peculiar substance. From the simulations done (Table 4.1), the gain had increased about 1.2 dB while the directivity had increased approximately 1.7 dB. The extension result also shows an increasing of gain from 5.3 dB to 8.6 dB. Besides, the Return Loss had reduced around 10 dB. This suggested that LH MTM could improve the coupling efficiency of the antenna as well as focusing the wave propagating though it.

CHAPTER 5

CONCLUSION

5.1   Conclusion

The design and simulation processes of the LH MTM were presented and all the objectives within the scope of the project were met. All fabrication work was done manually in the Wireless Communication Centre, Universiti Teknologi Malaysia.

From the whole project, it was proven that LH MTM was indeed a peculiar substance with the double negative parameters that could enhance the performance of a microstrip antenna. This was because whenever the polarity of the permittivity and permeability were reversed, a lot of other theories follow suit and as a result, new modified theories were being created. As in this thesis, the 2 most obvious results of the negative parameters that were presented were the negative refractive index and the backward wave propagation.

In addition, the presence of LH MTM could improve the gain and directivity of a microstrip antenna as well as reducing the Return Loss of the antenna. This was proven true by means of the simulation results. Besides, the modified NRW Approach was proven to yield reliable results from the outcome of the whole project.

On the other hand, the applications of LH MTM are also being discovered in other fields and a lot of new findings are surfacing at the current press time. More theories are bound to be bent and modified with such peculiar properties of LH MTM.

5.2 Proposed Future Work

As this is the pioneer project in Universiti Teknologi Malaysia, there is still a lot of room for improvement either in the field of microwave propagation or in other fields that might only be scarcely involved with microwave engineering. However, since this project had focused particularly on the enhancement of microstrip antenna, the following suggestions would be presented.

i.   Shifting the frequency of the LH MTM region to ISM Band or other more well-known frequency range so that the application of LH MTM would be increased.

ii. Miniaturization of LH MTM by using other approaches such as the Transmission Line Approach [1].

iii. Designing a new LH MTM structure different from the current available ones (S-Shape LH MTM, Ω-Shape LH MTM, SRR LH MTM, etc.)

iv. More in-depth discovery of this peculiar substance and seek its application within the microwave engineering study. For example, the integration of LH MTM in the cellular phone technology.

REFERENCES

1. Christophe Caloz and Tatsuo Itoh, Electromagnetic Metamaterials Transmission Line Theory and Microwave Applications, John Wiley & Sons, Inc. 2006

2. J.B. Pendry, A.J. Holden, D.J. Robbins and W.J. Stewart, Low Frequency Plasmons for Thin-Wire Structure, *J. Phys*. Condens. Matter 10 4785 – 4809, 20 March 1998

3. Jiunn-Nan Hwang, and Fu-Chiarng Chen, Study of SAR Reduction with Split Ring Resonators, IEEE, 2005

4. Hu Jun, Yan Chun-sheng, Lin Qing-chun, New Patch Antenna with MTM Cover, *J Zhejiang University SCIENCE A* 7(1), 89-94, 2006

5. Shah Nawaz Burokur, Mohamed Latrach and Sergre Toutain, Theoritical Investigation of a Circular Patch Antenna in the Presence of a Left-Handed Mematerial, *IEEE Antennas and Wireless Propagation Letters*, Vol. 4, 2005

6. I. Gil, J. Bonache, J.Garcia-Garcia, F. Falcone, F. Martin, Metamaterials in Microstrip Technology for Filter Applications, IEEE, 2005

7. Tie Jun Cui et. al., Study of Lossy Effects on the Propagation of Propagating and Evanescent Waves in Left-Handed Materials *Physics Letters* pg. 484-494, 2004

8. Shah Nawaz Burokur, Mohamed Latrach, Serge Toutain, Theoretical Investigation of a Circular Patch Antenna in the Presence of a Left-Handed Medium, *IEEE Antennas and Wireless Propagation Letters*, Vol. 4, 2005

9. Jorge Carbonell, Luis J. Rogla, Vicente E. Boria, Didier Lippens, Design and Experimental Verification of Backward-Wave Propagation in Periodic Waveguide Structures, *IEEE Transactions on Microwave Theory and Techniques*. Vol. 54, No. 4, 4 April 2006

10. Silvio Hrabar, Juraj Bartolic, Backward Wave Propagation in Waveguide Filled with Negative Permeability Meta Material, 2003

11. Silvio Hrabar, Gordan Jankovic, Berislav Zickovic, Zvonimir Sipus, Numerical and Experimental Investigation of Field Distribution in Waveguide Filled with Anisotropic Single Negative Metamaterial

12. Qun Wu, Fan Yi-Meng, Ming-Feng Wu, Jian Wu, Le-Wei Li, Design of Planar LHM with Broad Bandwidth and Miniaturized Cell, IEEE, 2006

13. Richard R. Ziolkowski, Double Negative Metamaterial Design, Experiments and Applications, *IEEE Transactions on Microwave Theory and Techniques*, Vol.51, No. 7, July 2003

14. Ching-Ying Cheng, Richard R. Ziolkowski, Tailoring Double-Negative Metamaterial Response to Achieve Anomalous Propagation Effects along Microstrip Transmission Lines, No. 12, December 2003

15. D.M. Pozar, Microwave Engineering, 2nd Ed., New York: Wiley, pg. 211, 1998

16. D.R. Jackson and N.G. Alexopoulos, Gain Enhancement Methods for Printed Circuit Antennas, *IEEE Trans. Antennas Propagation*, vol.AP-33, no.9, Sep. 1985

17. H. Nakano, M. Ikeda, K. Hitosugi and J. Yamauchi, A Spiral Antenna sandwiched by dielectric layers, *IEEE Trans Antennas Propagation*, vol. 52, no. 6, Jun 2004

18. D.R. Smith, S. Schultz, P. Markos, and C.M. Soukoulis, Determination of effective permittivity and permeability of metamaterials from reflection and transmission coefficient, *Phys. Rev. B*, vol. 65, pg. 195 104, Apr. 2002.

19. D. Seetharamdoo, R. Sauleau, A.C. Tarot, and K. Mahdjoubi, Homogenization of negative refractive index metamtaerials: Influence of physical parameters on the effective permittivity and permeability, *Proc. 27th ESA Antenna Technology Workshop Innovative Periodic Antennas, Santiago de Compostela*, Spain, pp. 5781-578, Mar. 2004

20. F. Martin, F. Falcone, J. Bonache, R. Marques and M Sorolla, Split ring resonator based on left handed coplanar waveguide, *Appl. Phys. Lett.*, vol. 83, pp4652 - 4654, December 2003.

21. Irfan Bulu, Humeyra Caglayan, Koray Aydin and Ekmel Ozbay, Compact Size Highly Directive Antennas based on the SRR Metamaterial Medium, *New Journal of Physics 7*, pg 223, 2005

APPENDIX A

CST Microwave Studio Manual

This manual is specially prepared to guide a beginner in CST Microwave Studio (CST MWS) to construct and simulate a simple Coaxial Feed Square Patch Antenna (CFSPA). After executing the CST MWS programme, one could follow the steps below:

1. Choose a template. There are many available templates to choose from and whenever the right template is chosen, the unit of the parameters (e.g. mm, GHz, ns) would be predefined correctly. Below is the sample of the design template.
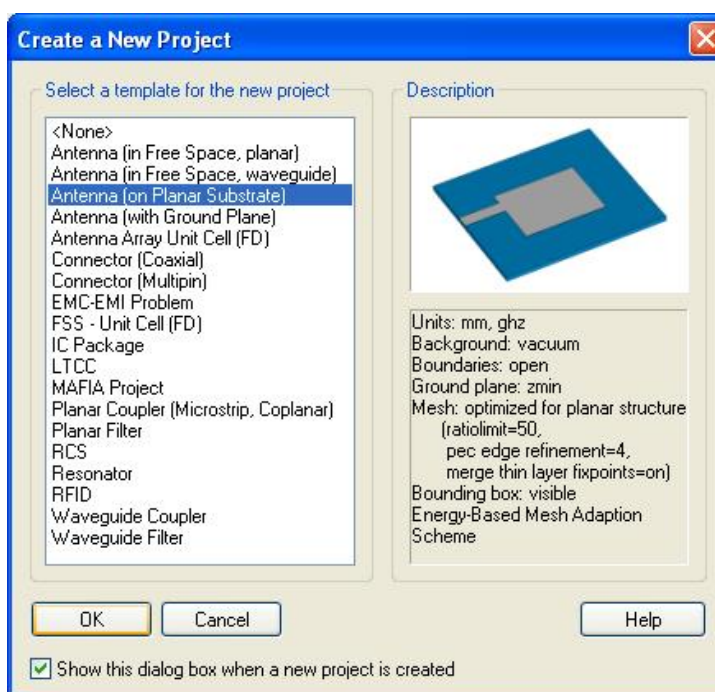
2. Construct the structure. This is done by using the building blocks available. In building the CFSPA, the rectangular and cylindrical blocks are used most often. For further practice on the designing skills, one could refer to the CST website where some videos are available for their promotion purposes. The address of the website that

showcases the ways to construct a model could be found at http://www.cst.com/Content/Showroom/01/01.html.

3. After designing the structure the way one desires, the excitation port needs to be designed as well. This step requires some creativity in the designer to construct the port that mimics the real life coaxial port. In other words, considerations need to be given from the conductor in the coaxial port, the Teflon layer and the exterior ground plane.

4. Whenever a user would like to undo his actions in the design or simply wanting to know the procedures involved in a particular design, he/she could click on the History List ![icon].
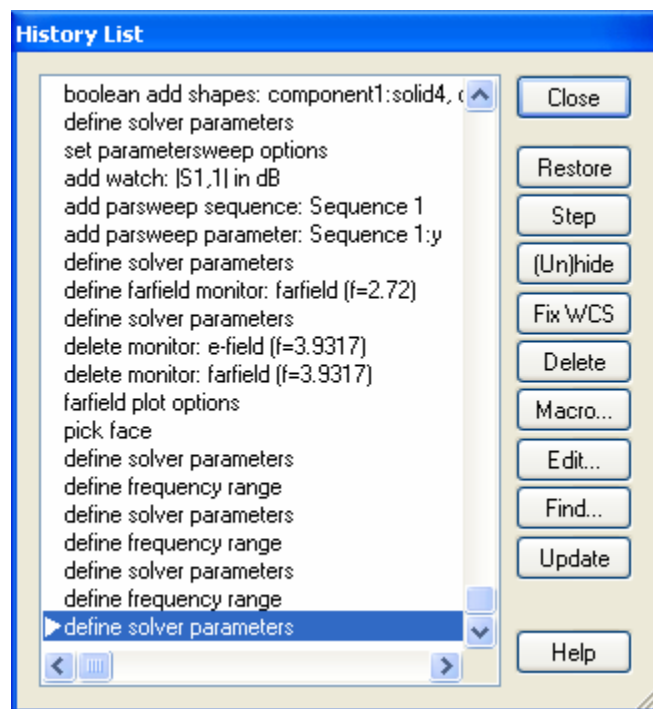
5. When the design is complete, it is essential to define the excitation port by picking the face of the structure where the port is intended to be placed. Then, the waveguide port icon ![icon] is chosen as the excitation port.
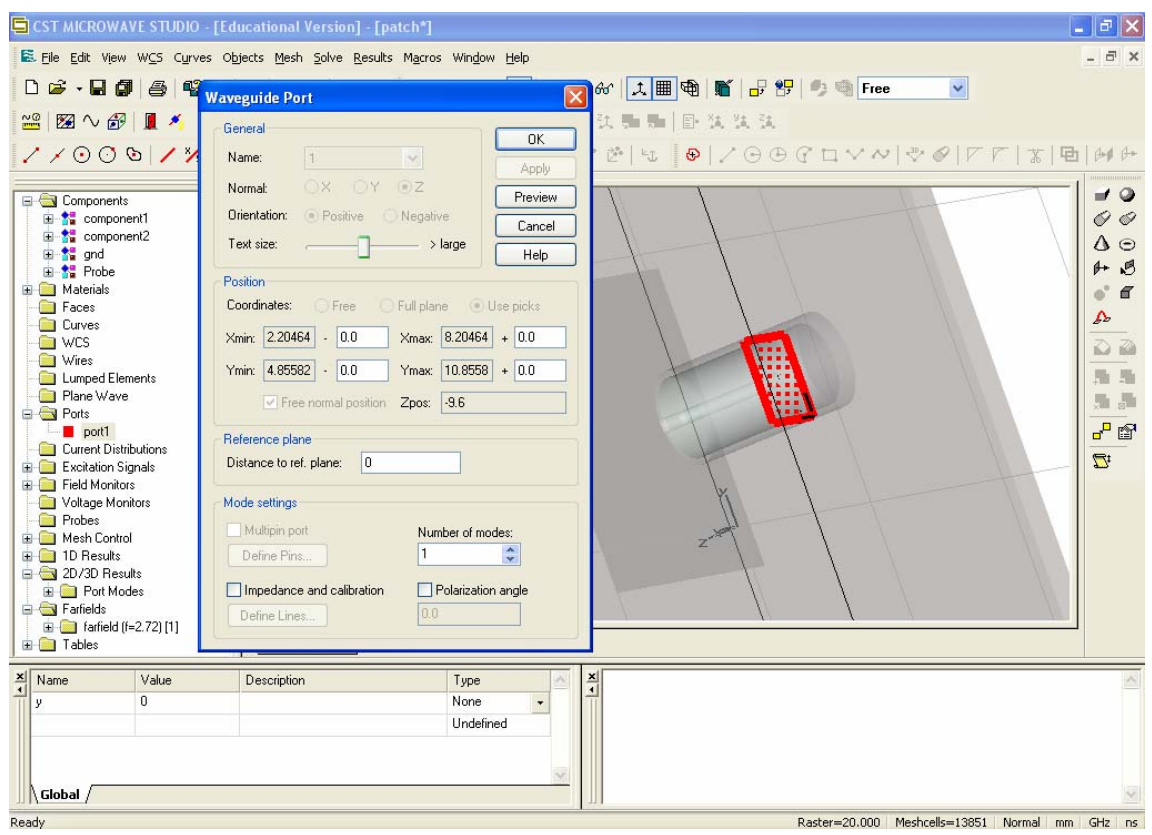
6. Before proceeding any further, one should double check the parameters unit in to ensure that the design has the desired dimensions and operates in the correct frequency.
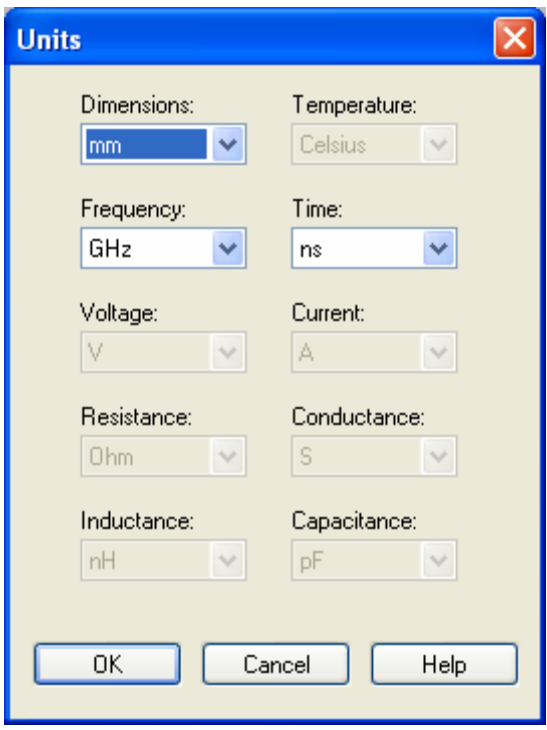
7. Subsequently, the frequency range of the simulation should be chosen by clicking on the $\sim$ icon. For the number of frequency steps to be simulated, it is chosen in the Special tab when the Time Solver icon is clicked later.
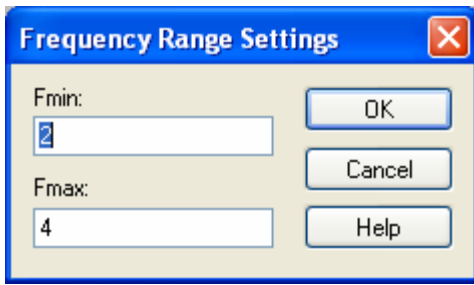
8. In addition, the boundary conditions should also be set. This could be done by choosing the icon and for CFSPA, the boundary conditions should be chosen as Open.
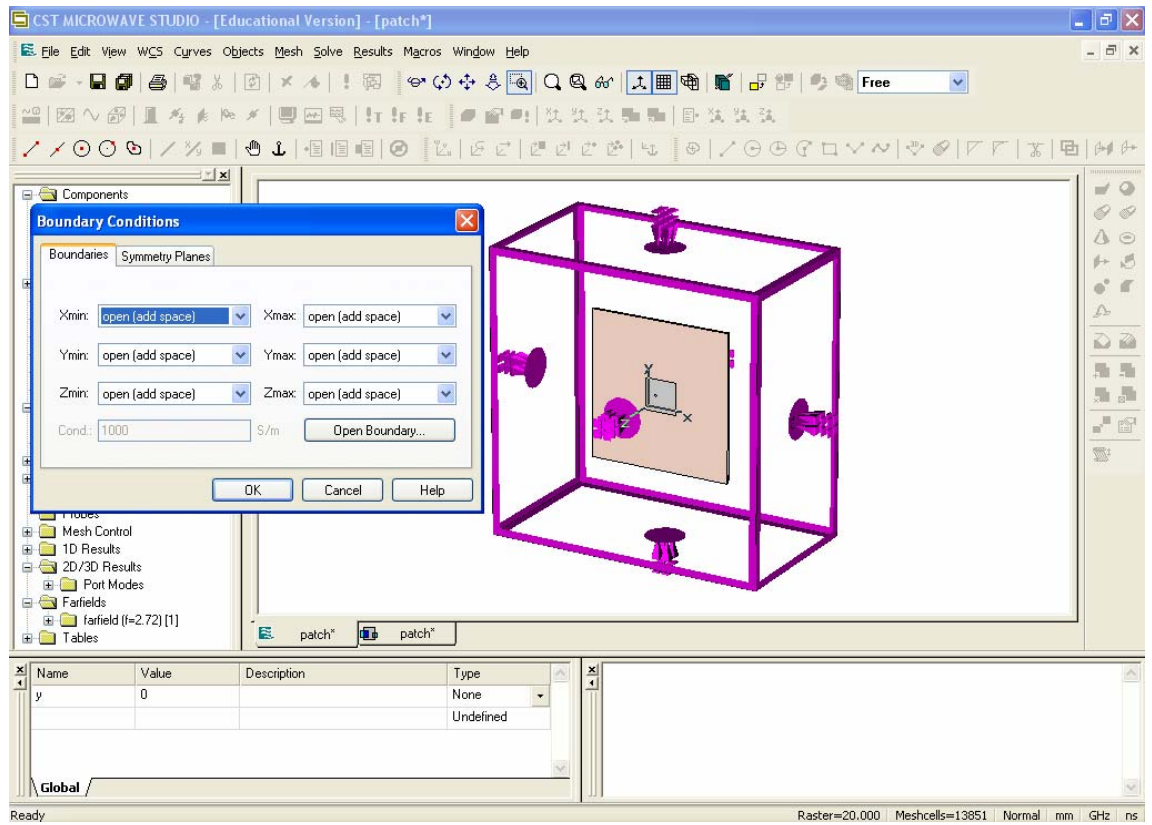
9. In the occasion where the E-Field, H-Field, the Far-field are needed in the end result of the simulation, the Field Monitor 🖥 should be set before any simulation is done. After selecting the appropriate field to be monitored, it is also crucial to check the frequency of interest for the field chosen.
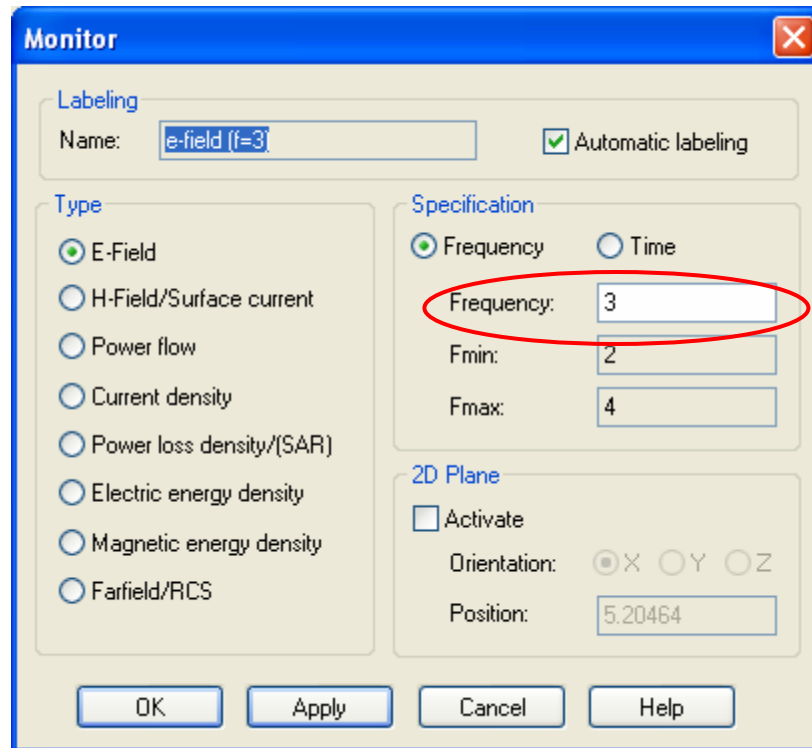
10. Next, the Time Solver icon ![icon] is chosen to run the simulation and the pop up window would appear as shown below. Usually, the sensitivity level is set to -50dB for a more accurate result. As for the frequency steps to be simulated as stated in 6, one has to click on the Special tab in the solver menu which is in the following figure. One can see that the number of samples of frequency could be altered accordingly.
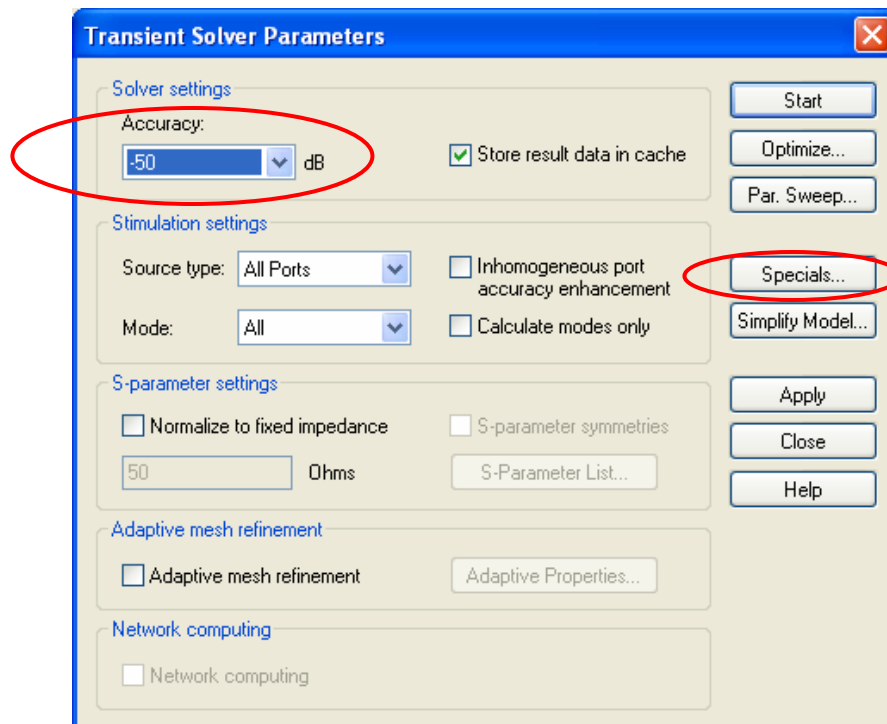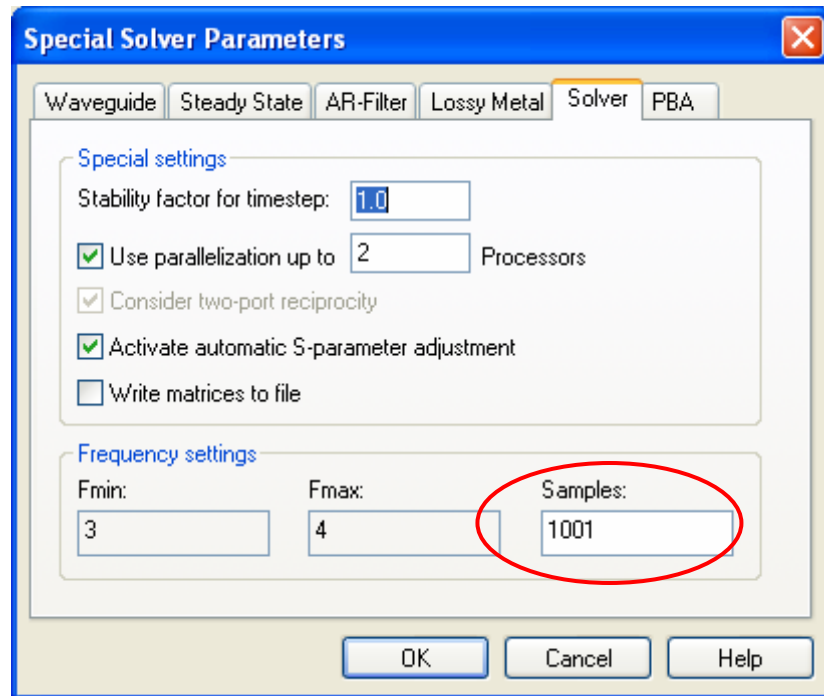
11. All the results simulated would by default stored and saved. Then, one could view the results on the 1D result tab on the left side of the screen (as shown in the following figure). Among the important simulated results are the S parameters (in dB, Polar and Linear), the Excitation Signal, the Smith Chart and so on. If the user had chosen to simulate the 2D results from the Field Monitors as stated in 9, the results would also appear below the 1D results.
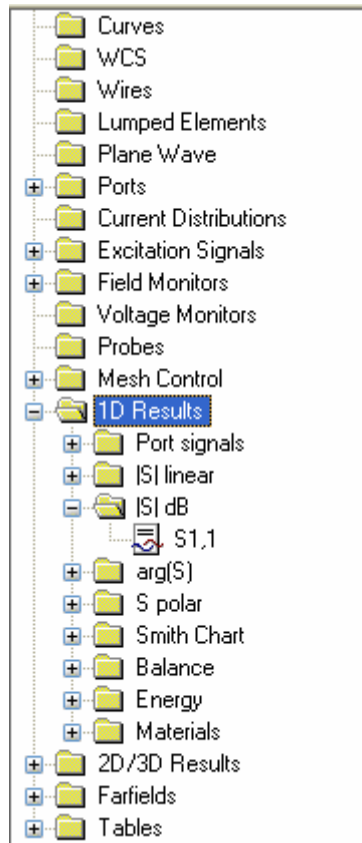
12. To add to the finishing touch of the simulation, perhaps one would like to export the image of the video from CST to other applications like Microsoft Powerpoint to present the findings. In order to perform this, one could simply click on the Macros tab on top of the main window as shown in the following 4 figures.
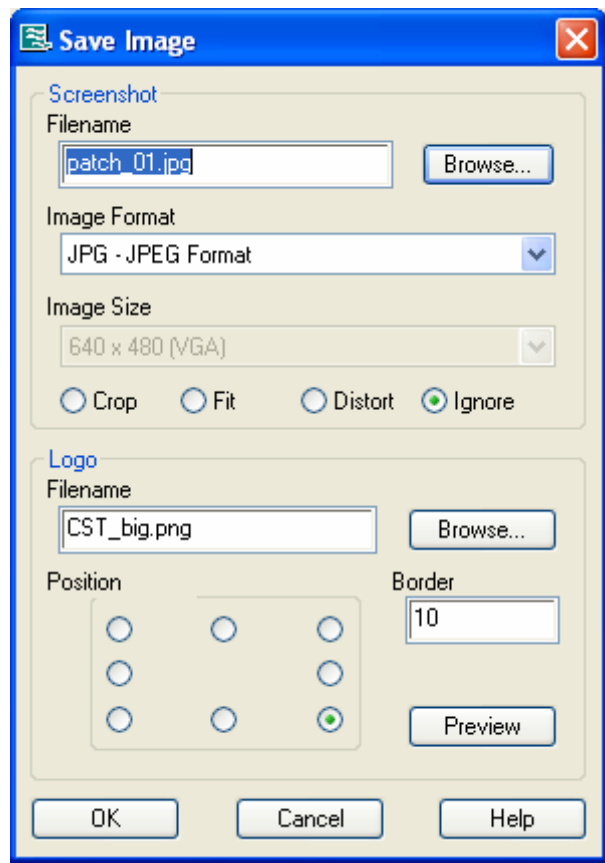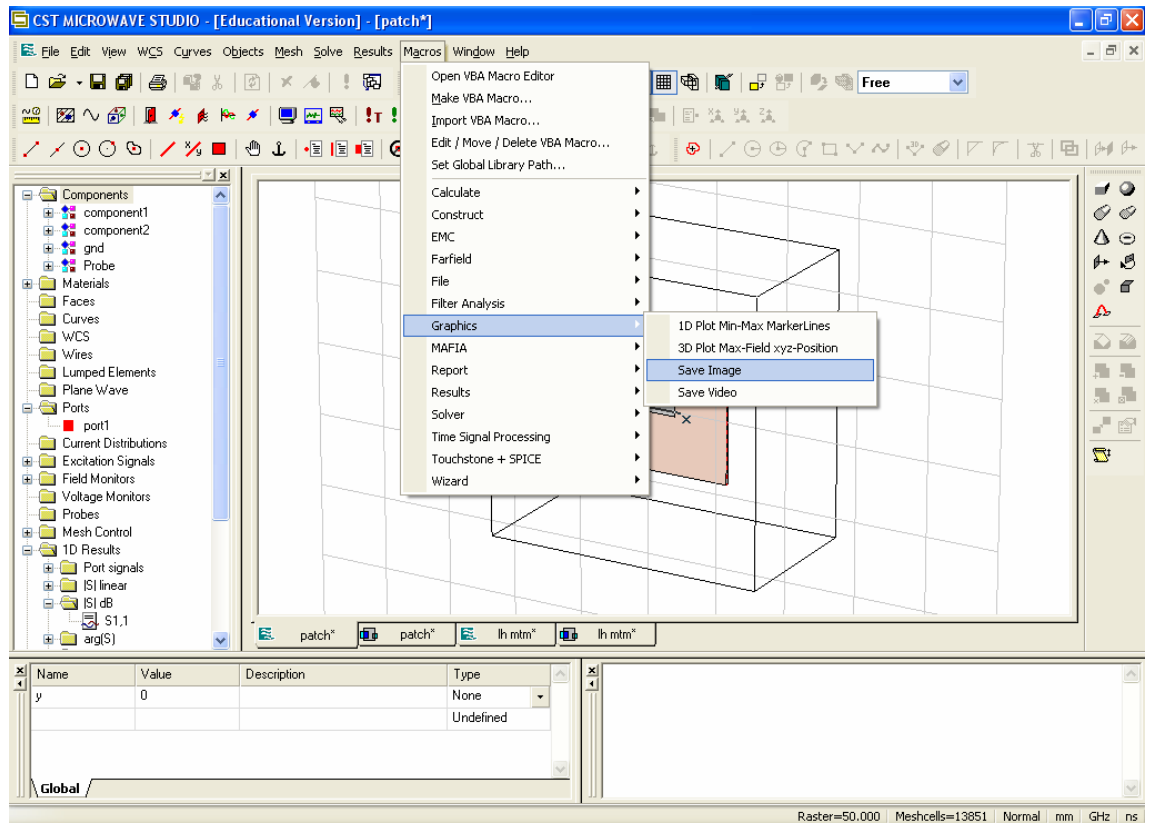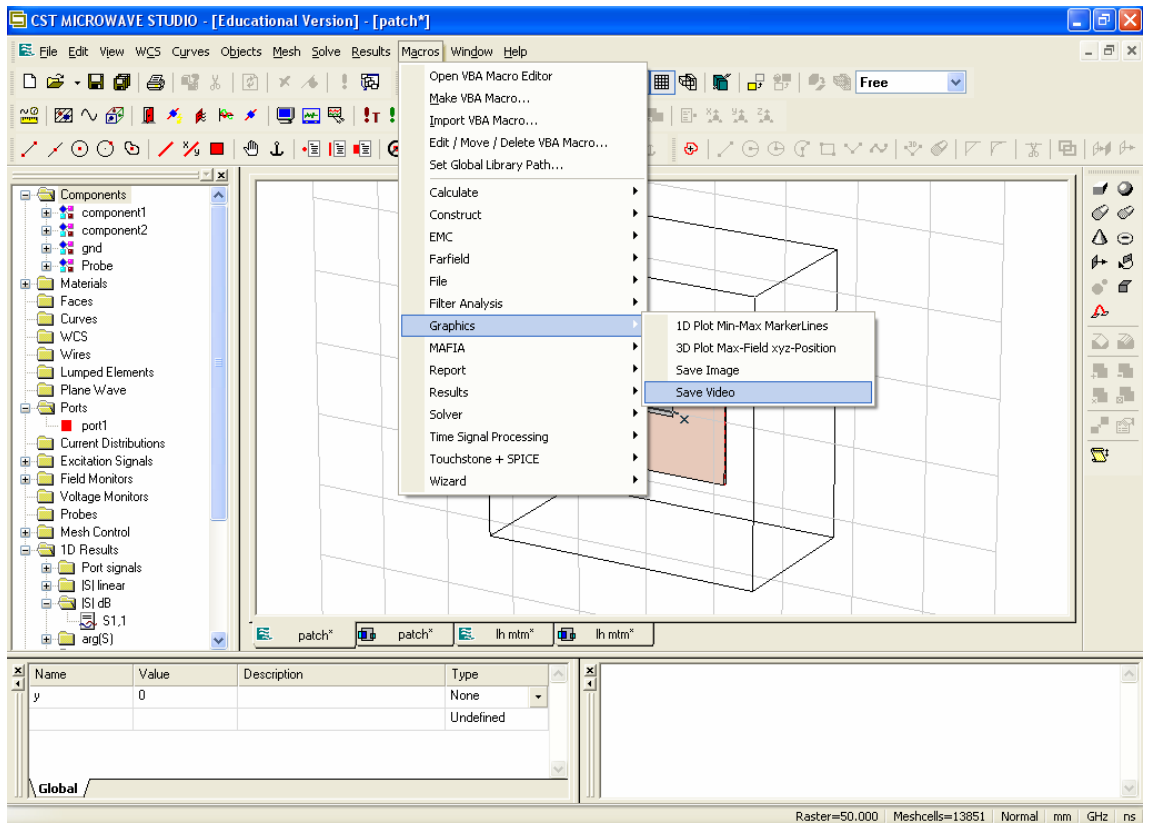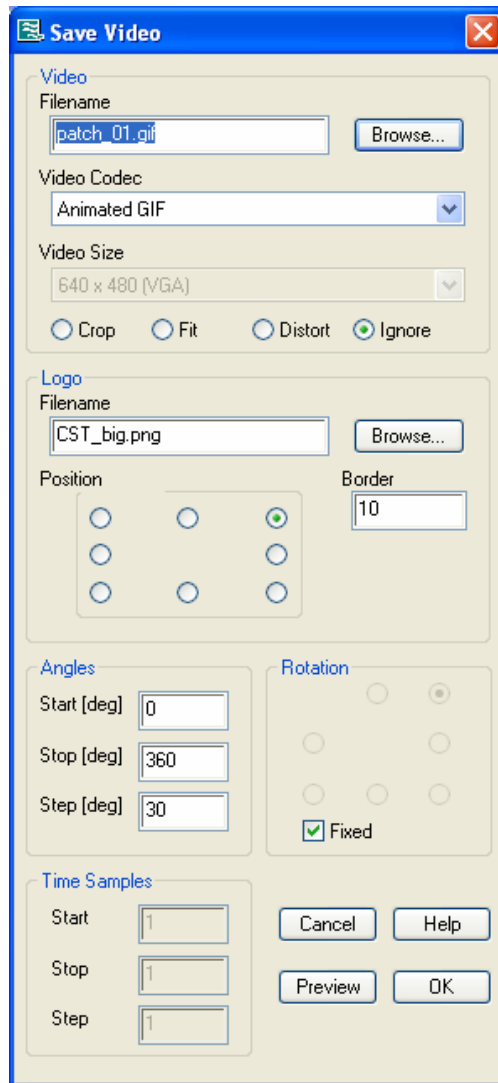
13. Besides, one may be interested to export the S parameters for record or further calculation purposes. This could be simply done by clicking on the parameter on the left side of the screen. Then, the format of the file to be exported should be chosen in the File tab and eventually defining the destination of the exported file. For example, when one wants to export the S_{11} parameter (dB) for record purposes, he/she would follow the precedence relationship as follows:

    a.   Click on S_{11}

    b.   File > Export > Plot Data ASCII

    c.   Choose the destination of the file
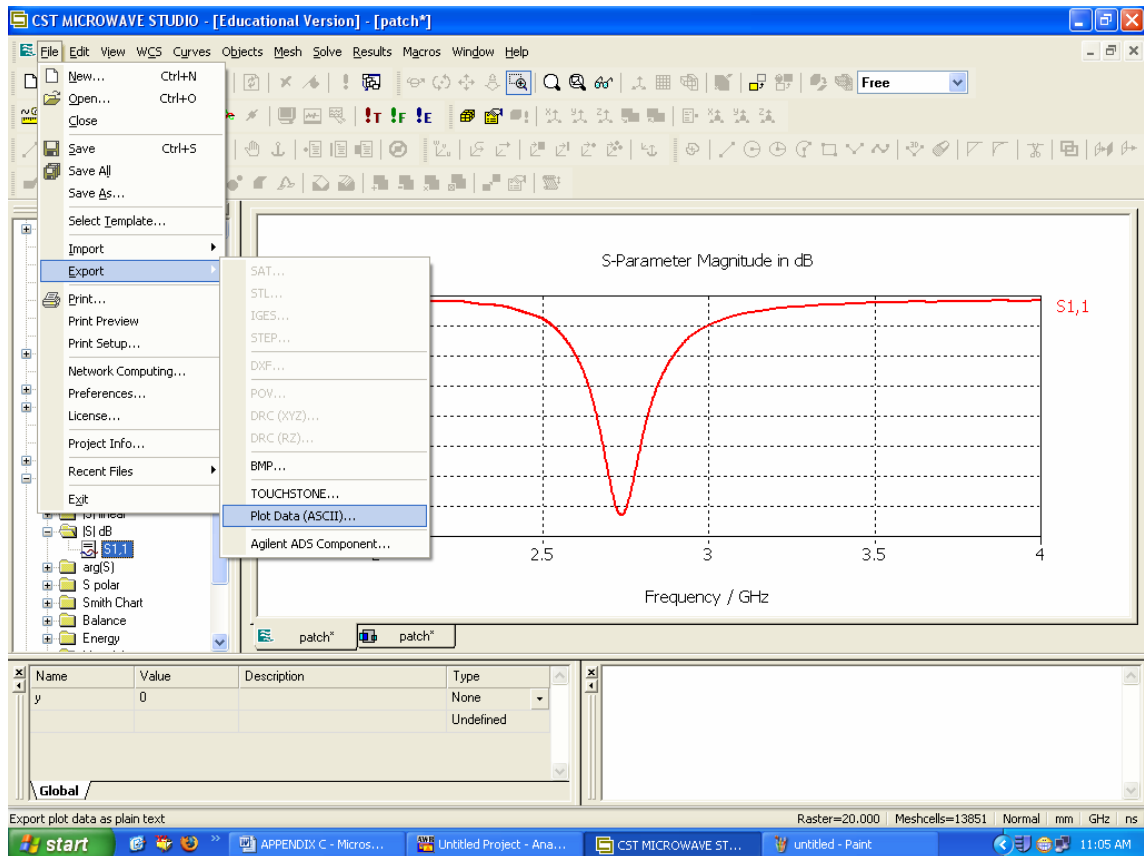
14. Lastly, in order to fabricate the structure, one has to print out the exact dimension of the structure. Therefore, CST MWS has design a very convenient tool to transfer the design into AutoCAD with the widely used extension .dxf. However, one must first correctly define the face of the structure to be exported by assigning the local coordinate system (U, V, W). Then, he/she has to click on the Component tab on the left side of the screen and subsequently choose the export function in the File tab. Then, choose the destination of the file.
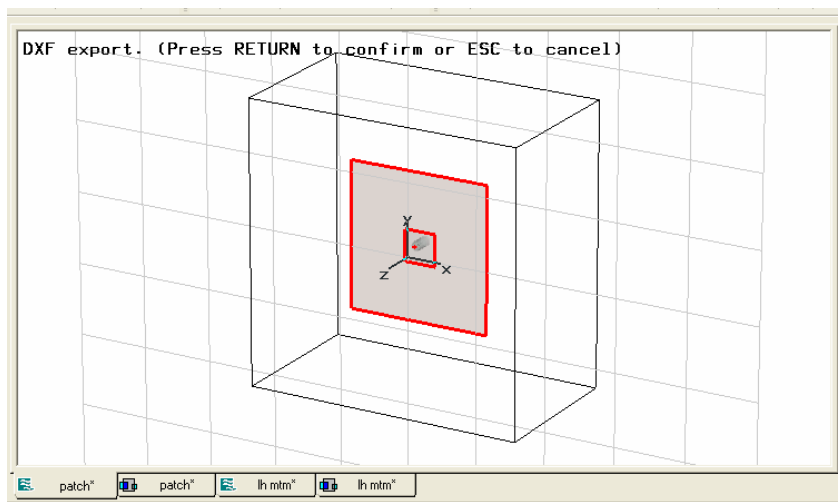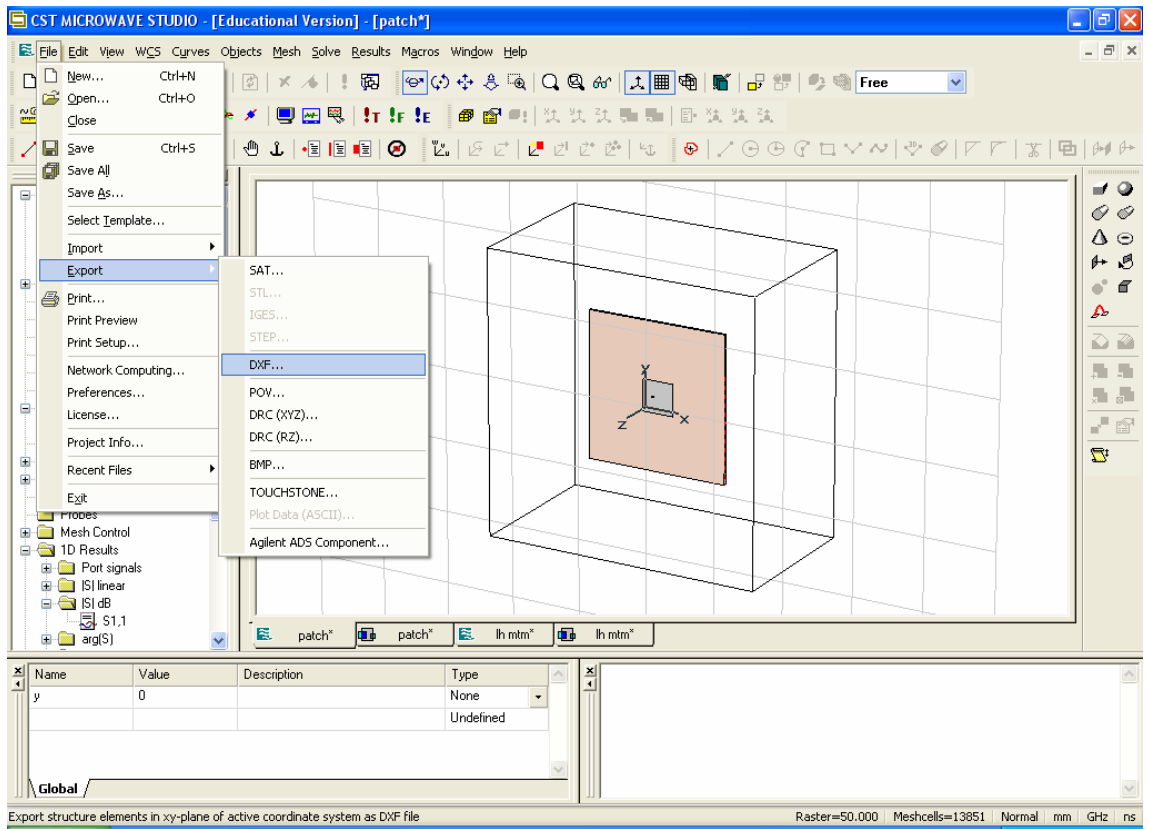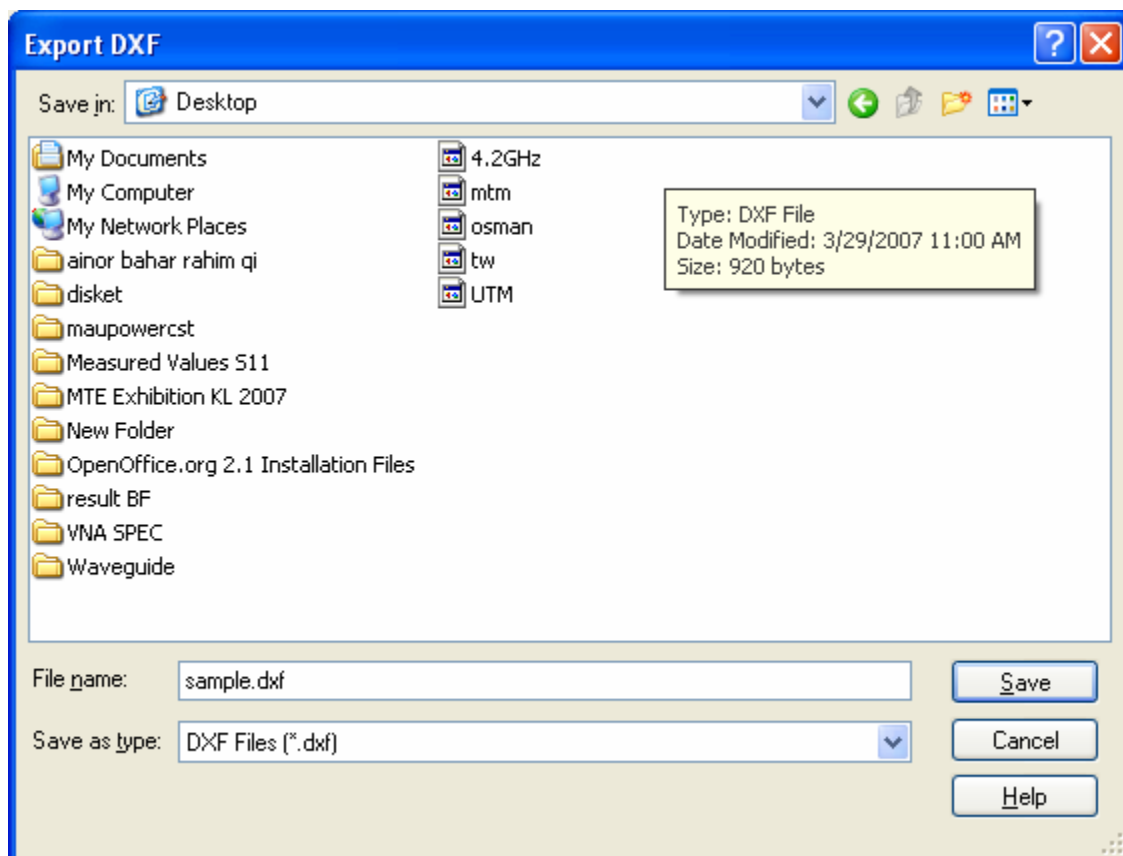
APPENDIX B

Results and Discussion of the LH MTM Array
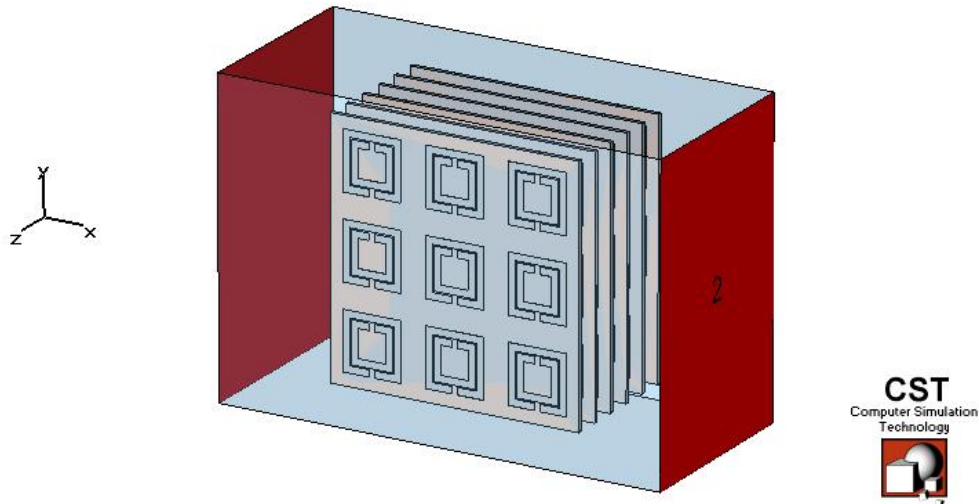
LH MTM Array
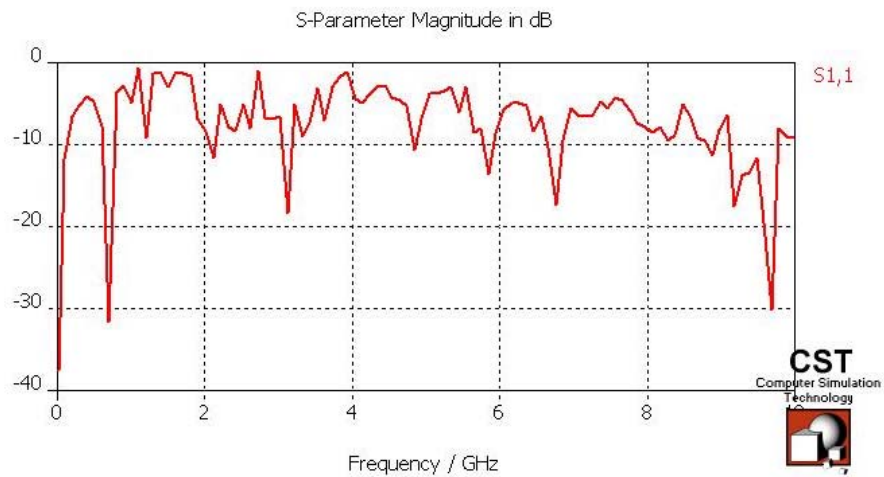
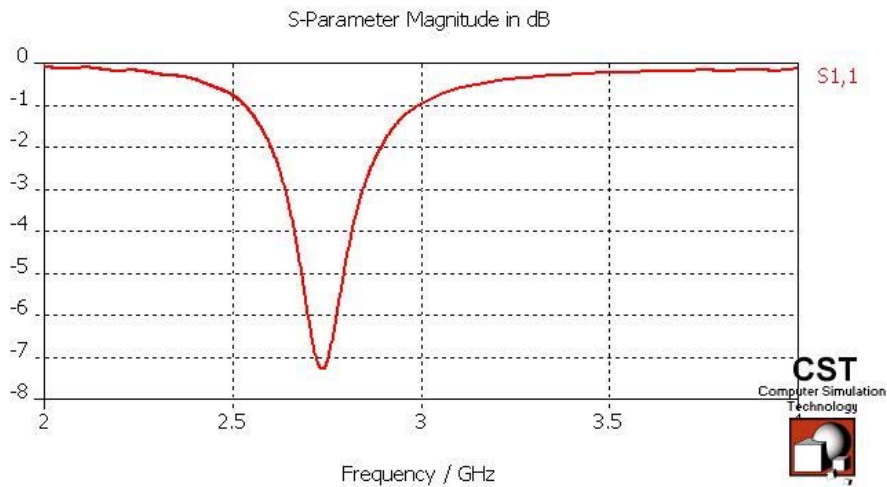Simulated Return Loss S_{11} Parameter
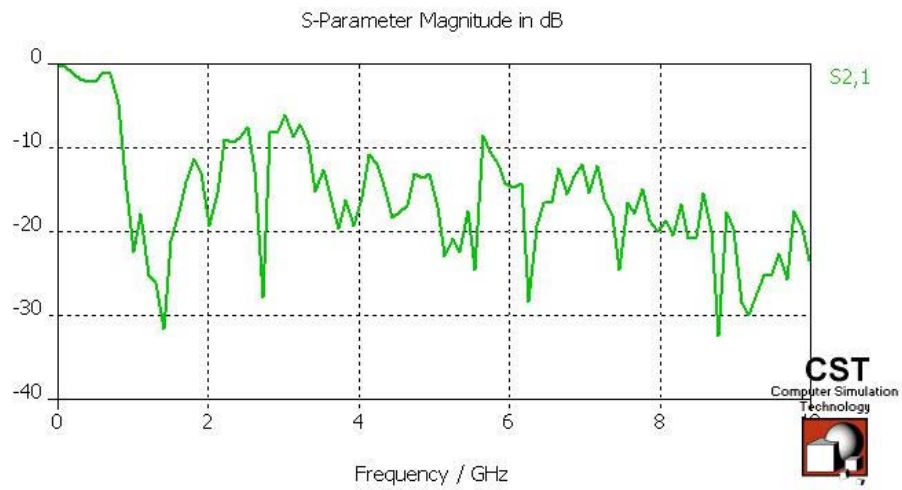
Simulated S$_{21}$ Parameter
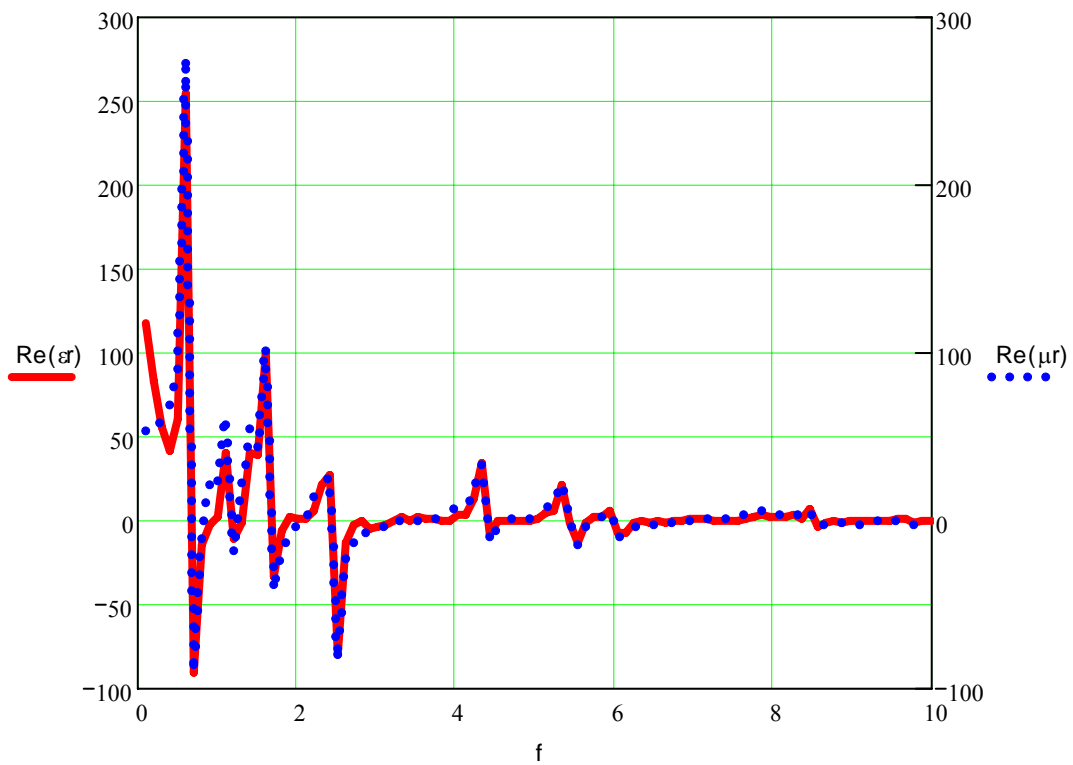
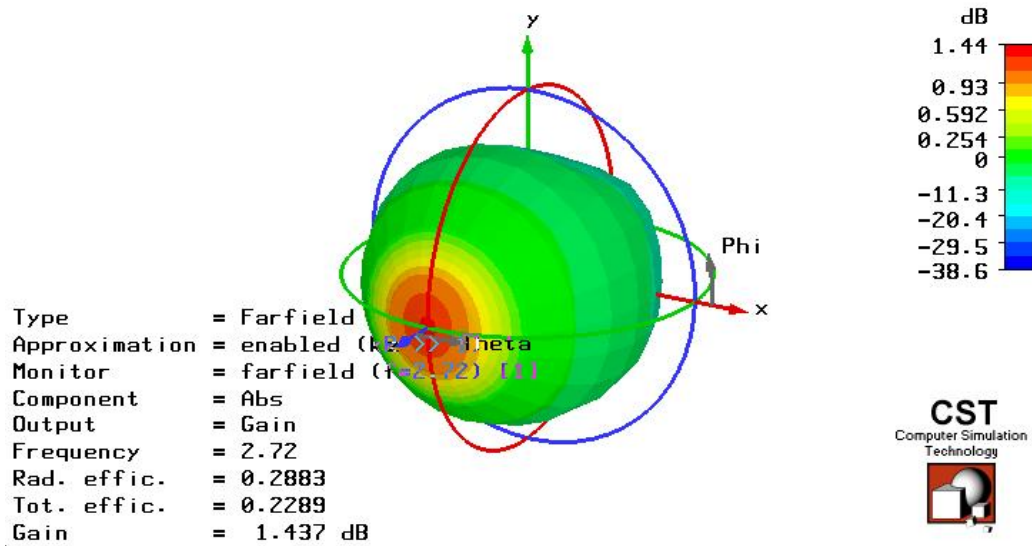Calculated DNG Parameters from MathCAD
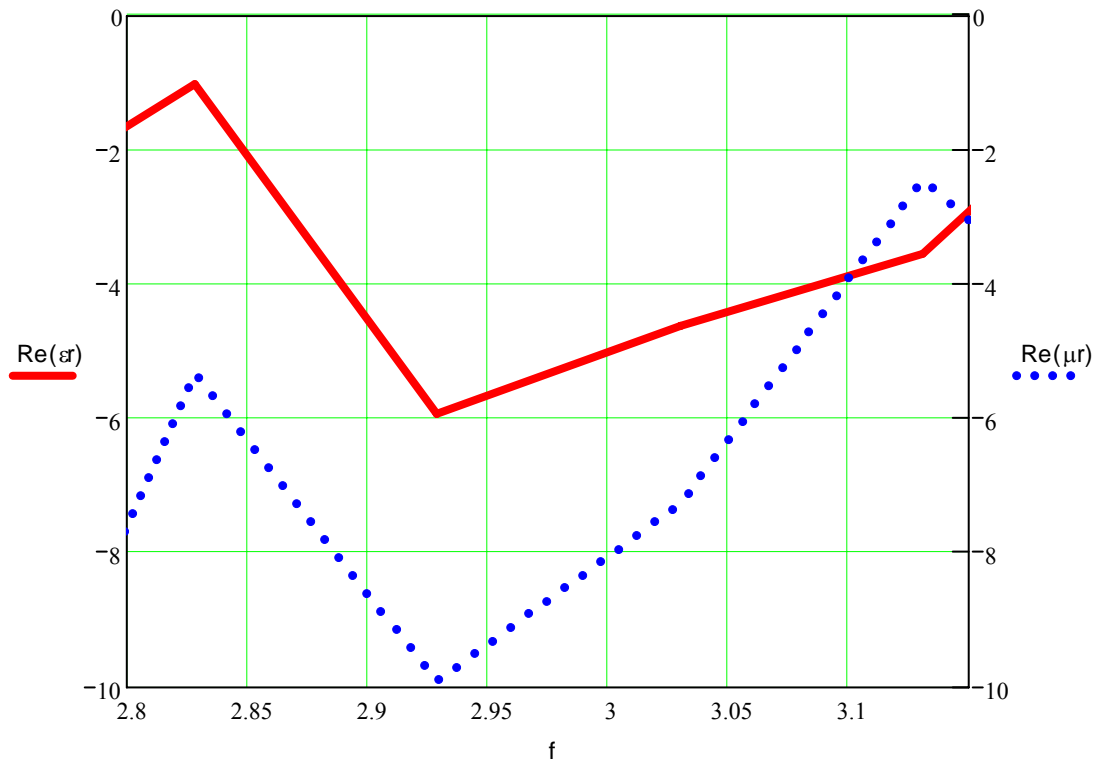
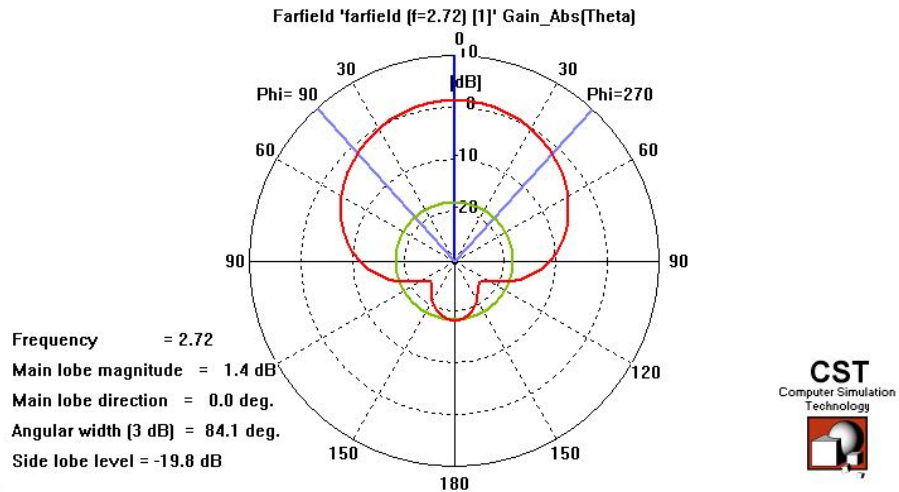Zoomed-in (2.8GHz – 3.15GHz) Calculated DNG Parameters from MathCAD
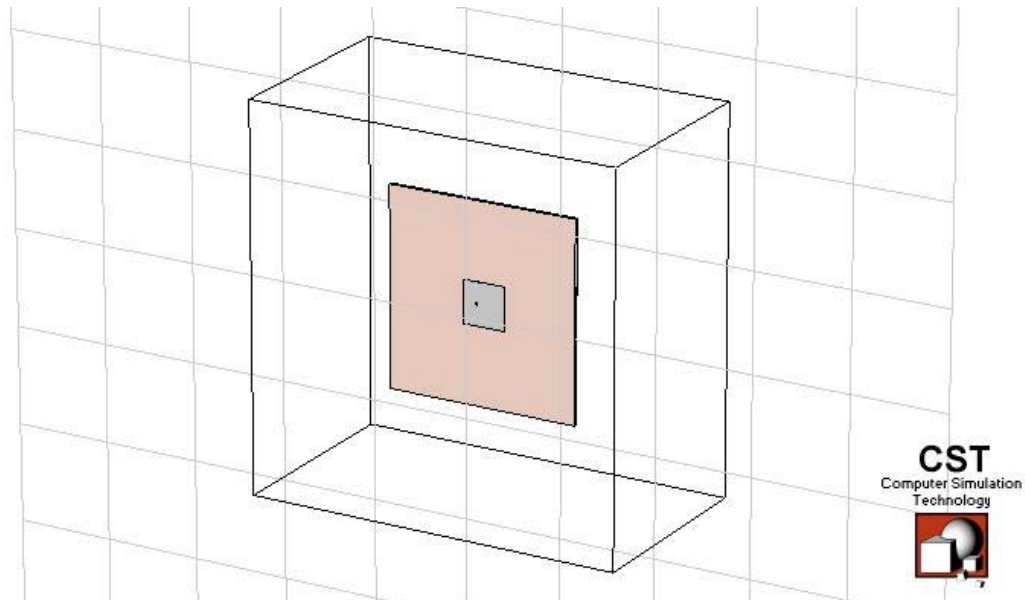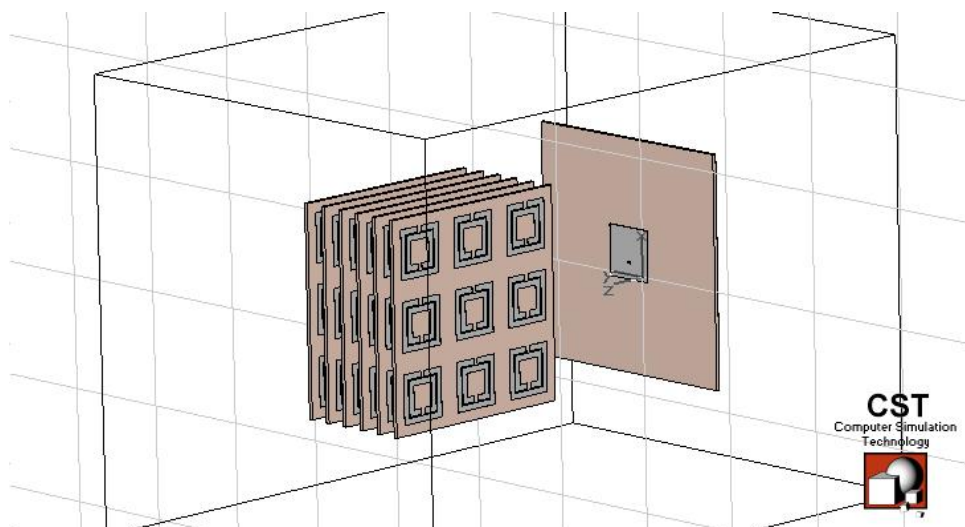

Patch Antenna

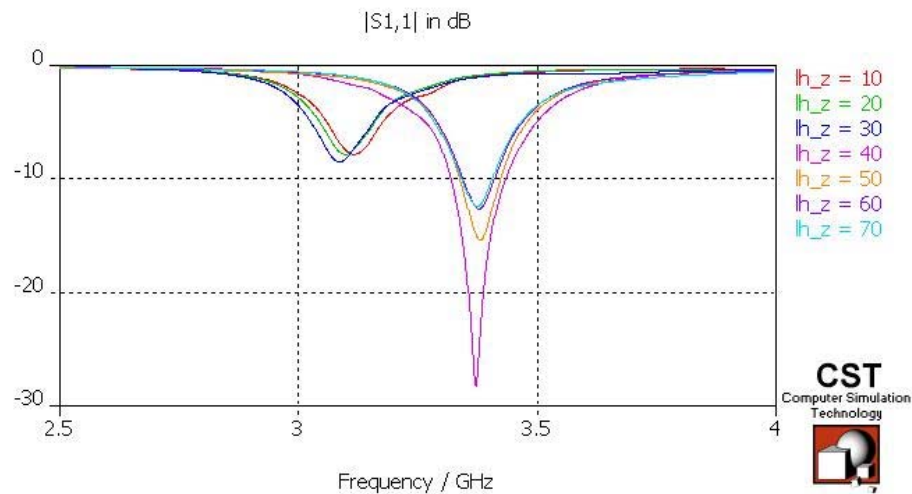Simulated Return Loss S_{11} Parameter of Patch Antenna

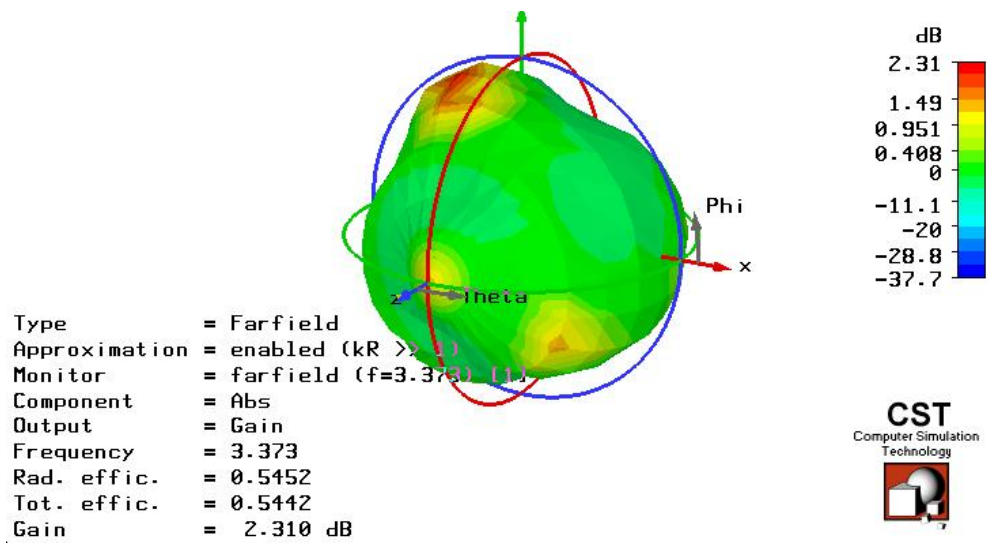
3D Farfield Results of Patch Antenna

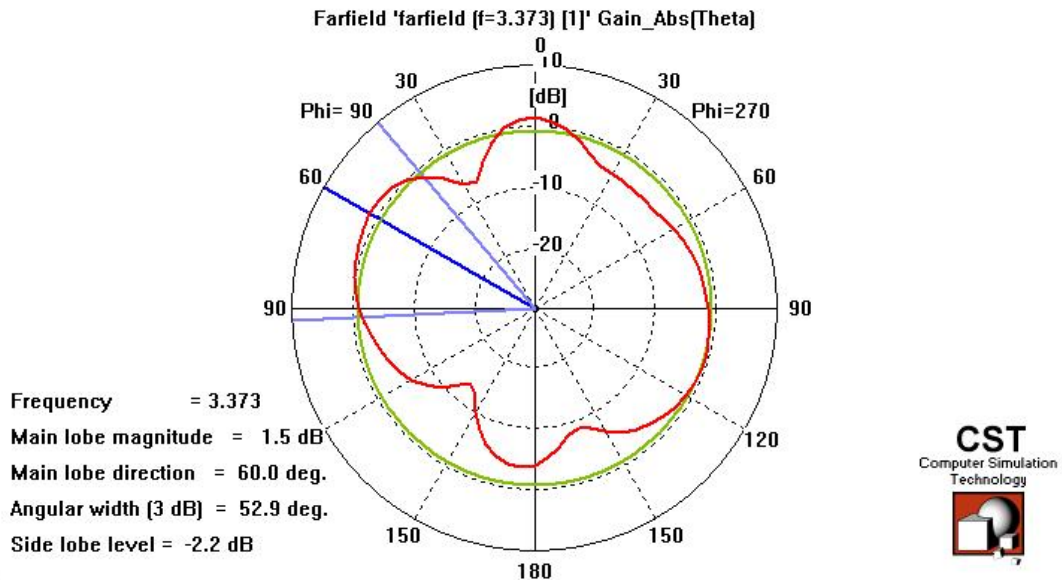2D Farfield Results of Patch Antenna
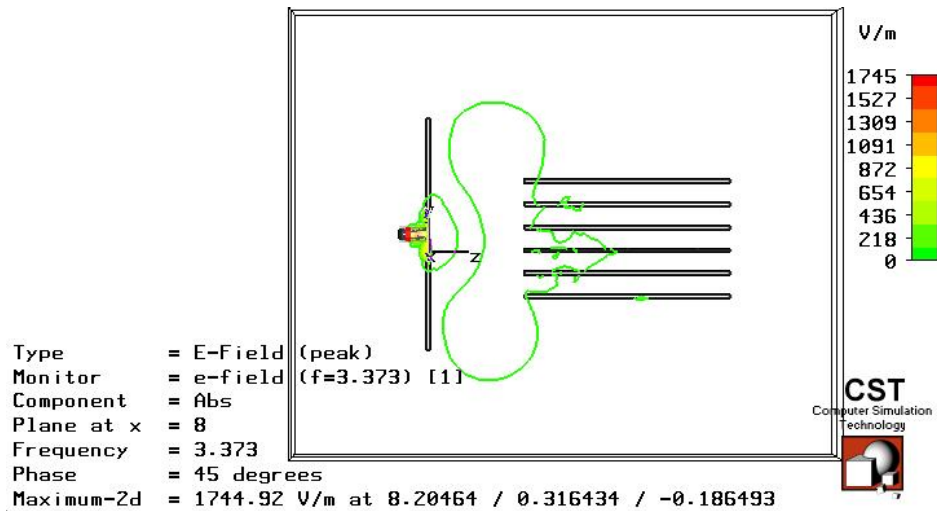

LH MTM Integrated with Patch Antenna

Simulated Return Loss S$_{11}$ Parameter of LH MTM Integrated with Patch Antenna

(lh_z = distance between LH MTM and Patch Antenna)

3D Farfield Results of LH MTM Integrated with Patch Antenna

Farfield 'farfield (f=3.373) [1]' Gain_Abs(Theta)

Frequency = 3.373
Main lobe magnitude = 1.5 dB
Main lobe direction = 60.0 deg.
Angular width (3 dB) = 52.9 deg.
Side lobe level = -2.2 dB

2D Farfield Results of LH MTM Integrated with Patch Antenna

Type = E-Field (peak)
Monitor = e-field (f=3.373) [1]
Component = Abs
Plane at x = 8
Frequency = 3.373
Phase = 45 degrees
Maximum-2d = 1744.92 V/m at 8.20464 / 0.316434 / -0.186493

E-Field Results of LH MTM Integrated with Patch Antenna